

Taming Thiemann’s Hamiltonian constraint in canonical loop quantum gravity: reversibility, eigenstates and graph-change analysis

T. L. M. Guedes,^{1,2,*} G. A. Mena Marugán,^{3,†} M. Müller,^{1,2,‡} and F. Vidotto^{3,4,§}

¹*Institute for Quantum Information, RWTH Aachen University, D-52056 Aachen, Germany*

²*Peter Grünberg Institute, Theoretical Nanoelectronics,
Forschungszentrum Jülich, D-52425 Jülich, Germany*

³*Instituto de Estructura de la Materia, IEM-CSIC, C/ Serrano 121, 28006 Madrid, Spain*

⁴*Department of Physics and Astronomy, Department of Philosophy,
and Rotman Institute, Western University, N6A5B7 London, Ontario, Canada.*

The Hamiltonian constraint remains an elusive object in loop quantum gravity because its action on spinnetworks leads to changes in their corresponding graphs. As a result, calculations in loop quantum gravity are often considered unpractical, and neither the eigenstates of the Hamiltonian constraint, which form the physical space of states, nor the concrete effect of its graph-changing character on observables are entirely known. Much worse, there is no reference value to judge whether the commonly adopted graph-preserving approximations lead to results anywhere close to the non-approximated dynamics. Our work sheds light on many of these issues, by devising a new numerical tool that allows us to implement the action of the Hamiltonian constraint without the need for approximations and to calculate expectation values for geometric observables. To achieve that, we fill the theoretical gap left in the derivations of the action of the Hamiltonian constraint on spinnetworks: we provide the first complete derivation of such action for the case of 4-valent spinnetworks, while updating the corresponding derivation for 3-valent spinnetworks. Our derivations also include the action of the volume operator. By proposing a new approach to encode spinnetworks into functions of lists and the derived formulas into functionals, we implement both the Hamiltonian constraint and the volume operator numerically. We are able to transform spinnetworks with graph-changing dynamics perturbatively and verify that volume expectation values have rather different behavior from the approximated, graph-preserving results. Furthermore, using our tool we find a family of potentially relevant solutions of the Hamiltonian constraint. Our work paves the way to a new generation of calculations in loop quantum gravity, in which graph-changing results and their phenomenology can finally be accounted for and understood.

I. INTRODUCTION

Although current experiments are still far from observing any traces of quantum behavior in gravity [1–3], the necessity of a convergence between quantum physics and general relativity has been conceptually established since the pioneering works of Bronstein [4], Dirac [5, 6] and Hawking [7], among others [8, 9]. The search for a quantum theory of gravity led to several proposals, one of which, loop quantum gravity (LQG), has at its core the idea of quantized spacetime geometry. The theory is based on a recasting of the Einstein equation in terms of holonomies in a compact gauge group and fluxes of canonically conjugate densitized triads, constructed with the so-called Ashtekar-Barbero variables [10–12]. These new fields allowed for a derivation of Hamiltonian constraints for the gravitational field [13] and a quantization protocol in the molds of Dirac’s quantization [6, 14].

One of the bases commonly used in LQG is spanned by eigenstates of certain geometric operators, namely the so-called spinnetworks (these are closely related, for instance, to ribbon graphs and string nets [15–17]). These

are graphs with spins/colors [or more formally representations of the $SU(2)$ group] assigned to their links and nodes that form singlets out of the spins of incoming and outgoing links (in other words, this enforces the decomposition of the input irreducible representations into the output ones). Spinnetworks provide a powerful graphical tool to perform and represent otherwise cumbersome calculations [18], and have been in use since the advent of the quantum mechanics of angular momenta [19–21]. A major difficulty in canonical-LQG calculations, however, is the graph-changing effect of the Hamiltonian constraint on spinnetworks, which generates superpositions of spinnetworks with different graphs from each input spinnetwork, and therefore can exponentially increase the number of intervening states in computations. This work aims at contributing to fill this gap by providing a complete derivation of the action of the Hamiltonian constraint on 3- and 4-valent nodes. A related goal is to numerically implement the corresponding formulas through a novel spinnetwork-encoding approach in order to understand the effect of graph changes on geometric observables, like the volume. In addition, in this way we can also elucidate the validity of the commonly employed graph-preserving approximations, as well as search for new solutions of the Hamiltonian constraint.

This article is the companion paper of a letter, where we summarize and highlight the most important results of our investigation without details about technical as-

* t.guedes@fz-juelich.de

† mena@iem.cfmac.csic.es

‡ markus.mueller@fz-juelich.de

§ fvidotto@uwo.ca

pects [22]. It is structured as follows. In Sec. II we summarize the main findings of our work, before delving into them. In Sec. III, we introduce the Hamiltonian constraint and its basic building blocks. In Sec. IV, we introduce the mathematical machinery used throughout the calculations, namely, recoupling theory. Sections VI and VII use recoupling theory to derive the action of the Hamiltonian constraint on 3- and 4-valent node-like spinnetworks, respectively. In Sec. VIII we consider the action of the volume operator. In Sec. IX, we introduce our encoding of spinnetworks and operators, showing how we are able to apply the Hamiltonian constraint on spinnetworks and evaluate the volume expectation values. In Sec. X, we present and discuss our results for the volume of spinnetworks perturbatively transformed by the unitary generated by the constraint. Finally, Sec. XI contains our closing remarks, briefly discussing the consequences of our findings.

II. MAIN RESULTS

We start with a brief overview of the theory and a derivation of the action of the (scalar) Euclidean Hamiltonian constraint (referred to simply as Hamiltonian whenever there is no risk of confusion) on 3-valent and 4-valent spinnetworks, the simplest duals to triangulations of bi- and tri-dimensional hypersurfaces. For the former case, as in Ref. [23], our derivations can be considered an update of those presented in Refs. [24, 25], in which an approach based on the much less manageable Temperley-Lieb algebra was employed [19]. Moreover, we show that working with modern conventions leads to somewhat different results (cf. Appendix A2). In the case of 4-valent nodes, our derivations are an extension, as well as a correction, of those presented in Ref. [26]. This is the first in-depth derivation of the action of the Euclidean Hamiltonian constraint on 4-valent nodes using the modern graphical-calculus machinery [18, 21]. It serves as a guide for both experts and beginners in LQG, as well as for those generally interested in spinnetwork calculus for other purposes, like studies of non-Abelian topological error-correction codes [15–17].

In addition, we introduce a new computational tool, implemented concretely as a Mathematica code, that implements the action of the Hamiltonian constraint at spinnetwork nodes through a newly devised numerical approach. A key feature of this approach is a map between spinnetworks and functions of lists, on which the Hamiltonian acts as a functional. The (symbolic) calculations, performed in a computer based on our analytical formulas, involve no approximations in the Hamiltonian and therefore represent the first complete, graph-changing, application of the Euclidean Hamiltonian constraint on low-valency spinnetwork nodes (and the second numerical work in canonical LQG to our knowledge [27]), as well as of the unitary transformation it generates, expanded perturbatively. We generate numerical data

for the volume expectation values of two perturbatively transformed fiducial spinnetworks of valency 4 using the lapse as a perturbation parameter and the Hamiltonian constraint as a unitary-transformation generator. Our perturbative expansion of the unitary goes up to the 3rd order in the absence of embedding (or alternatively when either embedding in four or more dimensions or a “topological model” is considered, as is the case in covariant LQG), and up to 4th order when embedding in a three-dimensional (3D) manifold is considered. We compare the results with the corresponding data generated with a graph-preserving Hamiltonian and present the first concrete indication that such Hamiltonians fail to capture the proper dynamics of LQG spinnetworks. As we anticipate in Fig. 1(c), the expectation values of the quantum volume are rather different between graph-changing and graph-preserving scenarios.

Furthermore, we use our code to look for low-spin eigenstates of the Euclidean Hamiltonian, showing that simple eigenstates do exist: states with only vanishing spins meeting at the intertwiner. Note that these eigenstates also include spinnetworks with large numbers of inner loops, as long as the innermost links meeting at the intertwiner are in the trivial representation. Lastly, we propose a more complex family of solutions built from any desired spinnetwork, whose properties should be investigated in follow-up works.

III. OVERVIEW

Using Ashtekar-Barbero variables, the Einstein-Hilbert action can be recast in terms of smearings over three sets of constraints corresponding to gauge invariance, diffeomorphism invariance and (Euclidean) time reparametrization [13]. In the quantum theory, gauge invariance is well understood and consideration solely of spinnetworks with spin singlets at every node (also called intertwiners) suffices to satisfy this constraint. In precise mathematical terms, gauge invariance enforces that the Cauchy-Schwarz inequalities are fulfilled at every node. Spatial diffeomorphism invariance is a key symmetry in general relativity and topological field theories [15], both of which participate in the construction of LQG. In terms of spinnetworks embedded in manifolds, spatial diffeomorphisms can be well understood as (invertible) analytic deformations of the spinnetwork graphs (i.e., analytic maps). In a very simplified description, to satisfy the diffeomorphism constraint, one needs to consider equivalence classes of (dual) spinnetworks with respect to diffeomorphisms [14, 28]: all graphs related to each other by analytic deformations should be superposed to compose states that satisfy the diffeomorphism constraint.

The last constraint, commonly known as scalar or Hamiltonian constraint, dictates the dynamics of spinnetworks, and we will sometimes refer to it simply as the Hamiltonian, for the sake of analogy with standard quantum mechanics. When neither matter nor a cos-

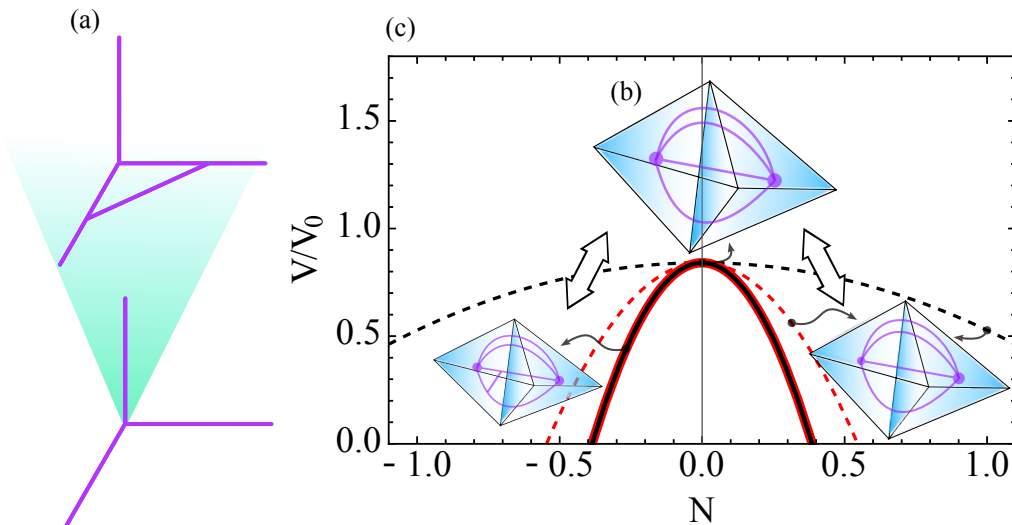


FIG. 1. Schematic representations of spinnetworks. (a) A 3-valent spinnetwork node (bottom) is transformed under the action of the Hamiltonian to give a modified structure containing an inner loop (top), exemplifying the graph-changing character of the non-approximated Hamiltonian constraint. (b) A minimal example of spinnetwork: the dipole model. Two 4-valent nodes are connected through their links pairwise, so that the dual to such graph is formed by two tetrahedra whose faces are pairwise glued (what cannot be visualized in 3D). These tetrahedra represent the quanta of volume. (c) Under the action of a unitary generated by the Hamiltonian, with a perturbative evolution parameter N called lapse (which mathematically behaves similarly to the time in standard quantum mechanics), a transformed spinnetwork node behaves differently when either graph-changing or graph-preserving dynamics are considered. The volume, with contributions up to 2nd order in N displayed, decreases much slower with N when the approximation of nonchanging graphs is adopted (dotted curve, right dipole), while the correct dynamics produces a steeper volume reduction with N at leading perturbative order (solid curve, left dipole). The data for the volume dependence on N for these two cases considers a single spinnetwork node with spins $1/2$ on its four links and spin 0 (red) or 1 (black) in the central link (not displayed in the dipole model)

and therefore does not entirely represent the dynamics of the dipole model, which was included for illustrative purposes.

mological constant are considered, the eigenstates of all three constraints with null eigenvalue are the physical states of the theory (strictly speaking, those normalizable with respect to a suitable inner product). On the other hand, for the scalar constraint, nonzero eigenvalues might represent, for example, physical states of the geometry in the presence of classical matter or a nonzero cosmological constant, both of which are common in the formulation of loop quantum cosmology [29, 30].

Thiemann [13] proposed a specific form for the scalar constraint constructed from the volume operator \hat{V} and holonomies $\hat{h}[p]$ (the link-related parallel-transport unitaries commonly encountered in lattice gauge theories) defined over a path p :

$$\hat{C}_s = -\frac{i}{3l_0^2} \lim_{\square \rightarrow 0} \sum_{\square} N_{\square} \epsilon_{ijk} \text{tr} \left\{ \hat{h}[\alpha_{ij}] - \hat{h}[\alpha_{ji}], \hat{h}[p_k] \hat{V} \hat{h}^{-1}[p_k] \right\}. \quad (1)$$

In this equation, the large curly brackets stand for the anticommutator, the symbol tr is the trace, the symbol \square represents a partition of the manifold into cubes and the limit $\square \rightarrow 0$ means that the size of those cubes goes to zero, while their number diverges. It must be noted, however, that different partition schemes using, e.g., prisms of choice, are possible, all of which lead to the same equa-

tions up to some prefactors [31]. As a result of this regularization procedure, only the cubes centered at the nodes of the spinnetworks will contribute to Eq. (1) and no cube will ever contain more than one node (in fact, shrinking the cubes to a size at which they contain either one or no nodes suffices to describe the effect of this limit) [28]. The prefactor N_{\square} is called lapse and results from the Riemannian discretization of a distribution that smears the constraint. In Eq. (1), the lapse serves as an amplitude modulator for the action of the constraint in each cube, which effectively translates a 3D foliation of spacetime along a timelike vector proportional in absolute value to N_{\square} . The paths α_{ij} and α_{ji} are triangular loops of opposite orientations (i.e., $\alpha_{ij} = \alpha_{ji}^{-1}$), with segments parallel to two perpendicular links (labelled by i and j) from a (physical) node. Here, perpendicularity is understood in the sense of the assumed Euclidean geometry in the embedding manifold. The path p_k is a line segment parallel to yet another link from the node (labelled k), perpendicular to both i and j links. The totally anti-symmetric symbol ϵ_{ijk} guarantees that only holonomies applied over three mutually perpendicular links from a given intertwiner contribute to the action of the scalar constraint. These holonomies couple additional spins (in the sense of Clebsch-Gordan spin addition) to the respective links of the spinnetwork acted upon by \hat{C}_s . Moreover, because

α_{ij} and α_{ji} are (closed) loops, the term $\hat{h}[\alpha_{ij}] - \hat{h}[\alpha_{ji}]$ can add one additional link (between i and j) to the spin-network [see Fig. 1(a)].

Finally, the volume operator is a key observable in LQG, extracting information about the (quantum) geometry of spacetime from quantum states. Discrete eigenvalues of the volume are based on the spins of the links connected to a certain node of valency 4 or higher, with l_0 being the Planck length. This provides an interpretation of spinnetworks as the dual to a triangulation of a manifold, associating a link to each face (2-simplex) of the triangulation and a node to each tetrahedron (3-simplex), or polyhedron in the most general case. In this sense, two nodes connected by four links can be seen as two tetrahedra with pairwise connected faces [see Fig. 1(b)]. The matrix elements of \hat{V} will be introduced later in the calculations.

IV. SU(2) RECOUPLING THEORY

Before deriving the action of Eq. (1) on spinnetwork nodes, we introduce the main working tools from recoupling theory, i.e., the graphical calculus involving elements and representations of the SU(2) group. Early papers in LQG [24, 25, 32, 33] made use of the now “old-fashioned”, yet more graphically intuitive description of such systems in terms of Temperley-Lieb tangles [19], which are closely related to knots [34]. Tangles are usually proportional to spinnetworks [32], but the complicated conversion factors between them, which lead to the need for normalization not only in the states, but also in commonly used functions like the Wigner 3j, 6j and 9j symbols, make the Temperley-Lieb approach less attractive when one aims at robust calculations that can be performed numerically. For completeness, we report the derivations using the Temperley-Lieb algebra in Appendix B, while here instead we focus on the modern convention for recoupling theory, mainly following the notation of Ref. [18], as well as some identities from Ref. [21]. In this convention, the Wigner 3j, 6j and 9j symbols are the same that are implemented in Mathematica.

The key idea of recoupling theory is to represent the SU(2) group elements g in a given representation $j \in \mathbb{N}/2$, as well as its coupling to other elements of the same group in possibly different representations, in graphical form. Starting from the simplest element in any representation, the identity, we write a single straight line with ends carrying the two indices of the identity matrix (e.g., for $j = 1/2$, the 2×2 matrix has two indices commonly associated with spin magnetic numbers $\pm 1/2$),

$$\delta_{m,n}^{(j)} = m \xrightarrow{j} n. \quad (2)$$

and with the representation indicated above the corresponding link. For a given j , there are $d_j = 2j+1$ possible

choices of indices, and once two matrices are contracted, summation over the indices at the corresponding connected ends of the graphical representation is implied. If one therefore connects the two opposite ends of the identity, forming a closed loop, one ends up with its trace, which is simply d_j .

Another SU(2) element that deserves its own graphical representation is given by the j -representation tensor $\epsilon^{(j)mn} = \epsilon_{mn}^{(j)} = (-1)^{j-m} \delta_{m,-n}^{(j)} = (-1)^{2j} \epsilon_{nm}^{(j)}$, for which $\epsilon_{mn}^{(j)} \epsilon^{(j)nk} = (-1)^{2j} \delta_m^{(j)k}$. Graphically, this tensor is represented by a small solid arrow pointing from m to n ,

$$\epsilon_{mn}^{(j)} = m \xrightarrow{j} n. \quad (3)$$

Consequently, one has the graphical relations

$$\epsilon_{mn}^{(j)} \epsilon^{(j)nk} = m \xrightarrow{j} k = (-1)^{2j} \delta_m^{(j)k}, \quad (4)$$

$$\epsilon_{mn}^{(j)} \epsilon^{(j)kn} = m \xrightarrow{j} \leftarrow k = \delta_m^{(j)k}. \quad (5)$$

It should be noted that flipping the arrow in Eq. (3) corresponds to swapping the order of the indices, which leads to a prefactor of $(-1)^{2j}$. Since $(-1)^{4j} = 1$, Eq. (5) can be derived from Eq. (4) through an arrow flip. The tensor $\epsilon^{(j)mn}$ is invariant under SU(2) transformations: given a Wigner matrix $D_n^{(j)m}(g)$ for the SU(2) element g , $D_n^{(j)m}(g) \epsilon_{mp}^{(j)} D_q^{(j)p}(g) = \epsilon_{nq}^{(j)} = D_m^{(j)n}(g) \epsilon_{mp}^{(j)} D_p^{(j)q}(g)$. Graphically, the Wigner matrix is represented by a triangle with the group element g within,

$$D_n^{(j)m}(g) = n \begin{array}{c} j \\ \triangleleft g \triangleright \\ m \end{array}. \quad (6)$$

The invariance of the tensor $\epsilon_{nq}^{(j)}$ is therefore graphically represented as

$$n \xrightarrow{j} q = n \begin{array}{c} j \\ \triangleleft g \triangleright \end{array} \begin{array}{c} j \\ \triangleleft g \triangleright \\ q \end{array}. \quad (7)$$

A similar relation holds when the triangles point toward the “free” ends of the links. It is worth noting that the invariance of $\epsilon_{nq}^{(j)}$ holds for any g as long as it is present on both Wigner matrices. Using Eq. (7), it is possible to show that the Wigner matrices can be inverted through contraction with $\epsilon_{mn}^{(j)}$ on both of their indices,

$$n \xrightarrow{j} \begin{array}{c} j \\ \triangleleft g \triangleright \end{array} \leftarrow q = n \begin{array}{c} j \\ \triangleleft g^{-1} \triangleright \end{array} q. \quad (8)$$

Equations (2)-(8) span the basic relations for representing single SU(2) elements graphically as links. Consideration of graphs, however, requires the coupling of several such links into nodes according to the SU(2) decomposition rule into irreducible representations. This

enforces the Clebsch-Gordan (also known as triangularity) conditions on the spins meeting at a certain node. Mathematically, the (nontrivial) minimal-valency coupling is enforced by a Wigner 3j symbol, an object proportional to the Clebsch-Gordan coefficients. The Wigner 3j symbol is graphically represented as a 3-valent node with a certain cyclicity that describes whether the columns of the 3j symbol are ordered clock-wise (-) or counter-clock-wise (+) on the node,

$$\begin{pmatrix} j_1 & j_2 & j_3 \\ m_1 & m_2 & m_3 \end{pmatrix} = \begin{array}{c} j_1 \\ | \\ \bigoplus \\ | \\ j_2 \quad j_3 \end{array} = \begin{array}{c} j_1 \\ | \\ \bigominus \\ | \\ j_3 \quad j_2 \end{array}. \quad (9)$$

Swapping the cyclicity of the node, which is also known as braiding, leads to a phase factor of $(-1)^{j_1+j_2+j_3}$. Since j_1, j_2, j_3 must fulfill the Clebsch-Gordan conditions, such that $j_1 + j_2 + j_3 \in \mathbb{N}$, a double braid leads to a prefactor of $(-1)^{2(j_1+j_2+j_3)} = 1$. On the leftmost side of Eq. (9), the Wigner 3j symbol contains an upper row of spins (irreducible representations) and a lower row of associated spin projections/magnetic numbers (matrix components in a given irreducible representation). The Wigner matrices $D_n^{(j)m}(g)$, represented as in Eq. (6) [which includes both Eqs. (2) and (3) as special cases] are then contracted with the node legs of the same representation in Eq. (9), which implies a summation over the lower entries in the latter. The Wigner 3j symbol is also invariant with respect to SU(2) transformations, i.e., it returns the node when this is contracted with three inwards oriented or three outwards oriented Wigner matrices representing the same SU(2) element g ,

$$\begin{array}{c} j_1 \\ | \\ \triangleup g \\ | \\ \bigoplus \\ | \\ \triangleleft g \\ | \\ j_2 \quad j_3 \end{array} = \begin{array}{c} j_1 \\ | \\ \bigoplus \\ | \\ j_2 \quad j_3 \end{array}. \quad (10)$$

The SU(2) invariance of the Wigner 3j symbol means that, regardless of their representations, the Wigner matrices can be partially or even entirely absorbed into the nodes in graphical notation, depending on which elements g are connected to each node. As an example, if all three legs of a given node are contracted with $\epsilon_{nq}^{(j)}$ symbols, therefore displaying three outwards or inwards oriented solid arrows in graphic form, they can be all simultaneously incorporated into the node. Lastly, there is a correspondence between $\epsilon_{nq}^{(j)}$ and the Wigner 3j symbols, which graphically takes the form

$$\begin{array}{c} j \\ | \\ \bigoplus \\ | \\ j' \end{array} = \delta_{j,j'} d_j^{-\frac{1}{2}} \begin{array}{c} j \\ | \\ \downarrow \end{array}. \quad (11)$$

Now that the coupling of three links into a node has been introduced, we present a few graphical relations involving nodes and links. The first two relations allow for

major simplifications during calculations,

$$+ \begin{array}{c} j_1 \\ | \\ \bigoplus \\ | \\ j_3 \end{array} = 1, \quad (12)$$

$$j_1 \begin{array}{c} | \\ \bigoplus \\ | \\ j' \end{array} j_2 = \delta_{j,j'} d_j^{-1} \begin{array}{c} | \\ \downarrow \end{array} j. \quad (13)$$

Note that these graphical relations are of topological nature, in the sense that rotating or deforming them without crossing links does not affect the outcomes.

Two (identity) links of arbitrary spins can be coupled by introducing two nodes connecting them according to

$$j_1 \begin{array}{c} | \\ | \\ | \end{array} j_2 = \sum_j d_j \begin{array}{c} j_1 \quad j_2 \\ | \quad | \\ \bigoplus \\ | \\ j \\ | \\ \bigominus \\ | \\ j_1 \quad j_2 \end{array}. \quad (14)$$

The sum on the right-hand side of Eq. (14) runs, in principle, over $j \in \mathbb{N}/2$, but considering that the two nodes enforce that the triangle inequality has to be fulfilled by the three spins meeting at them, the sum over j runs effectively from $|j_1 - j_2|$ to $j_1 + j_2$. Although Eq. (14) can also be used on links with arbitrary group elements assigned to them, this requires extending the corresponding Wigner-matrix links by contracting one of their ends with identities, so that the identity segments of the links can be merged through (14) and the Wigner matrices, in the form of Eq. (6), sit at the external legs of one of the nodes on the right-hand side of Eq. (14). When the same group element is assigned to both of the links merged through this relation, however, the node invariance [Eq. (10)] can be used to give an expression corresponding to the direct coupling of two Wigner matrices of the same g ,

$$\begin{array}{c} j_1 \\ | \\ \triangleleft g \\ | \\ \triangleleft g \\ | \\ j_2 \end{array} = \sum_j d_j \begin{array}{c} j_1 \quad j_2 \\ | \quad | \\ \bigoplus \\ | \\ \triangleleft g \\ | \\ j_1 \quad j_2 \end{array}, \quad (15)$$

$$\begin{array}{c} j_1 \\ | \\ \triangleleft g \\ | \\ \triangleleft g^{-1} \\ | \\ j_2 \end{array} = \sum_j d_j \begin{array}{c} j_1 \quad j_2 \\ | \quad | \\ \bigoplus \\ | \\ \triangleleft g \\ | \\ j_1 \quad j_2 \end{array}. \quad (16)$$

The manipulation of structures like the ones on the right-

hand side of Eqs. (14)-(16) is facilitated by

$$\begin{array}{c} j_4 \\ \diagup \\ + \\ \diagdown \\ j_2 \\ \uparrow \\ l \\ \downarrow \\ + \\ \diagdown \\ j_1 \\ \diagup \\ j_3 \end{array} = \sum_k d_k (-1)^{j_2+j_3+k+l} \left\{ \begin{array}{ccc} j_1 & j_2 & k \\ j_4 & j_3 & l \end{array} \right\} \begin{array}{c} j_4 \\ \diagup \\ + \\ \diagdown \\ j_3 \\ \uparrow \\ k \\ \downarrow \\ + \\ \diagdown \\ j_1 \\ \diagup \\ j_2 \end{array}, \quad (17)$$

which accounts for the swapping of the legs of spins j_2 and j_3 . The symbol within curly brackets in Eq. (17) is the Wigner 6j symbol, defined through the contraction of four Wigner 3j symbols [note that, for contraction, one needs $\epsilon_{nq}^{(j)}$ to convert upper into lower indices and vice versa]. In graphical form, this contraction is represented as

$$\begin{array}{c} + \\ \diagup \\ j_3 \\ \diagdown \\ k_1 \\ \diagup \\ + \\ \diagdown \\ k_2 \\ \diagup \\ + \\ \diagdown \\ j_1 \\ \diagup \\ + \end{array} = \left\{ \begin{array}{ccc} j_1 & j_2 & j_3 \\ k_1 & k_2 & k_3 \end{array} \right\}. \quad (18)$$

The three arguments in the upper row of the Wigner 6j symbol [right-hand side of Eq. (18)] are the spins of the three legs of any chosen node of the tetrahedron; the remaining arguments are the corresponding spins of opposite links of the tetrahedron (e.g., j_i is opposite to k_i) organized column-wise. The Wigner 6j symbol has a high degree of symmetry: permuting its columns gives the same outcome, as well as swapping the upper and lower arguments in any two chosen columns. On top of that, owing to the presence of four Wigner 3j symbols, the Wigner 6j symbol is nonzero only if the triangle inequalities are simultaneously satisfied in all of the nodes of the tetrahedron, i.e., for the sets $\{j_1, j_2, j_3\}$, $\{j_1, k_2, k_3\}$, $\{k_1, j_2, k_3\}$ and $\{k_1, k_2, j_3\}$. Similarly, contracting six Wigner 3j symbols gives the Wigner 9j symbol,

$$\begin{array}{c} + \\ \diagup \\ j_3 \\ \diagdown \\ l_1 \\ \diagup \\ + \\ \diagdown \\ k_3 \\ \diagup \\ + \\ \diagdown \\ j_2 \\ \diagup \\ + \end{array} = \left\{ \begin{array}{ccc} j_1 & j_2 & j_3 \\ k_1 & k_2 & k_3 \\ l_1 & l_2 & l_3 \end{array} \right\}. \quad (19)$$

$$\sum_j d_j (-1)^{k_1+k_2+j} \left\{ \begin{array}{ccc} l_1 & l_2 & j \\ l_3 & l_4 & k_1 \end{array} \right\} \left\{ \begin{array}{ccc} l_3 & l_4 & j \\ l_2 & l_1 & k_2 \end{array} \right\} = \left\{ \begin{array}{ccc} l_1 & l_4 & k_1 \\ l_2 & l_3 & k_2 \end{array} \right\}, \quad (24)$$

$$\sum_j d_j (-1)^{l_1+l_2+l_3+l_4+l_5+l_6+k_1+k_2+k_3+j} \left\{ \begin{array}{ccc} l_1 & l_2 & j \\ l_3 & l_4 & k_1 \end{array} \right\} \left\{ \begin{array}{ccc} l_3 & l_4 & j \\ l_5 & l_6 & k_2 \end{array} \right\} \left\{ \begin{array}{ccc} l_5 & l_6 & j \\ l_2 & l_1 & k_3 \end{array} \right\} = \left\{ \begin{array}{ccc} k_1 & k_2 & k_3 \\ l_5 & l_1 & l_4 \end{array} \right\} \left\{ \begin{array}{ccc} k_1 & k_2 & k_3 \\ l_6 & l_2 & l_3 \end{array} \right\}. \quad (25)$$

The SU(2) generators, being elements of the su(2) algebra, can also be represented similarly to Wigner matrices. However, the presence of an extra index, say i , means that they require one additional leg with respect

to Eq. (6), with spin 1. These elements are sometimes called grasps and are a key component of the quantum

Under permutations of any two of its rows or columns, the Wigner 9j symbol picks up a phase $(-1)^{j_1+j_2+j_3+k_1+k_2+k_3+l_1+l_2+l_3}$. If two of its columns or rows are identical and the phase factor is negative, the Wigner 9j symbol is therefore zero.

Combining Eq (17) with (3) and (9), one can derive the so-called 2-2 Pachner move (see Appendix A),

$$\begin{array}{c} j_1 \\ \diagdown \\ + \\ \diagup \\ j_3 \end{array} \begin{array}{c} j_4 \\ \diagup \\ + \\ \diagdown \\ j_2 \end{array} = \sum_k d_k (-1)^{j_1-j_2+j_3+j_4} \left\{ \begin{array}{ccc} j_1 & j_4 & k \\ j_2 & j_3 & l \end{array} \right\} \begin{array}{c} j_1 \\ \diagup \\ + \\ \diagdown \\ j_4 \\ \uparrow \\ k \\ \downarrow \\ + \\ \diagdown \\ j_3 \\ \diagup \\ j_2 \end{array}. \quad (20)$$

This transformation represents a change of intertwiner basis, which will be further discussed in the next section. The 2-2 Pachner move is also known as F-move in the field of non-Abelian anyonic quantum error correction and plays an important role in implementing lattice surgeries, Dehn-twists and braid-moves [15, 16].

Considering the large number of sums over spins, as well as of Wigner symbols summed over, it is advantageous to employ a few identities involving such quantities (cf. Ref. [21], Eqs. C.35a-e and C.37):

$$\left\{ \begin{array}{ccc} l_1 & l_2 & 0 \\ l_3 & l_4 & k \end{array} \right\} = \frac{(-1)^{l_1+l_3+k} \delta_{l_1 l_2} \delta_{l_3 l_4}}{\sqrt{d_{l_1} d_{l_3}}}, \quad (21)$$

$$\sum_j d_j (-1)^{2j} \left\{ \begin{array}{ccc} l_1 & l_2 & j \\ l_1 & l_2 & k \end{array} \right\} = 1, \quad (22)$$

$$\sum_j d_j \left\{ \begin{array}{ccc} l_1 & l_2 & j \\ l_3 & l_4 & k_1 \end{array} \right\} \left\{ \begin{array}{ccc} l_3 & l_4 & j \\ l_1 & l_2 & k_2 \end{array} \right\} = \delta_{k_1, k_2} d_{k_1}^{-1}, \quad (23)$$

to Eq. (6), with spin 1. These elements are sometimes called grasps and are a key component of the quantum

volume operator. Their graphical representation is

$$(\tau_i^{(j)})_n^m = i\sqrt{j d_{j/2} d_j} \begin{array}{c} j \quad + \quad j \\ \hline n \quad \rightarrow \quad m \\ | \\ i \end{array} \quad (26)$$

V. INTERTWINERS AND SPINNETWORKS

Intertwiners are equivariant multilinear maps between sets of $SU(2)$ representations. In other words, they are invariant tensors of the $SU(2)$ group. Given an arbitrary number of representations j_i acting on Hilbert spaces \mathcal{H}_{j_i} , the intertwiners are the elements of the space (of spin singlets) $\text{Inv}_{SU(2)}(\otimes_i \mathcal{H}_{j_i})$. The simplest (which we will refer as trivial) intertwiner is $\epsilon_{nq}^{(j)}$, which is the basis element of the 1-dimensional space $\text{Inv}_{SU(2)}(\mathcal{H}_j \otimes \mathcal{H}_j)$ for a given j . The next (nontrivial) intertwiner, corresponding to the Wigner 3j symbol, is the sole basis element of the space $\text{Inv}_{SU(2)}(\mathcal{H}_{j_1} \otimes \mathcal{H}_{j_2} \otimes \mathcal{H}_{j_3})$ for a given choice of j_1, j_2 and j_3 . As can be seen from Eq. (12), which can be recast as the contraction of two nodes with the same three spins but different cyclicities [cf. Eq. (9)], i.e., as an inner product of the basis element of $\text{Inv}(\mathcal{H}_{j_1} \otimes \mathcal{H}_{j_2} \otimes \mathcal{H}_{j_3})$ with itself, the norm of the Wigner 3j symbol is 1. The identity of this space can therefore be resolved simply as two (noncontracted) copies of the Wigner 3j symbols, a ket followed by a bra (in Dirac's notation).

In general, n -valent intertwiners can be built from 2- and 3-valent ones through contraction. The protocol for construction of n -valent intertwiners requires the use of $n - 2$ Wigner 3j symbols, each of which has one or two of its indices contracted with one out of $n - 3$ $\epsilon_{nq}^{(j)}$, which bridge the 3j symbols pairwise. The chain of 3-valent nodes so constructed has therefore one “free” 3-valent-intertwiner leg per inner node and two such legs in the nodes at the ends of the chain. These constructions, however, are in general not unique, as the corresponding space $\text{Inv}_{SU(2)}(\otimes_i \mathcal{H}_{j_i})$ might have several basis elements corresponding to all possible choices of inner-link spins. The identity $\mathbb{1}$ of such spaces can then be resolved as the weighted sum over all inner spins of the (noncontracted) doubled n -valent intertwiners,

$$\mathbb{1} = \sum_{\{i\}} \left(\prod_{l=1}^{n-3} d_{i_l} \right) \begin{array}{c} j_{n-2} \quad j_{n-1} \\ \diagdown \quad \diagup \\ \oplus \quad \oplus \\ \diagup \quad \diagdown \\ j_{n-3} \quad j_{n-2} \\ \vdots \\ j_2 \quad j_1 \\ \diagdown \quad \diagup \\ \oplus \quad \oplus \\ \diagup \quad \diagdown \\ j_3 \quad j_2 \end{array} \quad \begin{array}{c} j_2 \quad j_3 \\ \diagdown \quad \diagup \\ \oplus \quad \oplus \\ \diagup \quad \diagdown \\ i_1 \quad i_2 \\ \vdots \\ i_{n-2} \quad i_{n-3} \\ \diagdown \quad \diagup \\ \oplus \quad \oplus \\ \diagup \quad \diagdown \\ j_{n-1} \quad j_{n-2} \end{array} \quad (27)$$

For simplicity, we will not use Dirac's bra-ket notation explicitly, and instead we will merely present the spin-networks (or intertwiners at their nodes) as quantum

states, with “free” legs pointing in opposite directions for bras and kets, so that inner products tie legs of corresponding spins. The sum in Eq. (27) runs over all (Clebsch-Gordan-)allowed values for the set of $n - 3$ internal spins $\{i\}$. Using Eq. (13), it is possible to show that the squared norm of each of the n -valent intertwiners in Eq. (27) is $(\prod_l d_{i_l})^{-1}$, what explains the weighting factors in the sum. Eq. (27) can greatly simplify calculations, since introducing the intertwiner-space identity graphically accounts for “breaking” any number of links of a spinnetwork and introducing (27) for the corresponding number of external legs, which are contracted with the broken-link ends of the spinnetwork. The concept is similar to lattice surgery [15, 35, 36]. By introducing the resolution of the identity in spinnetwork calculations, one can therefore “surgically remove” portions of the spinnetwork which, once contracted with suitable intertwiners, form closed secondary spinnetworks that can be converted into functions through, e.g., Eqs. (18) and (19). As an example that will be useful for later calculations, we consider the following use of the resolution of the identity:

$$\begin{array}{c} j_2 \\ \diagdown \quad \diagup \\ \oplus \quad \oplus \\ \diagup \quad \diagdown \\ j_3 \quad j_1 \\ \vdots \\ k_2 \quad k_3 \end{array} = + \begin{array}{c} + \\ \diagdown \quad \diagup \\ \oplus \quad \oplus \\ \diagup \quad \diagdown \\ k_1 \quad j_2 \\ \vdots \\ k_2 \quad k_3 \end{array} + \begin{array}{c} j_2 \\ \diagdown \quad \diagup \\ \oplus \quad \oplus \\ \diagup \quad \diagdown \\ k_1 \quad j_1 \\ \vdots \\ k_3 \end{array} \quad (28)$$

In Eq. (28), the three (magenta) dots represent the specific locations chosen for “breaking” the links and contracting with the legs of the 3-valent intertwiners that resolve the identity of the space $\text{Inv}(\mathcal{H}_{j_1} \otimes \mathcal{H}_{j_2} \otimes \mathcal{H}_{j_3})$. Note that this contraction requires the braiding of the links of spins k_1, j_2 and k_3 on the right-hand side of Eq. (28), explaining the flip in cyclicity.

As a special case, which will be of great importance in the study of the action of the LQG Hamiltonian constraint on spinnetworks, we look at the 4-valent intertwiners. They are composed by two Wigner 3j symbols contracted by means of one $\epsilon_{nq}^{(j)}$. The choice of the legs that are paired leads to different bases of $\text{Inv}_{SU(2)}(\mathcal{H}_{j_1} \otimes \mathcal{H}_{j_2} \otimes \mathcal{H}_{j_3} \otimes \mathcal{H}_{j_4})$, which can be mapped into each other by the 2-2 Pachner move [cf. Eq. (20)]. The number of elements in these bases is determined solely by the number of allowed inner spin values connecting the two nodes: if the central link of spin i pairs the external links of spins j_1, j_2, j_3 and j_4 , forming triangularity-fulfilling sets $\{j_1, j_3, i\}$ and $\{j_2, j_4, i\}$, then i runs from $\max\{|j_1 - j_3|, |j_2 - j_4|\}$ to $\min\{|j_1 + j_3|, |j_2 + j_4|\}$. The 4-valent intertwiners have squared norm d_i^{-1} , as can be derived with the aid of Eq. (13) (which removes the “inner bubble”) followed by Eq. (5) (to remove the arrows)

and Eq. (12),

$$+ \begin{array}{c} \text{---} j_1 \text{---} \\ \text{---} i \text{---} \text{---} j_4 \text{---} \\ \text{---} j_2 \text{---} \\ \text{---} j_3 \text{---} \end{array} \text{---} = d_i^{-1} \delta_{i,i'} . \quad (29)$$

Note that the 4-valent intertwiner on the right part of the figure on the left-hand side of the equation (corresponding to Dirac's ket) has both its 3-valent nodes braided, so that the cyclicities are inverted. If the inner spins i and i' do not match, the inner product gives zero. Similarly, if the external spins of any of the contracted legs do not match, the inner product is also zero, but we will omit the corresponding Kronecker deltas whenever possible. In Eq. (29), in order to make its interpretation clearer, we have displayed the connection points between external links of the two 4-valent intertwiners participating in the inner product (represented in red). It is worth noting that, by choosing the intertwiners in a different basis, such as the one obtained after applying a 2-2 Pachner move, the same result can be obtained in a different way. First Eq. (13) is used to get rid of the upper and lower “bubbles” in the graph, then Eq. (5) merges the arrows, and finally the remaining loop, which represents the trace over the identity in the inner-spin representation, gives a factor of d_i . This calculation is represented as

$$+ \begin{array}{c} \text{---} j_1 \text{---} \\ \text{---} i \text{---} \text{---} j_4 \text{---} \\ \text{---} j_2 \text{---} \\ \text{---} j_3 \text{---} \end{array} \text{---} = d_i^{-2} \delta_{i,i'} \begin{array}{c} \text{---} i \text{---} \\ \text{---} \text{---} \\ \text{---} \text{---} \\ \text{---} i' \text{---} \end{array} = d_i^{-1} \delta_{i,i'} . \quad (30)$$

Note that the deformation of the lines in the graphs, e.g., rounded in Eq. (29) and blocky in Eq. (30), is irrelevant. All that matters is the adjacency between graphical elements. For the sake of visual simplicity, we will henceforth omit these (red) contraction points.

It might seem that once we have completed the study of bases of the $\text{Inv}_{\text{SU}(2)}(\otimes_i \mathcal{H}_{j_i})$ spaces, we are ready to proceed with the action of the Euclidean Hamiltonian constraint on general spinnetworks. This perspective, however, fails to acknowledge the importance of a fundamental component of spinnetworks, namely the Wigner matrices at the links. The holonomies in Eq. (1) act on spinnetworks according to Eqs. (15) and (16), so that the spinnetworks at both the domain and image of the map (1) contain $\text{SU}(2)$ group elements assigned to their links. Once the quantum states are described by spinnetworks, the inner product requires taking integrals with Haar measure over all $\text{SU}(2)$ elements at the links of the spinnetwork. These integrals couple two links with the same assigned $\text{SU}(2)$ element, one from the bra and an-

other one from the ket, according to

$$\int dg \begin{array}{c} \text{---} j' \text{---} \\ \text{---} g \text{---} \\ \text{---} g \text{---} \\ \text{---} j \text{---} \end{array} = d_j^{-1} \delta_{j,j'} \begin{array}{c} \text{---} j \text{---} \\ \text{---} \text{---} \\ \text{---} j \text{---} \end{array} . \quad (31)$$

Note that the orientation of the arrows in Eq. (31) is irrelevant: as long as they are parallel, flipping both of them gives a phase $(-1)^{4j} = 1$. We show below that the Kronecker delta in Eq. (31) is critical to ensure orthogonality of states in the image of the map (1).

The operator defined in Eq. (1) acts on 3-valent node-local spinnetworks (i.e., spinnetworks that include the intertwiner and its “neighborhood”, potentially representing a local component of a larger spinnetwork), henceforth denoted NLSNs, of the form

$$\begin{array}{c} \text{---} j_1 \text{---} \\ \text{---} a \text{---} \text{---} b \text{---} \\ \text{---} g \text{---} \\ \text{---} j_2 \text{---} \text{---} j_3 \text{---} \\ \text{---} \epsilon \text{---} \end{array} . \quad (32)$$

Using Eq. (10), it is possible to show that $\text{SU}(2)$ group elements can also be assigned to the links in the representations j_1 , a and b . Similarly, the same can be done in the other two nodes connected with the Wigner matrix of the element g in the representation ϵ , leading to different elements assigned to each of the links in (32). By comparison with Refs. [24–26], it might seem surprising that we are considering a 3-valent NLSN with an additional bridging link between two of its legs, even more when one considers the presence of a Wigner matrix there. As we will show in the next section, however, this is precisely the general form of the spinnetwork nodes generated by the scalar Euclidean Hamiltonian constraint (1). In fact, it is also the general form of the input nodes acted upon by Eq. (1). If one wants to consider a spinnetwork node with no added loops, applying Eq. (11) on both right and left lower nodes of Eq. (32) when $\epsilon = 0$ gives, up to a normalization factor, the “naked” spinnetwork node (i.e, the intertwiner). In order to investigate the effects of the self-adjointness of Eq. (1) (and therefore also the reversibility of its action) on spinnetworks, one must by any means start with a spinnetwork of the form (32) to be able to observe that the Hamiltonian both increases and decreases ϵ , therefore removing the Wigner matrix when $\epsilon \rightarrow 0$. In Ref. [26] the $\text{SU}(2)$ element in the bridging link is set equal to $g = 1$ in the output spinnetwork, yet, this move precludes the use of Eq. (31) when taking the inner product between spinnetworks, which basically destroys the orthogonality between NLSNs of the form (32). In order to enforce orthogonality between 3-valent NLSNs with different values of any of the spins j_1 , j_2 , j_3 ,

a , b or ε , one applies Eq. (31) on the contraction of two spinnetworks of the form (32) according to

$$\begin{aligned}
 & \int dg \begin{array}{c} \text{Diagram 1: A box with top leg } j_1 \text{ and bottom leg } j_2. \text{ Left leg } a, \text{ right leg } \alpha. \text{ Inside, } b \text{ and } j_3 \text{ are connected to } j_1. \text{ A triangle with } g^{-1} \text{ and } \varepsilon \text{ is on the left, and a triangle with } g \text{ and } \gamma \text{ is on the right.} \end{array} = \int dg \begin{array}{c} \text{Diagram 2: Similar to Diagram 1, but the triangles are swapped.} \end{array} \\
 & = \delta_{\varepsilon,\gamma} d_\varepsilon^{-1} \begin{array}{c} \text{Diagram 3: A box with top leg } j_1 \text{ and bottom leg } j_2. \text{ Left leg } a, \text{ right leg } \alpha. \text{ Inside, } b \text{ and } \beta \text{ are connected to } j_1. \text{ A triangle with } \varepsilon \text{ is on the left, and a triangle with } \varepsilon \text{ is on the right.} \end{array} = \delta_{\varepsilon,\gamma} \delta_{a,\alpha} \delta_{b,\beta} d_a^{-1} d_b^{-1} d_\varepsilon^{-1} \\
 & \times \begin{array}{c} \text{Diagram 4: A box with top leg } j_1 \text{ and bottom leg } a. \text{ Inside, } b \text{ is connected to } j_1. \end{array} = \delta_{\varepsilon,\gamma} \delta_{a,\alpha} \delta_{b,\beta} d_a^{-1} d_b^{-1} d_\varepsilon^{-1}. \tag{33}
 \end{aligned}$$

Note that, since the bra spinnetwork is Hermitian conjugated, its Wigner matrix in Eq. (33) (left of the graph) is inverted. In the first row of Eq. (33), we use Eq. (8), then perform the integral over g according to Eq. (31) and finally use Eq. (5) to achieve the form in the second row. After application of Eq. (13), the graph in the second row of Eq. (33) can be converted into the graph in the third row. The bottom-most graph is then converted into a function with the aid of Eqs. (5) and (12). For spinnetworks of the form (32) with different spins at the external legs (say, $\{j_1, j_2, j_3\}$ on the bra and $\{j'_1, j'_2, j'_3\}$ on the ket), the inner product then gives $\delta_{\varepsilon,\gamma} \delta_{a,\alpha} \delta_{b,\beta} \delta_{j_1, j'_1} \delta_{j_2, j'_2} \delta_{j_3, j'_3} d_a^{-1} d_b^{-1} d_\varepsilon^{-1}$.

Similarly, the 4-valent NLSNs acted upon and generated by Eq. (1) have the form

$$\begin{array}{c} \text{Diagram 5: A 4-valent vertex with legs } j_1, j_2, j_3, j_4. \text{ Top-left leg } j_1, \text{ top-right leg } j_4, \text{ bottom-left leg } j_3, \text{ bottom-right leg } j_2. \text{ Inside, } a \text{ and } b \text{ are connected to the vertex. A triangle with } g \text{ and } \varepsilon \text{ is on the left.} \end{array} \tag{34}$$

Orthogonality between spinnetworks of the form (34) can

be shown through

$$\begin{aligned}
 & \int dg \begin{array}{c} \text{Diagram 6: Similar to Diagram 1, but with an additional leg } i' \text{ on the right.} \end{array} = \int dg \begin{array}{c} \text{Diagram 7: Similar to Diagram 6, but the triangles are swapped.} \end{array} \\
 & = \delta_{\varepsilon,\gamma} d_\varepsilon^{-1} \begin{array}{c} \text{Diagram 8: Similar to Diagram 3, but with an additional leg } i' \text{ on the right.} \end{array} = \delta_{\varepsilon,\gamma} \delta_{a,\alpha} \delta_{b,\beta} d_a^{-1} d_b^{-1} d_\varepsilon^{-1} \\
 & \times \begin{array}{c} \text{Diagram 9: Similar to Diagram 4, but with an additional leg } i' \text{ on the right.} \end{array} = \delta_{\varepsilon,\gamma} \delta_{a,\alpha} \delta_{b,\beta} \delta_{i, i'} d_a^{-1} d_b^{-1} d_\varepsilon^{-1} d_{i'}^{-1}. \tag{35}
 \end{aligned}$$

The derivation of Eq. (35) follows the same steps as in Eq. (33), with one additional step in the last row, where Eqs. (13) and (5) have to be used before Eq. (12). For spinnetworks of the form (34) with different spins at the external legs (say $\{j_1, j_2, j_3, j_4\}$ on the bra and $\{j'_1, j'_2, j'_3, j'_4\}$ on the ket), the inner product then gives $\delta_{\varepsilon,\gamma} \delta_{a,\alpha} \delta_{b,\beta} \delta_{i, i'} \delta_{j_1, j'_1} \delta_{j_2, j'_2} \delta_{j_3, j'_3} \delta_{j_4, j'_4} d_a^{-1} d_b^{-1} d_\varepsilon^{-1} d_{i'}^{-1}$. It is easy to show that changing the basis of 4-valent intertwiners in both bra and ket does not affect the inner product.

When applying Eq. (1) several times on spinnetworks, patterns with deeper and deeper inner loops connecting pairs of legs emerge. Equation (11) shows that, by considering the inner product between two such spinnetworks with different inner-loop structures, their graphs can be made the same through inclusion of links in the trivial representation [e.g., $\varepsilon = 0$ in Eq. (34)]. The group elements assigned (pairwise) to the corresponding links on each of the spinnetworks participating in the inner product are the same, and through Eq. (31) it is possible to see that, when the representations do not coincide, as is the case when any inner loop is missing in one of the spinnetworks, the inner product is zero [owing to the Kronecker delta in Eq. (31)]. We emphasize that such orthogonality is a direct result of the integration (31), and neglecting the presence of a Wigner matrix on any of the inner loops makes sets of non-equivalent spinnetworks non-orthogonal. One is therefore left only with the task of calculating the norm of such complicated spinnet-

works. This can be performed by induction. Let us assume that we know the squared norm N_{n-1} of a spinnetwork s_{n-1} with $n-1$ inner loops. Adding one extra inner loop as close as possible to the intertwiner (i.e., deeper than any of the $n-1$ loops), gives us the spinnetwork s_n . On the other hand, N_{n-1} can be cast as $N_{n-1}^{>1} d_i^{-1}$, where $N_{n-1}^{>1}$ is the coefficient obtained from all inner loops and d_i^{-1} is the norm of the intertwiner, which remains after the contributions of all inner loops are factored out of the graph. If we now consider s_n , its squared norm will be $N_{n-1}^{>1} N_1$, where N_1 is the squared norm of the spinnetwork (34), s_1 , which remains after converting the $n-1$ outermost loops into coefficients. If the innermost loop in s_1 contains links of spins i , a_n , b_n and ε_n , then, from Eq. (35), we see that $N_1/d_i^{-1} = d_{a_n}^{-1} d_{b_n}^{-1} d_{\varepsilon_n}^{-1}$, which means that adding a new loop as close as possible to the intertwiner will lead to a multiplicative factor of N_1/d_i^{-1} in the squared norm. By induction we then see that, if the “naked” intertwiner has squared norm d_i^{-1} , adding loops with external links with spins a_k , b_k and ε_k gives the total squared norm $d_i^{-1} \prod_k d_{a_k}^{-1} d_{b_k}^{-1} d_{\varepsilon_k}^{-1}$, to which the only spins that do not contribute are those of the outermost links of the NLSN.

It will be useful to work with normalized spinnetworks for some calculations, such as the derivation of the quantum volume operator, which requires diagonalization. Normalization of spinnetworks can be achieved by multiplying them with the inverse of their norm, rendering orthonormal the set of spinnetworks of the form (32) or (34).

VI. ACTION OF THE SCALAR CONSTRAINT ON 3-VALENT SPINNETWORKS

We start with a spinnetwork of the form (32). Following Refs. [24, 25], both the links (i.e., the Wigner matrices) and the paths of the holonomies in Eq. (1) will be oriented towards the node, so that inverse holonomies are associated with segments oriented away from the node. The orientation is important, since the consecutive application of the holonomies in Eq. (1) should follow a chain of contractions closed by the trace.

We proceed with the application of the first holonomy of the first term on the right-hand side of Eq. (1) to the fiducial spinnetwork. At first, we will consider the action of $\hat{h}^{-1}[p_k]$ only along the path p_1 parallel to the link of

spin j_1 , i.e.,

$$\hat{h}^{-1}[p_1] \begin{array}{c} j_1 \\ | \\ \oplus \\ / \quad \backslash \\ a \quad b \\ \oplus \quad \oplus \\ | \quad | \\ g \quad \varepsilon \\ \oplus \quad \oplus \\ j_2 \quad j_3 \end{array} = \begin{array}{c} j_1 \\ | \\ \oplus \\ / \quad \backslash \\ a \quad b \\ \oplus \quad \oplus \\ | \quad | \\ g \quad \varepsilon \\ \oplus \quad \oplus \\ j_2 \quad j_3 \end{array} \begin{array}{c} \frac{1}{2} \\ | \\ \triangle \\ | \\ \oplus \end{array} \quad (36)$$

$$= \sum_m d_m \begin{array}{c} j_1 \\ | \\ \oplus \\ | \\ m \\ | \\ \oplus \\ | \\ \frac{1}{2} \\ | \\ \oplus \\ / \quad \backslash \\ a \quad b \\ \oplus \quad \oplus \\ | \quad | \\ g \quad \varepsilon \\ \oplus \quad \oplus \\ j_2 \quad j_3 \end{array}$$

As previously explained, the Wigner matrices of inverse SU(2) elements corresponding to inverse holonomies are directed outward from the node. The holonomies are in the fundamental representation, i.e., spin 1/2, as shown in Eq. (36). We extend the lower end of the spin-1/2 Wigner matrix on the right-hand side of Eq. (36) by contracting it with the 1/2-representation identity, Eq. (2), so that the latter can be coupled to the spinnetwork link of spin j_1 with the aid of Eq. (14). The spin resulting from the coupling assumes all values m allowed by the Clebsch-Gordan conditions, namely $m = j_1 \pm 1/2$. Note that the lower “free” link of spin 1/2 in Eq. (36) is technically one of the legs of the node, the intertwiner of which temporarily becomes 4-valent, having an inner link with spin j_1 . The action of the holonomies $\hat{h}^{-1}[p_2]$ and $\hat{h}^{-1}[p_3]$ along the links of spins j_2 and j_3 , which we will not explicitly show, follow analogous relations with permuted labels.

Spinnetworks like the one in the lower row of Eq. (36) are eigenstates of the volume operator. The latter acts on the (physical) nodes of the graph, giving zero contribution from nodes with valency below 4, while the central node contributes with a volume defined by the spins of the links attached to it. We will provide a detailed derivation of the action of the volume operator on such spinnetworks in Sec. VIII, but for now we merely represent the eigenvalues of the operator as $V_{m,j_1,a,b}^{(3,5)}$, where the superscript denotes that the intertwiner has valency 4, but one of its links (the holonomy one) is merely temporary. The next operator on the right-hand side of Eq. (1) is the holonomy $\hat{h}[p_k]$. For the specific case of the path p_1 along the j_1 -representation link, $\hat{h}[p_1]$ is graphically represented by a Wigner matrix directed toward the node, with its lower index contracted with the upper index of $\hat{h}^{-1}[p_1]$. It is worth noting that, since $\hat{h}[p_1]\hat{h}^{-1}[p_1] = 1$, the contraction of these holonomies, graphically shown

as a contraction between two Wigner matrices, one for g

and one for g^{-1} , leads to temporary spin-1/2 links corresponding only to identities (straight lines):

$$\begin{aligned}
 & \hat{h}[p_1] \sum_m d_m V_{m,j_1,a,b}^{(3.5)} \\
 & \begin{array}{c} j_1 \\ | \\ - \\ m \\ + \\ j_1 \\ \begin{array}{c} a \quad b \\ \nearrow \quad \searrow \\ + \quad + \\ \triangleleft \quad \triangleright \\ \epsilon \end{array} \end{array} \begin{array}{c} \triangle \\ \uparrow \\ g^{-1} \\ \downarrow \\ \frac{1}{2} \end{array} \\
 & = \sum_m d_m V_{m,j_1,a,b}^{(3.5)} \begin{array}{c} j_1 \\ | \\ - \\ m \\ + \\ j_1 \\ \begin{array}{c} a \quad b \\ \nearrow \quad \searrow \\ + \quad + \\ \triangleleft \quad \triangleright \\ \epsilon \end{array} \end{array} \begin{array}{c} \triangle \\ \uparrow \\ g^{-1} \\ \downarrow \\ \frac{1}{2} \\ \triangle \\ \uparrow \\ g \\ \downarrow \\ \frac{1}{2} \end{array} \\
 & = \sum_m d_m V_{m,j_1,a,b}^{(3.5)} \begin{array}{c} j_1 \\ | \\ - \\ m \\ + \\ j_1 \\ \begin{array}{c} a \quad b \\ \nearrow \quad \searrow \\ + \quad + \\ \triangleleft \quad \triangleright \\ \epsilon \end{array} \end{array} \begin{array}{c} \triangle \\ \uparrow \\ g^{-1} \\ \downarrow \\ \frac{1}{2} \\ \triangle \\ \uparrow \\ g \\ \downarrow \\ \frac{1}{2} \end{array} \\
 & = \sum_m d_m V_{m,j_1,a,b}^{(3.5)} \begin{array}{c} j_1 \\ | \\ - \\ m \\ + \\ j_1 \\ \begin{array}{c} a \quad b \\ \nearrow \quad \searrow \\ + \quad + \\ \triangleleft \quad \triangleright \\ \epsilon \end{array} \end{array} \begin{array}{c} \triangle \\ \uparrow \\ g^{-1} \\ \downarrow \\ \frac{1}{2} \end{array}
 \end{aligned} \tag{37}$$

Note that the deformation of the links on the last two rows of Eq. (37) is irrelevant, i.e., only the arrangement of the ends of the links matters, as we will show below.

The holonomies over the triangular loop, $\hat{h}[\alpha_{ij}] - \hat{h}[\alpha_{ji}]$, should be applied on the final NLSN obtained in Eq. (37) in such a way that the sequence of contractions in Eq. (1) is properly ordered and closed. Since α_{ij} and α_{ji} have opposite orientations, they will be attached to the loose ends of the two spin-1/2 temporary links (which are physically at the same point of the manifold) in different ways. The presence of a trace in Eq. (1) enforces that all virtual links should be tied together, such that no loose virtual links remain. As a result, for $\hat{h}[\alpha_{23}]$ we get

$$\begin{aligned}
 & \hat{h}[\alpha_{23}] \sum_m d_m V_{m,j_1,a,b}^{(3.5)} \\
 & \begin{array}{c} j_1 \\ | \\ - \\ m \\ + \\ j_1 \\ \begin{array}{c} a \quad b \\ \nearrow \quad \searrow \\ + \quad + \\ \triangleleft \quad \triangleright \\ \epsilon \end{array} \end{array} \begin{array}{c} \triangle \\ \uparrow \\ g^{-1} \\ \downarrow \\ \frac{1}{2} \end{array} \\
 & = \sum_m d_m V_{m,j_1,a,b}^{(3.5)} \begin{array}{c} j_1 \\ | \\ - \\ m \\ + \\ j_1 \\ \begin{array}{c} a \quad b \\ \nearrow \quad \searrow \\ + \quad + \\ \triangleleft \quad \triangleright \\ \epsilon \end{array} \end{array} \begin{array}{c} \triangle \\ \uparrow \\ g^{-1} \\ \downarrow \\ \frac{1}{2} \\ \triangle \\ \uparrow \\ g \\ \downarrow \\ \frac{1}{2} \end{array} \\
 & = \sum_{m,\alpha,\beta,\gamma} d_m d_\alpha d_\beta d_\gamma V_{m,j_1,a,b}^{(3.5)} \\
 & \begin{array}{c} j_1 \\ | \\ - \\ m \\ + \\ j_1 \\ \begin{array}{c} a \quad b \\ \nearrow \quad \searrow \\ + \quad + \\ \triangleleft \quad \triangleright \\ \epsilon \end{array} \end{array} \begin{array}{c} \triangle \\ \uparrow \\ g^{-1} \\ \downarrow \\ \frac{1}{2} \\ \triangle \\ \uparrow \\ g \\ \downarrow \\ \frac{1}{2} \\ \triangle \\ \uparrow \\ g \\ \downarrow \\ \frac{1}{2} \end{array}
 \end{aligned} \tag{38}$$

While transitioning from the left-hand to the right-hand side in the upper row of the above equation, Eq. (10) has been used on the node joining the links of spins $\{j_3, b, \varepsilon\}$. In the (upper) right-hand side of Eq. (38), the holonomy along the loop α_{ij} has been graphically represented as a Wigner matrix in the fundamental representation with ends that have been extended by identities, one of which, on the right side, is converted into two $\varepsilon^{(1/2)}$ symbols with the aid of Eq. (5). The trace in Eq. (1), which we do not write explicitly in Eq. (38), enforces the contraction of each of the free indices of this Wigner matrix (or of its identity-extended version) to the temporary links introduced by the holonomies along the link p_1 (“vertical” direction in the graphs), leading to the formation of “square” loops in the bottom row of Eq. (38) after a braiding operation on the uppermost node according to Eq. (9) (notice that the kinks have no physical meaning and serve merely for graphical convenience). Additionally, in the node containing spins $\{a, \alpha, 1/2\}$, Eq. (10) has been used to introduce three solid arrows. The effect of coupling the identity extensions of the Wigner matrix of g to the links of spins a and b can be accounted for by applying Eq. (14) to each of these links. In particular, for the right fundamental-representation identity, the coupling to the spin- b link involves only the segment between the two $\varepsilon^{(1/2)}$ symbols, which then become integrated into loops. Similarly, the $\varepsilon^{(a)}$ symbol is moved down in order for the identities in the a and $1/2$ representations to be coupled. The Wigner matrix of the holonomy is coupled through Eq. (15) to the Wigner matrix of g in the spinnetwork. Each of the sums resulting from couplings between the spinnetwork and the holonomy runs over the original spinnetwork-link spin plus or minus $1/2$. These three couplings leave triangular loops at the links with spins j_2 and j_3 , which, alongside with the small “square” loop, can be factored out of the spinnetwork with the help of the resolution of the identity [cf. Eq. (28)]:

$$\begin{aligned}
& \text{Diagram 1} = \text{Diagram 2} - \text{Diagram 3} - \text{Diagram 4} \\
& = (-1)^{-\frac{1}{2}+a+2b+2j_1+j_2+j_3+m+\varepsilon+\gamma+\alpha+2\beta} \left\{ \begin{matrix} a & j_2 & \varepsilon \\ \gamma & \frac{1}{2} & \alpha \end{matrix} \right\} \left\{ \begin{matrix} \frac{1}{2} & \gamma & \varepsilon \\ j_3 & b & \beta \end{matrix} \right\} \left\{ \begin{matrix} \frac{1}{2} & m & j_1 \\ a & b & \beta \end{matrix} \right\} \cdot \text{Diagram 5} \\
& = (-1)^{\frac{1}{2}-a+2b-j_1+j_2+j_3+m+\varepsilon+\gamma+2\alpha-\beta} \left\{ \begin{matrix} a & j_2 & \varepsilon \\ \gamma & \frac{1}{2} & \alpha \end{matrix} \right\} \left\{ \begin{matrix} \frac{1}{2} & \gamma & \varepsilon \\ j_3 & b & \beta \end{matrix} \right\} \left\{ \begin{matrix} \frac{1}{2} & m & q \\ a & b & \beta \end{matrix} \right\} \left\{ \begin{matrix} \frac{1}{2} & \alpha & a \\ \beta & m & j_1 \end{matrix} \right\} \cdot \text{Diagram 6}
\end{aligned} \tag{39}$$

Note that the tetrahedra in the first row of Eq. (39) contain a different number and arrangement of ε symbols when compared to Eqs. (18) and (28). Yet, through Eqs. (10) and (5), it is possible to see that these are equivalent up to phase terms [cf. Eq. (A3)]. The latter can originate either from changes in the cyclicity of nodes [cf. Eq. (9)] or changes in the direction of the solid arrows [see text preceding Eq. (3)]. After the three loops are removed in the first row of Eq. (39), a fourth loop can be removed, as shown in the second row of the same equation. The four tetrahedral structures factored out of the spinnetwork with Eq. (28) can be converted into Wigner $6j$ symbols according to Eq. (18), and for some of the tetrahedra braiding at the nodes or flips in the direction of solid arrows are required, leading to the phase factor in the third row of Eq. (39).

We now proceed with the application of $\hat{h}[\alpha_{32}]$ on the outcome of Eq. (37):

$$\begin{aligned}
& \hat{h}[\alpha_{32}] \sum_m d_m V_{m,j_1,a,b}^{(3.5)} = \sum_m d_m V_{m,j_1,a,b}^{(3.5)} \\
& = \sum_{m,\alpha,\beta,\gamma} d_m d_\alpha d_\beta d_\gamma V_{m,j_1,a,b}^{(3.5)}
\end{aligned}
\tag{40}$$

Similar to the procedure in Eq. (38), Eq. (10) has been used in the node joining the links of spins $\{j_3, b, \varepsilon\}$ between the right- and left-hand sides in the upper row of the above equation. Furthermore, the holonomy along the loop α_{32} has been graphically represented as the inverse Wigner matrix to the one representing $\hat{h}[\alpha_{23}]$, with ends also extended by identities. The contraction of each of the free indices of this Wigner matrix to the temporary links introduced by the holonomies along the link p_1 therefore happens in opposite order, leading to the formation of new “square” loops in the bottom row of Eq. (40) after a braiding operation on the $\{m, j_1, 1/2\}$

node [cf. Eq. (9)]. The effect of coupling the identity extensions of the Wigner matrix of g to the links of spins a and b is described by Eq. (14). The $\varepsilon^{(a)}$ symbol has been moved up in order for the identities in the a and $1/2$ representations to be coupled. The Wigner matrix itself is coupled through Eq. (16) to the Wigner matrix of the NLSN, and the intertwiners contracted to the resulting Wigner matrix are braided to properly contract with the free legs from adjacent coupled links. After introducing pairs of arrows through Eq. (5) at the links of spins j_2, β and m , the resulting triangular loops at the links with spins j_2 and j_3 , alongside with the small “square” loop, can be factored out of the spinnetwork with the help of the resolution of the identity [cf. Eq. (28)]:

$$\begin{aligned}
&= (-1)^{-b+j_1+j_2+j_3-\varepsilon-\gamma+2\alpha+\beta} \left\{ \begin{matrix} \frac{1}{2} & \alpha & a \\ j_2 & \varepsilon & \gamma \end{matrix} \right\} \left\{ \begin{matrix} \varepsilon & j_3 & b \\ \beta & \frac{1}{2} & \gamma \end{matrix} \right\} \left\{ \begin{matrix} a & b & j_1 \\ m & \frac{1}{2} & \alpha \end{matrix} \right\} \\
&= (-1)^{-\frac{1}{2}+b+j_1+j_2+j_3+m-\varepsilon-\gamma-\alpha+2\beta} \left\{ \begin{matrix} \frac{1}{2} & \alpha & a \\ j_2 & \varepsilon & \gamma \end{matrix} \right\} \left\{ \begin{matrix} \varepsilon & j_3 & b \\ \beta & \frac{1}{2} & \gamma \end{matrix} \right\} \left\{ \begin{matrix} a & b & j_1 \\ m & \frac{1}{2} & \alpha \end{matrix} \right\} \left\{ \begin{matrix} m & \alpha & b \\ \beta & \frac{1}{2} & j_1 \end{matrix} \right\}
\end{aligned}
\tag{41}$$

Between the second and third rows of Eq. (41) we have used Eq. (10) to introduce ε tensors in the node connecting the spins $\{j_2, \alpha, \gamma\}$, leading to a double arrow on the spin- γ link or, through Eq. (5), a $(-1)^{2\gamma}$ phase factor instead. As in Eq. (39), the conversion between the tetrahedra in the first row of Eq. (41) and the one in Eq. (18) requires braiding operations and flips in the directions of the solid arrows, resulting in the appearance of phases.

The contributions from terms inversely ordered in the anticommutator in Eq. (1) require the application of holonomies in a different order. First, the holonomies along the loops α_{ij} or α_{ji} are applied, leaving virtual spin-1/2 links connected to two different spinnetwork links. And then the holonomies along the path p_k , interleaved by the volume operator, are applied in such a way that all virtual links form closed loops to be factored out. The application of $\hat{h}[\alpha_{23}]$ on the spinnetwork (32) gives

$$\hat{h}[\alpha_{23}]$$

$$=$$

$$= \sum_{\alpha, \beta, \gamma} d_\alpha d_\beta d_\gamma$$

In Eq. (42), just as in Eq. (38), a pair of solid arrows has been created on one of the identity extensions of the Wigner matrix to be coupled to the spinnetwork. The coupling between the spin-1/2 identity segment between the two arrows and the spin- b link of the spinnetwork leads to the splitting of the ϵ tensors as seen in the bottom row of Eq. (42). We then proceed with the application of the inverse holonomy $\hat{h}^{-1}[p_1]$,

$$\hat{h}^{-1}[p_1] \sum_{\alpha, \beta, \gamma} d_\alpha d_\beta d_\gamma$$

$$= \sum_{\alpha, \beta, \gamma} d_\alpha d_\beta d_\gamma$$

$$= \sum_{m, \alpha, \beta, \gamma} d_m d_\alpha d_\beta d_\gamma$$

Note that, to pass from the second to the third row of Eq. (43), a braiding [cf. Eq. (9)] has been performed in the uppermost node of the spinnetwork after applying Eq. (14). Before applying the volume operator in the last row of Eq. (43), we can factor out the loops introduced on the spinnetwork by the coupling to the holonomies:

The diagram shows a sequence of transformations. On the left is a complex spinnetwork with multiple vertices and links labeled with $j_1, j_2, j_3, m, a, b, \alpha, \beta, \gamma, \epsilon, g^{-1}$. This is equal to the sum of three intermediate spinnetworks, each with a different internal structure. Finally, it is equal to a single spinnetwork where the top part is simplified, with a link labeled k connecting the top vertex to the middle vertex.

$$= (-1)^{-\frac{1}{2}+a+2b+2j_1+j_2+j_3+m+\epsilon+\gamma+\alpha+2\beta} \left\{ \begin{matrix} a & j_2 & \epsilon \\ \gamma & \frac{1}{2} & \alpha \end{matrix} \right\} \left\{ \begin{matrix} \frac{1}{2} & \gamma & \epsilon \\ j_3 & b & \beta \end{matrix} \right\} \left\{ \begin{matrix} \frac{1}{2} & m & j_1 \\ a & b & \beta \end{matrix} \right\}$$

$$\times \sum_k d_k (-1)^{\frac{1}{2}-\beta+\alpha+j_1} \left\{ \begin{matrix} \frac{1}{2} & m & k \\ \beta & \alpha & a \end{matrix} \right\}$$

The diagram shows a simplified spinnetwork with vertices and links labeled $j_1, j_2, j_3, m, k, \alpha, \beta, \gamma, g$. It is labeled (44).

In the second row of Eq. (44) we have used the 2-2 Pachner move (20) to convert the spinnetwork into a form on which the action of the volume operator is well known. Since this spinnetwork is one of the eigenstates of the volume operator, one merely gets a coefficient from \hat{V} . The action of the holonomy $\hat{h}[p_1]$ on this spinnetwork then simply ties the temporary spin-1/2 links together,

The diagram shows the action of the holonomy operator $\hat{h}[p_1]$ on the spinnetwork. It is equal to a coefficient $(-1)^{\frac{1}{2}+m+j_1} V_{m,k,\alpha,\beta}^{(3,5)}$ times a spinnetwork with a link labeled k connecting the top vertex to the middle vertex. This is further equal to $(-1)^{\frac{1}{2}+m+j_1} V_{m,j_1,\alpha,\beta}^{(3,5)} d_{j_1}^{-1} \delta_{k,j_1}$ times a spinnetwork where the link k is now labeled j_1 . The equation is labeled (45).

In the first equality of this equation, we have made use of Eq. (10) in the central intertwiner of the spinnetwork

to recover the desired arrangement of ϵ tensors. In the resulting term, the two contracted Wigner matrices leave

an identity behind, forming a loop that can be removed with Eq. (13). For this loop to be factored out, however, a braiding according to Eq. (9) has to be implemented in one of the nodes forming the loop, leading to the phase factor $(-1)^{\frac{1}{2}+m+j_1}$.

Finally, we look at the action of the holonomy $\hat{h}[\alpha_{32}]$ on the spinnetwork (32),

$$\begin{aligned}
 & \hat{h}[\alpha_{32}] \\
 & \begin{array}{c} j_1 \\ | \\ \triangle \\ / \quad \backslash \\ a \quad b \\ | \quad | \\ + \quad + \\ \backslash \quad / \\ j_2 \quad j_3 \\ \epsilon \end{array} \\
 & = \\
 & \begin{array}{c} j_1 \\ | \\ \triangle \\ / \quad \backslash \\ a \quad b \\ | \quad | \\ + \quad + \\ \backslash \quad / \\ j_2 \quad j_3 \\ \epsilon \end{array} \\
 & = \sum_{\alpha, \beta, \gamma} d_\alpha d_\beta d_\gamma \\
 & \begin{array}{c} j_1 \\ | \\ \triangle \\ / \quad \backslash \\ a \quad b \\ | \quad | \\ + \quad + \\ \backslash \quad / \\ j_2 \quad j_3 \\ \epsilon \end{array}
 \end{aligned} \tag{46}$$

As in the case of Eq. (39), the couplings between links in Eq. (46) are dictated by Eqs. (14) and (16). We then

proceed with the application of $\hat{h}^{-1}[p_1]$,

$$\begin{aligned}
 & \hat{h}^{-1}[p_1] \sum_{\alpha, \beta, \gamma} d_\alpha d_\beta d_\gamma \\
 & \begin{array}{c} j_1 \\ | \\ \triangle \\ / \quad \backslash \\ a \quad b \\ | \quad | \\ + \quad + \\ \backslash \quad / \\ j_2 \quad j_3 \\ \epsilon \end{array} \\
 & = \sum_{\alpha, \beta, \gamma} d_\alpha d_\beta d_\gamma \\
 & \begin{array}{c} \triangle \\ / \quad \backslash \\ a \quad b \\ | \quad | \\ + \quad + \\ \backslash \quad / \\ j_2 \quad j_3 \\ \epsilon \end{array} \\
 & = \sum_{m, \alpha, \beta, \gamma} d_m d_\alpha d_\beta d_\gamma \\
 & \begin{array}{c} \triangle \\ / \quad \backslash \\ a \quad b \\ | \quad | \\ + \quad + \\ \backslash \quad / \\ j_2 \quad j_3 \\ \epsilon \end{array}
 \end{aligned} \tag{47}$$

The loops in the spinnetwork in the third row of Eq. (47) can then be factored out with the aid of the resolution of the identity [cf. Eq. (27)]. We thus obtain

The diagrammatic equation (48) shows the simplification of a complex spin network. On the left, a large triangle with vertices \$j_1, j_2, j_3\$ and internal lines \$a, b, m, \alpha, \beta, \gamma, \epsilon\$ is shown. It is equal to the product of three smaller triangles: a triangle with spins \$\{a, j_2, \alpha\}\$, a triangle with spins \$\{b, j_3, \beta\}\$, and a triangle with spins \$\{j_1, m, \alpha\}\$. This product is then multiplied by a phase factor \$(-1)^{\frac{1}{2}-b+2j_1+j_2+j_3+m-\epsilon-\gamma+2\alpha+\beta}\$ and a sum over \$k\$ of \$d_k(-1)^{m-\beta+\alpha+\frac{1}{2}}\$ times a triangle with spins \$\{m, \frac{1}{2}, k\}\$. The final result is a single triangle with vertices \$j_1, j_2, j_3\$ and internal lines \$m, \alpha, \beta, \gamma, g^{-1}\$, with a phase factor \$(-1)^{\frac{1}{2}-b+2j_1+j_2+j_3+m-\epsilon-\gamma+2\alpha+\beta}\$.

$$\begin{aligned}
&= (-1)^{\frac{1}{2}-b+2j_1+j_2+j_3+m-\epsilon-\gamma+2\alpha+\beta} \left\{ \begin{matrix} \frac{1}{2} & \alpha & a \\ j_2 & \epsilon & \gamma \end{matrix} \right\} \left\{ \begin{matrix} \epsilon & j_3 & b \\ \beta & \frac{1}{2} & \gamma \end{matrix} \right\} \left\{ \begin{matrix} a & b & j_1 \\ m & \frac{1}{2} & \alpha \end{matrix} \right\} \\
&\quad \times \sum_k d_k (-1)^{m-\beta+\alpha+\frac{1}{2}} \left\{ \begin{matrix} m & \frac{1}{2} & k \\ \beta & \alpha & b \end{matrix} \right\}
\end{aligned}$$

(48)

Note that on the right-hand side of the upper row of Eq. (48) we have used the invariance of intertwiners, Eq. (10), on the node of spins $\{\alpha, b, m\}$. The same property has also been used later on the node of spins $\{\alpha, j_2, \gamma\}$, and the resulting double $\epsilon^{(\gamma)}$ has directly been converted into a phase factor $(-1)^{2\gamma}$ at the last row of

Eq. (48).

The last step in this calculation is precisely the application of $\hat{h}[p_1]\hat{V}$, as explained in Eq. (45).

To summarize Eqs. (36)-(48), the action of Eq. (1) on a spinnetwork of the form (32) for a fixed choice of directions for the holonomies reads

$$\begin{aligned}
& \frac{i}{2} \text{tr} \left\{ \hat{h}[\alpha_{23}] - \hat{h}[\alpha_{32}], \hat{h}[p_1] \hat{V} \hat{h}^{-1}[p_1] \right\} \\
& \quad \begin{array}{c} j_1 \\ | \\ \triangle \\ / \quad \backslash \\ a \quad b \\ \triangle \\ + \quad - \\ \backslash \quad / \\ j_2 \quad j_3 \\ \epsilon \end{array} = \frac{i}{2} \sum_{\alpha, \beta, \gamma, m, q} d_\alpha d_\beta d_\gamma d_m \left\{ \begin{array}{c} a \quad j_2 \quad \epsilon \\ \gamma \quad \frac{1}{2} \quad \alpha \end{array} \right\} \\
& \times \left\{ \begin{array}{c} \frac{1}{2} \quad \gamma \quad \epsilon \\ j_3 \quad b \quad \beta \end{array} \right\} \left[(-1)^{1/2-a+2b+\epsilon+\gamma+j_1+j_2+j_3+m+2\alpha-\beta} (V_{m,j_1,a,b}^{(3.5)} + V_{m,j_1,\alpha,\beta}^{(3.5)}) \left\{ \begin{array}{c} \frac{1}{2} \quad m \quad j_1 \\ a \quad b \quad \beta \end{array} \right\} \left\{ \begin{array}{c} \frac{1}{2} \quad \alpha \quad a \\ \beta \quad m \quad j_1 \end{array} \right\} \right. \\
& \quad \left. - (-1)^{-1/2-b-\epsilon-\gamma-j_1+j_2+j_3-m-\alpha} (V_{m,j_1,\alpha,\beta}^{(3.5)} + V_{m,j_1,a,b}^{(3.5)}) \left\{ \begin{array}{c} a \quad b \quad j_1 \\ m \quad \frac{1}{2} \quad \alpha \end{array} \right\} \left\{ \begin{array}{c} m \quad \frac{1}{2} \quad j_1 \\ \beta \quad \alpha \quad b \end{array} \right\} \right] \\
& \quad \begin{array}{c} j_1 \\ | \\ \triangle \\ / \quad \backslash \\ \alpha \quad \beta \\ \triangle \\ + \quad - \\ \backslash \quad / \\ j_2 \quad j_3 \\ \gamma \end{array} .
\end{aligned} \tag{49}$$

In this equation, we have used $(-1)^{2a+2m+2\beta} = 1$ in the first term within square brackets [namely in the prefactor of $V_{m,j_1,\alpha,\beta}^{(3.5)}$] and $(-1)^{2b+2m+2\beta+2j_1} = (-1)^{4\alpha} = 1$ in the second one [in the prefactor of $V_{m,j_1,a,b}^{(3.5)}$]. Note that taking $a \leftrightarrow \alpha$, $b \leftrightarrow \beta$ and $\epsilon \leftrightarrow \gamma$ in Eq. (49), what swaps input and output states, only affects the coefficient on the right-hand side of the equation by interchanging the two terms within square brackets, which effectively corresponds to a -1 prefactor [to help in the conversion of prefactors, note that $(-1)^{2b+2j_1+2\alpha} = (-1)^{2a+2\alpha} = -1$, $(-1)^{\epsilon+\gamma} = (-1)^{1-\epsilon-\gamma}$ and $(-1)^{m+j_1} = (-1)^{m+j_1+2(1/2+m+j_1)} = (-1)^{1-j_1-m}$]. The negative prefactor is in consonance with the definition of self-adjointness, i.e., for any two spinnetworks $|s\rangle$ and $|s'\rangle$, $\langle s' | \hat{C}_s | s \rangle = \langle s | \hat{C}_s | s' \rangle^*$ [note that Eq. (49) contains an imaginary prefactor i as well]. The complete action of \hat{C}_s on the spinnetwork requires considering all possible rotations of p_k and α_{jk} , with the caveat that new loops α_{jk} should be applied deeper (i.e., closer to the intertwiner) if other loops $\alpha'_{j'k'}$ with $j' \neq j$ or $k' \neq k$ are already present in the input spinnetwork.

VII. ACTION OF THE SCALAR CONSTRAINT ON 4-VALENT SPINNETWORKS

We now investigate the action of the scalar constraint (1) on spinnetworks of the form (34). As in the previous section, we start with the action of the first

holonomy of the first term on the right-hand side of Eq. (1) on a NLSN. It is important to notice that, for each possible inclusion of an inner loop (say, connecting links along the directions p_2 and p_3), there are up to two possible choices of a third direction along which the holonomies $\hat{h}[p_k]$ and $\hat{h}^{-1}[p_k]$ can be applied. Since the directions of p_k and of the support links of α_{ij} should be mutually perpendicular [owing to the ϵ_{ijk} factor in Eq. (1)], whether or not p_k can be chosen to be directed along one or two legs of the spinnetwork depends on whether the spinnetwork is assumed to be embedded in a manifold (and, in this case, what is the geometric arrangement of the spinnetwork links relative to each other) or not (in which case a ‘‘topological’’ approach is considered). In the canonical approach, it is usually assumed that the spinnetworks are embedded in 3D (as a consequence of the foliation adopted for the definition of the Ashtekar-Barbero variables), while in the covariant approach a ‘‘topological’’ approach (somewhat closer to embedding in four or higher dimensions, where mutual perpendicularity of all links is possible) is usually considered. Thus, we will derive contributions to the action of the scalar constraint arising from both choices of p_k for each choice of inner loop. Our choice provides the most general possible result, so that consideration of an embedding in 3D, allowing for mutual perpendicularity of only three links of the spinnetwork, can be attained by selectively excluding certain terms from our expressions or tuning their coefficients by geometric prefactors. Let us first consider the application of the holonomy $\hat{h}^{-1}[p_1]$ along the path p_1 parallel to the link of spin j_1 ,

$$\begin{aligned}
\hat{h}^{-1}[p_1] &= \sum_m d_m \text{ (Diagram with } g^{-1} \text{ triangle on } j_1 \text{)} \\
&= \sum_{m,l} d_m d_l (-1)^{j_1+j_4-n-l} \begin{Bmatrix} b & j_1 & l \\ a & j_4 & n \end{Bmatrix} \text{ (Diagram with } g^{-1} \text{ triangle on } j_1 \text{ and half-link } 1/2 \text{)}
\end{aligned}
\tag{50}$$

We reiterate that, after coupling the identity extension of the introduced Wigner matrix to the spin- j_1 link of the spinnetwork through Eq. (14), the new coupled spin takes values $m = j_1 \pm 1/2$. Note that the direction of the temporary link containing the Wigner matrix of g^{-1} is drawn off-parallel relative to the direction the holonomy is applied in, since the temporary link has actually no spatial extension and its direction is arbitrary as long as one remembers the correct order of contraction of its ends. In order for the spinnetwork structure to match the ones we investigate the action of the volume operator on [cf. Eq. (81)], we employ Eq. (17) to swap the upper legs of the spinnetwork at the end of Eq. (50) [note that the $-n-l$ terms in the phase factor come from flipping $\epsilon^{(l)}$ and $\epsilon^{(n)}$ before and after applying Eq. (17)]. When acting on the spinnetwork in the last row of Eq. (50), the volume operator

then gives

$$\begin{aligned}
& \hat{V} \text{ (diagram with } j_4, j_3, j_2, j_1, l, m, a, b, \epsilon, g, g^{-1} \text{)} \\
&= \sum_{p,q} \left(V_{l,j_1;j_4,b,a,l}^{(4.5)p,q} \sqrt{d_p d_q d_l^{-1} d_{j_1}^{-1}} \right) \text{ (diagram with } j_4, j_3, j_2, j_1, p, q, a, b, \epsilon, g, g^{-1} \text{)} \\
&= \sum_{p,q,k} d_k \left(V_{l,j_1;j_4,b,a,l}^{(4.5)p,q} \sqrt{d_p d_q d_l^{-1} d_{j_1}^{-1}} \right) (-1)^{j_4+q-p-k} \begin{Bmatrix} b & j_4 & k \\ a & q & p \end{Bmatrix} \text{ (diagram with } j_4, j_3, j_2, j_1, k, a, b, \epsilon, g, g^{-1} \text{)}.
\end{aligned} \tag{51}$$

Spinnetworks of this form are not eigenstates of the volume operator. As will be shown in Sec. VIII, the volume operator maps such (normalized) spinnetworks to linear combinations of spinnetworks with the same structure. Luckily, each such spinnetwork belongs to an equivalence class, and the action of the volume operator never maps spinnetworks from a certain equivalence class into another. For now, the coefficients of the linear combination resulting from the application of the volume operator on such spinnetworks will be denoted $(V_{l,j_1;j_4,b,a,l}^{(4.5)p,q} \sqrt{d_p d_q d_l^{-1} d_{j_1}^{-1}})$, where the square-root contribution comes from normalizing and denormalizing the spinnetwork prior and posterior to the action of the volume operator, respectively, and the superscript (4.5) denotes that the intertwiner has valency 5, but one of its links (the holonomy one) is merely temporary, while p and q , on the one hand, and n and j_4 , on the other hand, are the two-entry indices of its matrix elements. In the last row of Eq. (51), we employed again Eq. (17) to swap the upper legs of the spinnetwork.

We now apply the holonomy $\hat{h}[p_1]$ on these spinnetworks, resulting in a spinnetwork with two virtual spin-1/2 links located at the 4-valent node (note that the spin- k link has no physical extension). As in previous equations, the

Wigner matrices of g and g^{-1} cancel out. Accordingly,

Finally, we apply the holonomy $\hat{h}[\alpha_{32}]$, which is represented by a Wigner matrix with ends extended by identities, one of which, on the left side, includes two arrows introduced through Eq. (5). The trace is also applied to contract all the holonomy indices in the end, but we will not explicitly write it in the following equations.

The effect of coupling the identity extensions of the Wigner matrix of g to the links of spins a and b can be accounted for by applying Eq. (14) to each of these links. In particular, for the left fundamental-representation identity, the coupling to the spin- a link involves only the segment between the two $\epsilon^{(1/2)}$ symbols, which then become integrated into loops. The $\epsilon^{(a)}$ and $\epsilon^{(b)}$ symbols have both been moved up to get the identities in the a and b representations coupled to the fundamental-representation ones. The Wigner matrix of the holonomy is coupled through Eq. (15) to the Wigner matrix of the spinnetwork. Each of the sums resulting from couplings between the spinnetwork and the Wigner matrix corresponding to the holonomy runs over the original spin of the spinnetwork link plus or minus $1/2$. These three couplings leave triangular loops at the links with spins j_2 and j_3 . On top of that, contracting all the holonomies converts the temporary spin- $1/2$ links into two loops, one of which traverses the spinnetwork diagonally (with a “tilde” shape). This loop has to be removed before the other loop on the left upper side of the spinnetwork could be factored out through the resolution of the identity. We show in Appendix A, Eq. (A1), that the diagonal

link can also be factored out to give

$$\begin{aligned}
 & \text{Diagram 1} = \sum_u d_u (-1)^{2\varepsilon+1-a+2b-j_4+2q+m+2k+\beta} \left\{ \begin{matrix} k & \frac{1}{2} & u \\ m & a & q \end{matrix} \right\} \left\{ \begin{matrix} k & \frac{1}{2} & u \\ \beta & j_4 & b \end{matrix} \right\} \\
 & \text{Diagram 2}
 \end{aligned} \tag{54}$$

where we have made use of the invariance of intertwiners, Eq. (10), to create ϵ tensors on the nodes of spins $\{m, q, 1/2\}$, $\{q, a, k\}$ and $\{\gamma, \varepsilon, 1/2\}$ on the left-hand side of Eq. (54), as well as on the intertwiners of spins $\{m, a, u\}$ and $\{u, \beta, j_4\}$ on the right-hand side of the same equation. Note the factor $(-1)^{2\varepsilon}$ originating from the contraction of two $\epsilon^{(\varepsilon)}$ tensors and the use of the simplification $(-1)^{2u+2a+2m} = 1$.

The remaining loops can be also factored out with the aid of Eq. (28),

$$\begin{aligned}
 & \text{Diagram 1} = \text{Diagram 2} - \text{Diagram 3} - \text{Diagram 4} \\
 & = (-1)^{-b+j_1+j_2+j_3+u+\varepsilon-\gamma+2\alpha+2\beta} \left\{ \begin{matrix} \frac{1}{2} & \alpha & a \\ u & m & j_1 \end{matrix} \right\} \left\{ \begin{matrix} \frac{1}{2} & \alpha & a \\ j_3 & \varepsilon & \gamma \end{matrix} \right\} \left\{ \begin{matrix} \frac{1}{2} & \gamma & \varepsilon \\ j_2 & b & \beta \end{matrix} \right\} \\
 & \text{Diagram 5}
 \end{aligned} \tag{55}$$

For this specific contribution to the constraint, we use Eq. (25) to simplify the final expression.

Starting from the final spinnetwork in Eq. (52), we can also apply the inverse holonomy $\hat{h}[\alpha_{23}]$, with ends extended by identities. After reorganizing the arrows around the node joining the spins $\{j_2, \varepsilon, b\}$ using Eq. (10), the spin- a and spin- b links of the spinnetwork can be coupled to the identity extensions of the holonomy with the help of Eq. (14),

while the Wigner matrices can be merged through Eq. (16). We obtain

$$\hat{h}[\alpha_{32}] = \dots = \sum_{\alpha, \beta, \gamma} d_\alpha d_\beta d_\gamma \dots \quad (56)$$

In this case, however, Eq. (28) can be used right away to factor out three inner loops from the resulting spinnetwork, while the remaining diagonal link can be factored out afterwards (see Appendix A). To facilitate this factorization, we include pairs of arrows in the links of spins m , j_3 and β with the aid of Eq. (5) [and use $(-1)^{2u+2\alpha+2j_1}$ to simplify the final expression]. This leads to

$$= (-1)^{-\frac{1}{2}+b+j_2+j_3+q+k-\varepsilon+\gamma+2\alpha} \left\{ \begin{matrix} \frac{1}{2} & \alpha & a \\ j_3 & \varepsilon & \gamma \end{matrix} \right\} \left\{ \begin{matrix} a & k & q \\ m & \frac{1}{2} & \alpha \end{matrix} \right\} \left\{ \begin{matrix} \varepsilon & j_2 & b \\ \beta & \frac{1}{2} & \gamma \end{matrix} \right\} \\ \times \sum_u d_u (-1)^{-\frac{1}{2}+2b+2j_2-j_4+m+2k+2\gamma-\alpha+\beta} \left\{ \begin{matrix} j_1 & \alpha & u \\ k & \frac{1}{2} & m \end{matrix} \right\} \left\{ \begin{matrix} k & \frac{1}{2} & u \\ \beta & j_4 & b \end{matrix} \right\} \dots \quad (57)$$

While still considering $\hat{h}[p_1]$ to be directed along the link of spin j_1 , we now look at the other term in the anti-commutator of Eq. (1), namely, the contribution that starts with the application of $\hat{h}[\alpha_{32}]$ on the spinnetwork (34). For that, we include two $\epsilon^{(1/2)}$ tensors on the right identity extension of the applied Wigner matrix. Furthermore, we use the invariance of the nodes [cf. Eq. (10)] to reorganize the arrows in the node joining the spins $\{\epsilon, j_2, b\}$. Using Eq. (14), we couple the spin- b link of the spinnetwork to the spin-1/2 identity between the two $\epsilon^{(1/2)}$ tensors of the right extension of the Wigner matrix. Likewise, the section of the spin- a link of the spinnetwork right above the $\epsilon^{(a)}$ tensor is coupled to the left extension of the Wigner matrix. In sequence, using Eq. (10), we can rearrange the arrows in the negative-cyclicity node joining the spins $\{\epsilon, 1/2, \gamma\}$ [effectively creating an $\epsilon^{(\gamma)}$ out of $\epsilon^{(\epsilon)}$ and $\epsilon^{(1/2)}$] before applying Eq. (28) to factor out the two inner loops. This gives

$$\begin{aligned}
& \hat{h}[\alpha_{32}] \text{ (diagram)} = \text{ (diagram)} = \sum_{\alpha, \beta, \gamma} d_\alpha d_\beta d_\gamma \text{ (diagram)} \\
& = \sum_{\alpha, \beta, \gamma} d_\alpha d_\beta d_\gamma \text{ (diagram)} = \sum_{\alpha, \beta, \gamma} d_\alpha d_\beta d_\gamma (-1)^{\frac{1}{2} + j_2 + j_3 + 2b + \epsilon + \gamma + \alpha + \beta} \begin{Bmatrix} a & j_3 & \epsilon \\ \gamma & \frac{1}{2} & \alpha \end{Bmatrix} \begin{Bmatrix} \frac{1}{2} & \gamma & \epsilon \\ j_2 & b & \beta \end{Bmatrix} \text{ (diagram)} \\
& \hspace{15em} \text{(diagram)} \tag{58}
\end{aligned}$$

We then proceed with the application of $\hat{h}^{-1}[p_1]$. Its Wigner matrix contracts with one of the temporary spin-1/2 links created by $\hat{h}[\alpha_{32}]$. We apply a braid [cf. Eq. (9)] in the node where this link is connected, so that the latter can be moved to the “interior” of the spinnetwork. The resulting diagonal link can be factored out, as shown in Eq. (A1).

Thus, we obtain

$$\begin{aligned}
 \hat{h}^{-1}[p_1] &= \text{Diagram 1} = \text{Diagram 2} \\
 &= \sum_m d_m \text{Diagram 3} \\
 &= \sum_{m,u} d_m d_u (-1)^{-\frac{1}{2}+2j_1-j_4+a+b+2n-m+2u} \begin{Bmatrix} m & a & u \\ n & \frac{1}{2} & j_1 \end{Bmatrix} \begin{Bmatrix} n & \frac{1}{2} & u \\ \beta & j_4 & b \end{Bmatrix} \text{Diagram 4}
 \end{aligned} \tag{59}$$

For the spinnetwork in the last row of this equation, we then use Eq. (20) between the nodes of spins $\{\alpha, a, 1/2\}$ and

$\{a, u, m\}$. As before, we use Eq. (17) to swap the upper legs of the spinnetwork and braid the temporary links, getting

$$\begin{aligned}
 &= \sum_l d_l (-1)^{u-\frac{1}{2}+m+\alpha} \left\{ \begin{matrix} u & \alpha & l \\ \frac{1}{2} & m & a \end{matrix} \right\} \\
 &= \sum_l d_l (-1)^{u-\frac{1}{2}+m+\alpha} \left\{ \begin{matrix} u & \alpha & l \\ \frac{1}{2} & m & a \end{matrix} \right\} \sum_k d_k (-1)^{l+j_4-u-k} \left\{ \begin{matrix} \beta & l & k \\ \alpha & j_4 & u \end{matrix} \right\} (-1)^{l+1+2m+j_1}
 \end{aligned}
 \tag{60}$$

We can then use the invariance of intertwiners to rearrange the arrows around the nodes of spins $\{j_4, \alpha, k\}$ and $\{k, \beta, l\}$, followed by the application of the volume operator according to Eq. (51). Note that the rearrangement of arrows includes a flip in the tensor $\epsilon^{(k)}$, leading to a phase factor $(-1)^{2k}$.

Finally, we apply the holonomy $\hat{h}[p_1]$, which ties the two temporary spin-1/2 links of the spinnetwork while canceling the Wigner matrices of g and g^{-1} . The formed ‘‘bubble’’ can be factored out with the help of Eq. (13), resulting in the desired spin network:

$$\begin{aligned}
 \hat{h}[p_1] &= (-1)^{2\beta+m+\frac{1}{2}+j_1} \\
 &= d_{j_1}^{-1} \delta_{j_1, q} (-1)^{2\beta+m+\frac{1}{2}+j_1}
 \end{aligned}
 \tag{61}$$

The last contribution that considers holonomies applied along p_1 is the one starting with the application of $\hat{h}[\alpha_{23}]$.

Both indices of the corresponding Wigner matrix are contracted with identities, which extend themselves to embrace the NLSN as in the previous cases. Before coupling the holonomy to the spinnetwork, we use the invariance of the Wigner 3j symbols, Eq. (10), to reorganize the arrows associated with the node connecting the links of spins $\{j_2, \varepsilon, b\}$. After employing Eqs. (14) (coupling identity segments below the arrows) and (16), we apply Eq. (5) to the spin- j_3 and spin- β links to create a pair of arrows on each of them. One arrow from each pair can be extracted alongside the inner loops with the aid of Eq. (28), and we can then apply Eq. (10) to the nodes joining the spins $\{a, \alpha, 1/2\}$, $\{b, \beta, 1/2\}$ and $\{j_2, \gamma, \beta\}$ to obtain the final spinnetwork [note that the doubled $\epsilon^{(\alpha)}$ symbols are canceled via Eq. (5)]. This gives

$$\begin{aligned}
\hat{h}[\alpha_{23}] &= \text{Diagram 1} = \sum_{\alpha, \beta, \gamma} d_\alpha d_\beta d_\gamma \text{Diagram 2} \\
&= \sum_{\alpha, \beta, \gamma} d_\alpha d_\beta d_\gamma \left[\text{Diagram 3} - \text{Diagram 4} \right] \text{Diagram 5} \\
&= \sum_{\alpha, \beta, \gamma} d_\alpha d_\beta d_\gamma (-1)^{\frac{1}{2} + j_2 + j_3 + 2b + \varepsilon + \gamma + \alpha + \beta} \begin{Bmatrix} \frac{1}{2} & \alpha & a \\ j_3 & \varepsilon & \gamma \end{Bmatrix} \begin{Bmatrix} \varepsilon & j_2 & b \\ \beta & \frac{1}{2} & \gamma \end{Bmatrix} \text{Diagram 6}
\end{aligned} \tag{62}$$

Acting with $\hat{h}^{-1}[p_1]$ on the spinnetwork resulting from Eq. (62) allows for coupling the identity extension of $\hat{h}[\alpha_{23}]$ to the spin- j_1 link of the NLSN. Before and after applying Eq. (14), we braid the fundamental-spin links around the nodes joining the spins $\{a, \alpha, 1/2\}$ and $\{m, j_1, 1/2\}$, respectively. The Wigner matrix itself remains in one of the free ends of the temporary fundamental-spin links, while the other end is contracted with the corresponding temporary link resulting from the application of the holonomy on the loop α_{23} . The inner loop formed by this contraction can then be factored out employing Eq. (28). We can next use Eq. (10) to create a trio of arrows around the node where the links of spins $\{n, \alpha, m\}$ meet [see the third row of Eq. (63)]. One of these arrows, representing the $\epsilon^{(n)}$ symbol, allows us to use Eq. (17) to swap the upper legs of the spinnetwork. Similarly, creating a trio of arrows around the node with spins $\{b, \beta, 1/2\}$ allows us to use Eq. (20) in the connecting spin- b link. Note that, before applying the volume operator, one needs to reduce the tensors $\epsilon^{(u)}$, $\epsilon^{(1/2)}$ and $\epsilon^{(m)}$ on the third row of Eq. (63) to a prefactor $(-1)^{2m}$. As in Eq. (51), the action of the volume operator on the resulting spinnetwork [see the last row of Eq. (63)] gives a linear combination of spinnetworks with the same structure. We can then act on it with the holonomy $\hat{h}[p_1]$ to generate the desired spinnetworks, as in Eq. (61). In total, we obtain

$$\begin{aligned}
 & \hat{h}^{(-1)}[p_1] = \text{Diagram 1} = \text{Diagram 2} \\
 & = \sum_m d_m \text{Diagram 3} = \sum_m d_m \text{Diagram 4} \\
 & = \sum_m d_m (-1)^{1+2a+m+n+\alpha} \begin{Bmatrix} \frac{1}{2} & \alpha & a \\ n & j_1 & m \end{Bmatrix} \sum_l d_l (-1)^{m+j_4-n-l} \begin{Bmatrix} b & m & l \\ \alpha & j_4 & n \end{Bmatrix} \text{Diagram 5} \\
 & = \sum_{m,l,u} d_m d_l d_u (-1)^{-\frac{1}{2}+j_4+2a-m+\alpha-\beta} \begin{Bmatrix} \frac{1}{2} & \alpha & a \\ n & j_1 & m \end{Bmatrix} \begin{Bmatrix} b & m & l \\ \alpha & j_4 & n \end{Bmatrix} \begin{Bmatrix} m & \frac{1}{2} & u \\ \beta & l & b \end{Bmatrix} \text{Diagram 6}
 \end{aligned}
 \tag{63}$$

Since we are considering the most general case for the application of Eq. (1) acting on the spinnetwork (34), we must also take into account holonomies applied along the direction p_4 . For the first term in Eq. (1), we consider the application of the holonomy $\hat{h}^{-1}[p_4]$ on the spin network,

$$\hat{h}^{-1}[p_4] \text{ (Diagram)} = \text{ (Diagram)} \quad (64)$$

$$= \sum_m d_m \text{ (Diagram)} \quad (64)$$

The coupling of the identity extension of the Wigner matrix corresponding to $\hat{h}^{-1}[p_4]$ with the spin- j_4 link of the spinnetwork is described by Eq. (14). The resulting spinnetwork is already in the graphical form suitable for application of the volume operator, as described in Eq. (81), resulting in the linear combination

$$\hat{V} \sum_m d_m \text{ (Diagram)} = \sum_m d_m \sum_{p,q} (V_{n,j_4;j_1,b,a,m}^{(4,5)p,q} \sqrt{d_p d_q d_n^{-1} d_{j_4}^{-1}}) \text{ (Diagram)} \quad (65)$$

We then apply the holonomy $\hat{h}[p_4]$. Its Wigner matrix contracts with the free end of the g^{-1} Wigner matrix,

forming a temporary identity link. This gives

$$\hat{h}[p_4] = \text{Diagram 1} = \text{Diagram 2} = \text{Diagram 3} \quad (66)$$

The two temporary spin-1/2 links are then contracted by the trace with the identity extensions of the Wigner matrix representing the holonomy $\hat{h}[\alpha_{32}]$ after performing a braiding at the node of spins $\{m, 1/2, j_4\}$. We apply Eq. (5) in both identity extensions of the Wigner matrix, as well as Eq. (10) to the node of spins $\{\varepsilon, j_2, b\}$ in order to reorganize the arrows. The inter-arrow sections of the identity extensions are then coupled to the spin- a [namely the section below $\varepsilon^{(a)}$] and spin- b links by using Eq. (14). Similarly, the Wigner matrices are coupled by means of Eq. (15). We obtain

$$\hat{h}[\alpha_{32}] = \text{Diagram 1} = \text{Diagram 2} \quad (67)$$

$$= \text{Diagram 1} = \text{Diagram 2}$$

After using Eq. (4) on the spin-1/2 link with two arrows in the spinnetwork obtained in the last row of this equation and introducing new pairs of arrows at the links of spins β and j_3 via Eq. (5), we can use Eq. (28) to factor out three inner loops from the spinnetwork. We can then use Eq. (10) to redistribute the arrows around the resulting node of spins $\{j_2, \beta, \gamma\}$ [see the second row of Eq. (68)], leading to a double $\varepsilon^{(\beta)}$ that can be factored out employing Eq. (4). By braiding the node of spins $\{\alpha, 1/2, a\}$ [note the corresponding factor $(-1)^{\alpha+a+1/2}$] and rearranging arrows around that same node, as well as the node below, the remaining diagonal link can be factored out via Eq. (A2) (cf. Appendix

A). In this way, we get

$$\begin{aligned}
& \text{Diagram 1: A complex spinnetwork with four external legs } j_1, j_2, j_3, j_4. \text{ Internal nodes are labeled } p, q, a, b, \alpha, \beta, \gamma, \varepsilon, g. \text{ Edges are labeled } m, a, b, \alpha, \beta, \gamma, \varepsilon. \text{ Curved edges are labeled } \frac{1}{2}. \\
& = - \left[\text{Diagram 2} \right] - \left[\text{Diagram 3} \right] - \left[\text{Diagram 4} \right] (-1)^{\alpha+a-\frac{1}{2}} \left[\text{Diagram 5} \right] \\
& = (-1)^{a+2b+j_2+j_3+m+\varepsilon+\gamma+p+2\alpha+2\beta} \left\{ \begin{matrix} \frac{1}{2} & m & q \\ p & b & \beta \end{matrix} \right\} \left\{ \begin{matrix} \varepsilon & j_2 & b \\ \beta & \frac{1}{2} & \gamma \end{matrix} \right\} \left\{ \begin{matrix} \frac{1}{2} & \alpha & a \\ j_3 & \varepsilon & \gamma \end{matrix} \right\} \left[\text{Diagram 6} \right] \\
& = (-1)^{a+2b+j_2+j_3+m+\varepsilon+\gamma+p+2\alpha+2\beta} \left\{ \begin{matrix} \frac{1}{2} & m & q \\ p & b & \beta \end{matrix} \right\} \left\{ \begin{matrix} \varepsilon & j_2 & b \\ \beta & \frac{1}{2} & \gamma \end{matrix} \right\} \left\{ \begin{matrix} \frac{1}{2} & \alpha & a \\ j_3 & \varepsilon & \gamma \end{matrix} \right\} \\
& \quad \times \sum_k d_k (-1)^{1-\alpha+j_1+\beta-j_4} \left\{ \begin{matrix} \alpha & j_1 & k \\ p & \frac{1}{2} & a \end{matrix} \right\} \left\{ \begin{matrix} p & \frac{1}{2} & k \\ j_4 & \beta & m \end{matrix} \right\} \left[\text{Diagram 7} \right].
\end{aligned} \tag{68}$$

Starting from the spinnetwork in the last row of Eq. (66), we can apply $\hat{h}[\alpha_{23}]$ (and the trace), using Eqs. (14) and (16) [as well as Eq. (10) to reorganize arrows around the node $\{j_2, \varepsilon, b\}$] to obtain a spinnetwork with temporary

inner loops (note the double braiding on the leg along direction p_4 and the resulting phase factor):

$$\hat{h}[\alpha_{32}] = (-1)^{1+2m+q+j_4} \text{ (diagrammatic representation) } \quad (69)$$

$$= \sum_{\alpha, \beta, \gamma} d_\alpha d_\beta d_\gamma (-1)^{1+2m+q+j_4} \text{ (diagrammatic representation) } \quad (69)$$

In the spinnetwork in the last row of Eq. (69), we can use Eq. (A1) to factor out the diagonal link:

$$= \sum_k d_k (-1)^{1+\alpha-j_1+b-m} \begin{Bmatrix} \alpha & j_1 & k \\ p & \frac{1}{2} & a \end{Bmatrix} \begin{Bmatrix} p & \frac{1}{2} & k \\ m & \frac{1}{2} & q \end{Bmatrix} \text{ (diagrammatic representation) } \quad (70)$$

The remaining inner loops in Eq. (70) can be factored out with the help of Eq. (28). Note that we can use Eq. (5) on the links of spins β , j_4 and j_3 to introduce additional arrows that can be extracted when factoring out the tetrahedral

structures. This leads to

$$\begin{aligned}
 & \begin{array}{c} \text{Diagram 1: A central node with four outgoing links labeled } j_1, j_2, j_3, j_4. \text{ The links } j_1 \text{ and } j_2 \text{ are connected by a horizontal link } k. \text{ The links } j_3 \text{ and } j_4 \text{ are connected by a horizontal link } m. \text{ The links } j_1 \text{ and } j_3 \text{ are connected by a diagonal link } \alpha. \text{ The links } j_2 \text{ and } j_4 \text{ are connected by a diagonal link } \beta. \text{ The links } j_1 \text{ and } j_2 \text{ are connected by a diagonal link } \gamma. \text{ The links } j_3 \text{ and } j_4 \text{ are connected by a diagonal link } \epsilon. \text{ The links } j_1 \text{ and } j_2 \text{ are connected by a diagonal link } g. \text{ The links } j_3 \text{ and } j_4 \text{ are connected by a diagonal link } g. \end{array} \\
 & = - \begin{array}{c} \text{Diagram 2: A triangle with vertices } j_1, j_2, j_3. \text{ The link } j_1 \text{ is labeled } \frac{1}{2}. \text{ The link } j_2 \text{ is labeled } b. \text{ The link } j_3 \text{ is labeled } m. \text{ The link } j_1 \text{ and } j_2 \text{ are connected by a diagonal link } \beta. \text{ The link } j_1 \text{ and } j_3 \text{ are connected by a diagonal link } k. \end{array} \\
 & - \begin{array}{c} \text{Diagram 3: A triangle with vertices } j_1, j_2, j_3. \text{ The link } j_1 \text{ is labeled } a. \text{ The link } j_2 \text{ is labeled } \frac{1}{2}. \text{ The link } j_3 \text{ is labeled } \epsilon. \text{ The link } j_1 \text{ and } j_2 \text{ are connected by a diagonal link } \alpha. \text{ The link } j_1 \text{ and } j_3 \text{ are connected by a diagonal link } \gamma. \end{array} \\
 & - \begin{array}{c} \text{Diagram 4: A triangle with vertices } j_1, j_2, j_3. \text{ The link } j_1 \text{ is labeled } b. \text{ The link } j_2 \text{ is labeled } \epsilon. \text{ The link } j_3 \text{ is labeled } \frac{1}{2}. \text{ The link } j_1 \text{ and } j_2 \text{ are connected by a diagonal link } \beta. \text{ The link } j_1 \text{ and } j_3 \text{ are connected by a diagonal link } \gamma. \end{array} \\
 & \begin{array}{c} \text{Diagram 5: A central node with four outgoing links labeled } j_1, j_2, j_3, j_4. \text{ The links } j_1 \text{ and } j_2 \text{ are connected by a horizontal link } k. \text{ The links } j_3 \text{ and } j_4 \text{ are connected by a horizontal link } m. \text{ The links } j_1 \text{ and } j_3 \text{ are connected by a diagonal link } \alpha. \text{ The links } j_2 \text{ and } j_4 \text{ are connected by a diagonal link } \beta. \text{ The links } j_1 \text{ and } j_2 \text{ are connected by a diagonal link } \gamma. \text{ The links } j_3 \text{ and } j_4 \text{ are connected by a diagonal link } \epsilon. \text{ The links } j_1 \text{ and } j_2 \text{ are connected by a diagonal link } g. \text{ The links } j_3 \text{ and } j_4 \text{ are connected by a diagonal link } g. \end{array} \\
 & = (-1)^{1+a+j_2+j_3+j_4-k-\epsilon-\gamma+2\alpha} \left\{ \begin{array}{c} b \quad \beta \quad \frac{1}{2} \\ j_4 \quad m \quad k \end{array} \right\} \left\{ \begin{array}{c} \frac{1}{2} \quad \alpha \quad a \\ j_3 \quad \epsilon \quad \gamma \end{array} \right\} \left\{ \begin{array}{c} \epsilon \quad j_2 \quad b \\ \beta \quad \frac{1}{2} \quad \gamma \end{array} \right\} \\
 & \begin{array}{c} \text{Diagram 6: A central node with four outgoing links labeled } j_1, j_2, j_3, j_4. \text{ The links } j_1 \text{ and } j_2 \text{ are connected by a horizontal link } k. \text{ The links } j_3 \text{ and } j_4 \text{ are connected by a horizontal link } m. \text{ The links } j_1 \text{ and } j_3 \text{ are connected by a diagonal link } \alpha. \text{ The links } j_2 \text{ and } j_4 \text{ are connected by a diagonal link } \beta. \text{ The links } j_1 \text{ and } j_2 \text{ are connected by a diagonal link } \gamma. \text{ The links } j_3 \text{ and } j_4 \text{ are connected by a diagonal link } \epsilon. \text{ The links } j_1 \text{ and } j_2 \text{ are connected by a diagonal link } g. \text{ The links } j_3 \text{ and } j_4 \text{ are connected by a diagonal link } g. \end{array} .
 \end{aligned} \tag{71}$$

The phase factors in the last row of Eq. (71) are the result of recombining arrows using Eqs. (10), (4) and (5).

In order to consider the contribution arising from the other order of operators in the anticommutator of Eq. (1) for $p_k = p_4$, we start from Eq. (58) and apply $\hat{h}[p_4]$ on its final spinnetwork. The identity extension of the Wigner matrix of g^{-1} is coupled to the spin- j_4 link through Eq. (14), and its lower end is contracted with one of the spin-1/2 links produced by $\hat{h}[\alpha_{32}]$, forming an inner loop. We can factor out the inner loop with Eq. (28), braid the remaining temporary spin-1/2 link and use Eq. (10) to introduce three arrows around the node connecting the links of spins $\{a, n, j_1\}$ [this leads to the second row of Eq. (71)]. Using Eq. (20), we can then move the remaining spin-1/2 link to

the center of the spinnetwork,

$$\begin{aligned}
\hat{h}^{-1}[p_4] &= \text{Diagram 1} = \text{Diagram 2} \\
&= \sum_m d_m \text{Diagram 3} = \sum_m d_m \text{Diagram 4} \\
&= \sum_{m,l} d_m (-1)^{1+2b+n+m+\beta} \begin{Bmatrix} \frac{1}{2} & m & j_4 \\ n & b & \beta \end{Bmatrix} \sum_k d_k (-1)^{n+a+j_1+1} \begin{Bmatrix} n & \frac{1}{2} & k \\ \alpha & j_1 & a \end{Bmatrix} \text{Diagram 5}
\end{aligned} \tag{72}$$

After braiding the fundamental-spin link from the interior to the exterior of the NLSN and changing the cyclicity of its node, we apply once again Eq. (20), now to the spin- n link. We also use Eq. (10) to rearrange the arrows around the node of spins $\{\alpha, k, j_1\}$ [this gives the second row of Eq. (73)]. An additional braiding on the node of spins $\{1/2, l, m\}$, followed by the introduction of ϵ tensors on the node of spins $\{k, \beta, l\}$ [cf. Eq. (10)], gives the following

spinnetwork, on which the volume operator can be directly applied:

$$\begin{aligned}
 & (-1)^{\frac{1}{2}+k+n} \text{Diagram} \\
 &= (-1)^{\frac{1}{2}+k+n} \sum_l d_l (-1)^{\frac{1}{2}-\beta+k+m} \left\{ \begin{matrix} \frac{1}{2} & m & l \\ \beta & k & n \end{matrix} \right\} \text{Diagram} \\
 &= \sum_l d_l (-1)^{-\frac{1}{2}+2k+2m+n+l-\beta} \left\{ \begin{matrix} \frac{1}{2} & m & l \\ \beta & k & n \end{matrix} \right\} \text{Diagram}
 \end{aligned} \tag{73}$$

Finally, we apply $\hat{h}[p_4]$, which forms a closed loop that can be factored out with the aid of Eq. (13) to recover the

desired spin network,

$$\hat{h}[p_4] = \dots = d_{j_4}^{-1} \delta_{j_4, l} \dots \quad (74)$$

The last contribution in the scalar constraint (1) can be derived from the spinnetwork obtained in Eq. (62). We apply $\hat{h}^{-1}[p_4]$, using Eq. (14) to couple the identity extension of the Wigner matrix to the spin- j_4 link. The contraction of indices forms a diagonal link that can be factored out with the help of Eq. (A1). This gives

$$\begin{aligned}
\hat{h}^{-1}[p_4] &= \text{Diagram 1} = \text{Diagram 2} \\
&= \sum_m d_m (-1)^{\alpha+a+\frac{1}{2}} \text{Diagram 3} \\
&= \sum_m d_m \sum_l d_l (-1)^{-\frac{1}{2}+2l-j_1+a+b-m+2\alpha} \left\{ \begin{matrix} n & \frac{1}{2} & l \\ \alpha & j_1 & a \end{matrix} \right\} \left\{ \begin{matrix} n & \frac{1}{2} & l \\ m & b & j_4 \end{matrix} \right\} \text{Diagram 4}
\end{aligned} \tag{75}$$

After using Eq. (10) to reorganize the arrows around the node of spins $\{b, m, l\}$, we can employ Eq. (20) to move the temporary spin-1/2 link upwards. We thus obtain

$$\text{Diagram 5} = \sum_k d_k (-1)^{m-\beta+l+\frac{1}{2}} \left\{ \begin{matrix} m & \frac{1}{2} & k \\ \beta & l & b \end{matrix} \right\} \text{Diagram 6} \tag{76}$$

A simple rearrangement of arrows in the last spinnetwork in Eq. (76) allows us to apply the volume operator, Eq. (65), followed by the remaining holonomy, according to Eq. (74).

Putting our equations (50)–(63) together, we obtain all the contributions in Eq. (1) when a specific choice of loop, α_{32} , and holonomies along p_1 are considered,

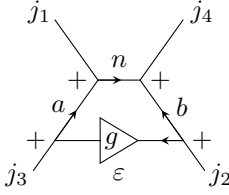
$$\frac{i}{2} \text{tr} \left\{ \hat{h}[\alpha_{23}] - \hat{h}[\alpha_{32}], \hat{h}[p_1] \hat{V} \hat{h}^{-1}[p_1] \right\} \cdot \begin{array}{c} j_1 \qquad \qquad j_4 \\ \qquad \qquad \qquad + \qquad \qquad \qquad \\ \qquad \qquad \qquad n \qquad \qquad \qquad \\ \qquad \qquad \qquad + \qquad \qquad \qquad \\ \alpha \qquad \qquad \qquad \qquad \qquad b \\ \qquad \qquad \qquad \qquad \qquad \qquad \\ j_3 \qquad \qquad \qquad g \qquad \qquad \qquad \\ \qquad \qquad \qquad \varepsilon \qquad \qquad \qquad \\ \qquad \qquad \qquad + \qquad \qquad \qquad \\ j_2 \end{array} = \frac{i}{2} \sum_{\alpha, \beta, \gamma, m, k, q} d_\alpha d_\beta d_\gamma d_m d_k$$

$$\begin{aligned} & \times \left\{ \begin{array}{c} \frac{1}{2} \ \alpha \ a \\ j_3 \ \varepsilon \ \gamma \end{array} \right\} \left\{ \begin{array}{c} b \ \beta \ \frac{1}{2} \\ \gamma \ \varepsilon \ j_2 \end{array} \right\} \left[\sum_{p, l} d_l (V_{l, j_1; j_4, b, a, m}^{(4.5)p, q} \sqrt{d_p d_q d_l^{-1} d_{j_1}^{-1}}) \left\{ \begin{array}{c} j_1 \ b \ l \\ j_4 \ a \ n \end{array} \right\} \left((-1)^{1/2+2j_1+j_2+j_3-\varepsilon-\gamma+2q-l-2p+2a-n+2\alpha-2\beta} \right. \right. \\ & \times \left\{ \begin{array}{c} p \ m \ \beta \\ \frac{1}{2} \ b \ q \end{array} \right\} \left\{ \begin{array}{c} p \ m \ \beta \\ k \ j_4 \ a \end{array} \right\} \left\{ \begin{array}{c} \frac{1}{2} \ \alpha \ a \\ k \ m \ j_1 \end{array} \right\} - \sum_u d_u (-1)^{1-b-j_1+j_2+j_3+j_4+2q+m-n-l-p+2u-\varepsilon-\gamma+\alpha+\beta} \left\{ \begin{array}{c} b \ j_4 \ u \\ a \ q \ p \end{array} \right\} \\ & \times \left. \left\{ \begin{array}{c} a \ u \ q \\ m \ \frac{1}{2} \ \alpha \end{array} \right\} \left\{ \begin{array}{c} j_1 \ \alpha \ k \\ u \ \frac{1}{2} \ m \end{array} \right\} \left\{ \begin{array}{c} u \ \frac{1}{2} \ k \\ \beta \ j_4 \ b \end{array} \right\} \right) - \sum_{p, l} d_l d_q d_{j_1}^{-1} (V_{l, q; j_4, \beta, \alpha, m}^{(4.5)p, j_1} \sqrt{d_p d_{j_1} d_l^{-1} d_q^{-1}}) \left\{ \begin{array}{c} \beta \ j_4 \ k \\ \alpha \ j_1 \ p \end{array} \right\} \\ & \times \left((-1)^{1/2+2j_1+j_2+j_3+2j_4+2a+2b+\varepsilon+\gamma+2m-p-k} \left\{ \begin{array}{c} \frac{1}{2} \ \alpha \ a \\ n \ j_1 \ m \end{array} \right\} \left\{ \begin{array}{c} b \ m \ l \\ \alpha \ j_4 \ n \end{array} \right\} \left\{ \begin{array}{c} m \ \frac{1}{2} \ q \\ \beta \ l \ b \end{array} \right\} - \sum_u d_u \right. \\ & \left. \times (-1)^{1+j_1+j_2+j_3+j_4+a-b+\varepsilon+\gamma+l+2q-m+2n-p+2u-k+2\alpha-\beta} \left\{ \begin{array}{c} \beta \ q \ l \\ \alpha \ j_4 \ u \end{array} \right\} \left\{ \begin{array}{c} m \ a \ u \\ n \ \frac{1}{2} \ j_1 \end{array} \right\} \left\{ \begin{array}{c} n \ \frac{1}{2} \ u \\ \beta \ j_4 \ b \end{array} \right\} \left\{ \begin{array}{c} u \ \alpha \ q \\ \frac{1}{2} \ m \ a \end{array} \right\} \right) \end{aligned}$$

$$\begin{array}{c} j_1 \qquad \qquad j_4 \\ \qquad \qquad \qquad + \qquad \qquad \qquad \\ \qquad \qquad \qquad k \qquad \qquad \qquad \\ \qquad \qquad \qquad + \qquad \qquad \qquad \\ \alpha \qquad \qquad \qquad \qquad \qquad \beta \\ \qquad \qquad \qquad \qquad \qquad \qquad \\ j_3 \qquad \qquad \qquad g \qquad \qquad \qquad \\ \qquad \qquad \qquad \gamma \qquad \qquad \qquad \\ \qquad \qquad \qquad + \qquad \qquad \qquad \\ j_2 \end{array} .$$

(77)

Similarly, Eqs. (64)–(76) give the result corresponding to Eq. (1) when α_{32} and holonomies along p_4 are considered,

$$\frac{i}{2} \text{tr} \left\{ \hat{h}[\alpha_{23}] - \hat{h}[\alpha_{32}], \hat{h}[p_4] \hat{V} \hat{h}^{-1}[p_4] \right\}$$


$$= \frac{i}{2} \sum_{\alpha, \beta, \gamma, m, k, q} d_\alpha d_\beta d_\gamma d_m$$

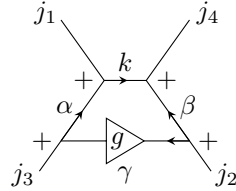
$$\times \left\{ \begin{matrix} \frac{1}{2} & \alpha & a \\ j_3 & \varepsilon & \gamma \end{matrix} \right\} \left\{ \begin{matrix} b & \beta & \frac{1}{2} \\ \gamma & \varepsilon & j_2 \end{matrix} \right\} \left[\sum_p d_k (V_{n, j_4; j_1, b, a, m}^{(4.5)p, q} \sqrt{d_p d_{j_1} d_l^{-1} d_q^{-1}}) \left((-1)^{1+j_1+j_2+j_3-j_4+a+2b+p+m+\varepsilon+\gamma+\alpha-\beta} \right. \right.$$

$$\times \left\{ \begin{matrix} p & \frac{1}{2} & k \\ j_4 & \beta & m \end{matrix} \right\} \left\{ \begin{matrix} \frac{1}{2} & m & q \\ p & b & \beta \end{matrix} \right\} \left\{ \begin{matrix} \alpha & j_1 & k \\ p & \frac{1}{2} & a \end{matrix} \right\} - (-1)^{1+j_1+j_2+j_3+2j_4-a-b-m+\varepsilon+\gamma-k+q-\alpha} \left\{ \begin{matrix} p & \frac{1}{2} & k \\ m & b & q \end{matrix} \right\} \left\{ \begin{matrix} p & \frac{1}{2} & k \\ \alpha & j_1 & a \end{matrix} \right\}$$

(78)

$$\times \left\{ \begin{matrix} \frac{1}{2} & j_4 & m \\ k & b & \beta \end{matrix} \right\} \left. \right) + \sum_p d_p d_q d_{j_4}^{-1} (V_{p, q; j_1, \beta, \alpha, m}^{(4.5)k, j_4} \sqrt{d_k d_{j_4} d_p^{-1} d_q^{-1}}) \left((-1)^{j_1+j_2+j_3+2j_4-a-\varepsilon-\gamma+q-\alpha+\beta+m+n} \left\{ \begin{matrix} \frac{1}{2} & m & j_4 \\ n & b & \beta \end{matrix} \right\} \right.$$

$$\times \left. \left\{ \begin{matrix} \alpha & j_1 & p \\ n & \frac{1}{2} & a \end{matrix} \right\} \left\{ \begin{matrix} \frac{1}{2} & m & q \\ \beta & p & n \end{matrix} \right\} - (-1)^{j_1+j_2+j_3+j_4+a+b+\varepsilon+\gamma-p+m+\alpha+2\beta} \left\{ \begin{matrix} n & \frac{1}{2} & p \\ \alpha & j_1 & a \end{matrix} \right\} \left\{ \begin{matrix} n & \frac{1}{2} & p \\ m & b & j_4 \end{matrix} \right\} \left\{ \begin{matrix} m & \frac{1}{2} & q \\ \beta & p & b \end{matrix} \right\} \right) \left. \right]$$



Note that Eqs. (77) and (78) are seemingly not simply related to each other by Eq. (17). In these equations, we explicitly wrote two separate sums over p [and also over l in the case of Eq. (77)] because the values summed over are different for each sum. Furthermore, there are five other different possible choices for the loop α_{ij} . For the loop α_{14} , bridging the links of spins j_1 and j_4 in our assignment of spins, Eqs. (50)-(76) can be directly used if preceded and followed by a flip in the direction of the central $\epsilon^{(i)}$ [cf. Eq. (34)]. For the loops α_{13} and α_{24} , however, application of the formulas derived in this section has to be preceded and followed by Eq. (20), which allows us to change the basis in the 4-valent intertwiner space so that the formulas hold. The last two loops, α_{12} and α_{34} , extend themselves diagonally through the spin-network and require a braid between either legs in the

p_1 and p_3 directions or p_2 and p_4 directions, both before and after employing Eqs. (50)-(76). It can be shown that applying the derived Hamiltonian between braid moves gives the same result as directly employing Eq. (1) with holonomies applied along the twisted loops α_{12} and α_{34} .

A last relevant point concerning the action of the Euclidean scalar constraint on 4-valent NLSN is how Eqs. (77) and (78) can be modified to render their action graph-preserving. The general approach in LQG is based on an extension of the loops $\alpha_{ij} \rightarrow \tilde{\alpha}_{ij}$, so that the enlarged loops $\tilde{\alpha}_{ij}$ cover an entire spinnetwork “patch” with borders defined by links and intertwiners. The precise form of the loops $\tilde{\alpha}_{ij}$ therefore depends on the spin-network of choice, as well as on which “patch” the graph-preserving Hamiltonian is acting on. This renders the NLSN-limited analysis of graph-preserving dynamics im-

possible: one is forced to extend the fiducial intertwiner in such a way that all its legs are connected to other intertwiners, forming closed loops $\tilde{\alpha}_{ij}$ on which the graph-preserving Hamiltonian can act. We note that a small modification of the NLSN studied here can still cover a small range of (modular segments of) connected spinnetworks on which a few such loops $\tilde{\alpha}_{ij}$ can be applied. If we include one inner loop at location 2 and one at location 4, promoting their “additional” links to virtual central links of two other independent intertwiners, we can apply Eqs. (77) and (78) limiting their action solely to these loops at locations 2 and 4. As a result, one considers a ladder-like spinnetwork with intertwiners connected by their upper or lower pairs of legs and loop couplings restricted to solely happen above and below the fiducial intertwiner, neglecting large loops coupled from the sides (for which the action of the graph-preserving Hamiltonian depends on the precise number and connectivity of intertwiners through the entire “side patches” of the spinnetwork). It is worth noting that these modified NLSNs can cover five other (modular segments of) spinnetwork graphs, namely by setting one or two of the spins at the outermost links to zero (e.g., by having all of them equal to zero, one creates a spinnetwork “bubble” in which the two lower legs of the intertwiner are connected to each other, and similarly for the two upper legs).

VIII. ACTION OF THE QUANTUM VOLUME OPERATOR

The quantum volume operator is a key observable in LQG, both due to its presence in the scalar Hamiltonian constraint (1) and to the conceptual implications of its eigenvalues and expectation values (which imply, among other things, that geometric properties of spacetime itself can have quantum features). There are, however, some open questions regarding the most suitable regularization approach to obtain the action of the quantum volume operator on spinnetworks. Several different regularizations (e.g., by decomposing the manifold into cubes or into tetrahedra) lead nonetheless to the same expression for the quantum volume operator up to a constant prefactor [28, 31]. We therefore leave an arbitrary prefactor V_0 on the volume operator, proportional to the Planck volume. This approach allows for some freedom of choice of a preferred regularization and renders dimensionless results that can be later properly scaled by the desired prefactor.

It is important to emphasize that, when acting with the scalar constraint on an n -valent NLSN, the volume operator appearing in Eq. (1) actually acts on an $(n+1)$ -valent node, since the holonomy $\hat{h}^{(-1)}[p_k]$ temporarily raises the valency of the node. Still, this increased valency does not imply that the volume operator simply acts on an $(n+1)$ -valent NLSN, since the volume cannot directly “grasp” the temporary spin-1/2 link introduced by the holonomy, and therefore acts on n out of the $n+1$ legs of the spin-

network [24, 25]. When the volume operator is directly applied on an n -valent NLSN, however, its action is different, and all triplets of (mutually perpendicular) links (or more generally linear independent triplets) selected out of all the n node legs can be “grasped”, without exclusions [32].

In the basis of spinnetworks, the volume operator is composed of other operators \hat{W} that can be represented as spinnetworks which attach themselves to the input spinnetwork through so-called “grasps”. The resulting spinnetwork contains additional inner structures that can be factored out (with the help of the expressions obtained with recoupling theory and introduced in Secs. IV and V) to recover the input graphical structure, rendering \hat{W} a map between spinnetworks with the same graph. In fact, when acting on the entire Hilbert space of spinnetworks, the volume operator forms an infinite block-diagonal matrix, and we can without loss of generality restrict the analysis to the specific block to which each spinnetwork of interest belongs, forming equivalence classes of spinnetworks that can be mapped into each other by \hat{W} . The matrices corresponding to these operators have to be diagonalized in the normalized-spinnetwork basis in order to build the (desired block of the) volume-operator matrix. Formally, for each possible choice of three nonparallel links from each node, one applies the operator \hat{W} on all spinnetworks of the same equivalence class to build its matrix. The corresponding matrices for each choice of three links are summed, taking the square root of the absolute value of the result. The sum over all nodes of such square-root matrices gives the volume-operator matrix representation in the normalized-spinnetwork basis. It is worth noting that this protocol for construction of the quantum-volume matrix follows Ref. [37], yet more complicated protocols, requiring the sum of absolute values of \hat{W} for each triplet of links before calculating the square root (which demands multiple diagonalization steps to derive a single volume matrix) are also found in the literature [32]. For details on the derivation of the quantum-volume operator, we refer to Refs. [32, 37].

Smearing densitized triads (the conjugated fields to the holonomies) results in angular-momentum-like operators $\hat{J}_i^{(e,v)}$. The index i refers to a choice of SU(2) generator and (e, v) is an assignment of link e incoming to or outgoing from a node v of the spinnetwork. The operator $\hat{J}_i^{(e,v)}$ acts on holonomies, given as in Eq. (6), by applying on them the generators of SU(2) [cf. Eq. (26)]. If e is the link along which the holonomy is applied, $\hat{J}_i^{(e,v)} D_k^{(j)m}(g) = -i(\tau_i^{(j)})_n^m D_k^{(j)n}(g)$ when e is incoming to v and $\hat{J}_i^{(e,v)} D_k^{(j)m}(g) = iD_n^{(j)m}(g)(\tau_i^{(j)})_k^n$ when e is outgoing from v , otherwise $\hat{J}_i^{(e,v)} D_k^{(j)n}(g) = 0$.

We define $\hat{W}_{\{e_\alpha, e_\beta, e_\gamma\}}^{(v)} = \eta^{ijk} \hat{J}_i^{(e_\alpha, v)} \hat{J}_j^{(e_\beta, v)} \hat{J}_k^{(e_\gamma, v)}$, where η^{ijk} is the structure constant of su(2) and $\{e_\alpha, e_\beta, e_\gamma\}$ is a set of links meeting at the node v . Following Ref. [37], we define the operator $\hat{Q} = (1/48) \sum_{\{e_\alpha, e_\beta, e_\gamma\}} \kappa(\{e_\alpha, e_\beta, e_\gamma\}) \hat{W}_{\{e_\alpha, e_\beta, e_\gamma\}}^{(v)}$, where

$\kappa(\{e_\alpha, e_\beta, e_\gamma\})$ is a factor that usually depends on the regularization scheme. Through a process of averaging, $\kappa(\{e_\alpha, e_\beta, e_\gamma\})$ can be made independent of the regularization, assuming values ± 1 depending on the relative orientation of the mutually perpendicular links in its argument (with respect to the natural orientation of reference frames on the manifold). For the sake of simplicity, we equivalently assume from here on that in 3D $\kappa(\{e_\alpha, e_\beta, e_\gamma\}) = 6$ whenever the set $\{e_\alpha, e_\beta, e_\gamma\}$ has an ascending index order and $\kappa(\{e_\alpha, e_\beta, e_\gamma\}) = 0$ otherwise (note, e.g., that for $\{e_1, e_2, e_3\}$ there are six ordering choices, three for which $\kappa = 1$ and three with $\kappa = -1$, but in this last case a rearrangement in the indices of η_{ijk} gives an extra factor of -1), while in 4D $\kappa(\{e_2, e_3, e_4\}) = \kappa(\{e_1, e_2, e_4\}) = 6 = -\kappa(\{e_1, e_2, e_3\}) = -\kappa(\{e_1, e_3, e_4\})$, and $\kappa(\{e_\alpha, e_\beta, e_\gamma\}) = 0$ otherwise [38]. The volume operator for a single node is then given by $\hat{V} = V'_0 \sqrt{|\hat{Q}|}$ (or

a sum thereof over different nodes, for general spinnetworks), where V'_0 differs from V_0 by a numerical factor extracted from $\sqrt{|\hat{Q}|}$.

The structure constant in $\hat{W}_{\{e_\alpha, e_\beta, e_\gamma\}}^{(v)}$, which is given by the Levi-Civita symbol, can be graphically represented by a 3-valent node with spin-1 links up to a factor of $i\sqrt{6}$, which we include into V'_0 together with the $1/48$ factor arising from \hat{Q} . The operator $\hat{W}_{\{e_\alpha, e_\beta, e_\gamma\}}^{(v)}$ can therefore be represented by three grasps [cf. Eq. (26)], connected via spin-1 links to a single node.

We first consider the action of $\hat{W}_{\{e_\alpha, e_\beta, e_\gamma\}}^{(v)}$ on a 3-valent spinnetwork previously modified by a holonomy, as in the last row of Eq. (36) (with the Wigner matrix omitted). In this case

$$6^{-1/2} \hat{W} \begin{array}{c} m \\ + \\ | \\ j_1 \\ + \\ \swarrow \quad \searrow \\ a \quad b \end{array} = -i [m(m+1)(2m+1)a(a+1)(2a+1)b(b+1)(2b+1)]^{\frac{1}{2}} \begin{array}{c} m \\ + \\ | \\ j_1 \\ + \\ \swarrow \quad \searrow \\ a \quad b \end{array} \begin{array}{c} \nearrow \quad \searrow \\ 1 \quad 1 \\ + \quad + \\ \nearrow \quad \searrow \\ 1 \quad 1 \\ + \quad + \end{array} \quad (79)$$

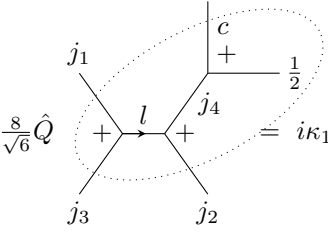
In Eq. (79), the three grasps are contracted with the spinnetwork links of spins a , b and m , while the temporary spin- $1/2$ link is “ignored” by the grasps. The orientation chosen for attaching the grasps follows the order of contraction of the indices assuming that holonomies for the spin- a , spin- b and spin- j_1 links are directed towards the node. Using Eq. (10), applied on the node with spins $\{m, 1/2, j_1\}$, the holonomy along the spin- j_1 link can be shifted to the links of spins m and $1/2$, both of which will be directed outwards from the node, resulting in an opposite order for the grasp with the spin- m link compared to the other two grasps. The prefactor in Eq. (79) comes from the three grasps [cf. Eq. (26)]. We can then factor out the spin-1 structure of the spinnetwork on the right-hand side of Eq. (79) as follows:

$$\begin{aligned}
& (-1)^{1+m+m} (-1)^{2m} \begin{array}{c} m \\ \downarrow + \\ 1 \curvearrowright \\ j_1 \\ \uparrow + \\ a \quad 1 \quad b \end{array} = (-1) \sum_k d_k (-1)^{m-j_1+1+\frac{1}{2}} \left\{ \begin{array}{c} m \quad \frac{1}{2} \quad k \\ j_1 \quad 1 \quad m \end{array} \right\} \begin{array}{c} m \\ \downarrow + \\ k \\ j_1 \\ \uparrow + \\ a \quad 1 \quad b \end{array} \\
& = (-1)^{1+2k+(k+1+j_1)} \sum_k d_k (-1)^{m-j_1+\frac{1}{2}+1} \left\{ \begin{array}{c} m \quad \frac{1}{2} \quad k \\ j_1 \quad 1 \quad m \end{array} \right\} \begin{array}{c} m \\ \downarrow + \\ k \\ j_1 \\ \uparrow + \\ a \quad 1 \quad b \end{array} \quad (80) \\
& = \sum_k d_k (-1)^{\frac{1}{2}+2a-k+m} \left\{ \begin{array}{c} m \quad \frac{1}{2} \quad k \\ j_1 \quad 1 \quad m \end{array} \right\} \left\{ \begin{array}{c} j_1 \quad 1 \quad k \\ a \quad 1 \quad a \\ b \quad 1 \quad b \end{array} \right\} \begin{array}{c} m \\ \downarrow + \\ j_1 \\ \uparrow + \\ a \quad b \end{array} .
\end{aligned}$$

In the first equality of Eq. (80), the arrows around the node joining the spins $\{m, 1/2, m\}$ have been rearranged using Eq. (9) and a braiding has been performed in the same node, moving the spin-1 link to the left. After changing the direction of $\epsilon^{(m)}$, giving a phase factor of $(-1)^{2m}$, the Pachner move, Eq. (20), gives the spinnetwork in the second equality of (80), in which the spin-1 has been braided back to the right side. Applying then Eq. (10) simultaneously to the nodes of spins $\{a, b, j_1\}$ and $\{k, 1, j_1\}$, as well as Eq. (5) to the spin- k link, allows us to get rid of all the arrows, obtaining the expression in the second row of Eq. (9). Finally, using relation (A2) (cf. Appendix A2), we can extract a hexagonal spinnetwork of the form (19), which is represented in the last row of Eq. (9) as a Wigner 9j symbol. It is worth noting that summation over k only covers the values j_1 or $j_1 \pm 1$, but the choice of sign is constrained by the value of m : if $m = j_1 + 1/2$, the Clebsch-Gordan conditions only allow $k = j_1$ or $k = j_1 + 1$. The Wigner 9j symbol has the interesting property that swapping any two of its columns or rows gives the unswapped symbol up to a phase factor of $(-1)^s$, with s being the sum of all entries of the symbol. For the 9j symbol in the last row of Eq. (9),

$s = 3 + 2a + 2b + j_1 + k$, while $a + b + j_1 \in \mathbb{N}$ by the gauge invariance of spinnetworks. This implies that, for $k = j_1$, swapping the rows or columns in the Wigner 9j symbol gives the same symbol multiplied by -1 . Therefore the symbol has to be zero. As a result, the action of the operator \hat{W} on the considered spinnetwork leads to two possible anti-Hermitian 2×2 matrices. One of them couples the spinnetworks with $k = j_1$ and $k = j_1 + 1$ for $m = j_1 + 1/2$, whereas the other couples the spinnetworks with $k = j_1 - 1$ and $k = j_1$ for $m = j_1 - 1/2$. It is easy to show that such matrices have two real eigenvalues with the same absolute value. Therefore, taking the square root of the absolute value of \hat{Q} gives a matrix proportional to the identity. The volume operator in this case acts diagonally.

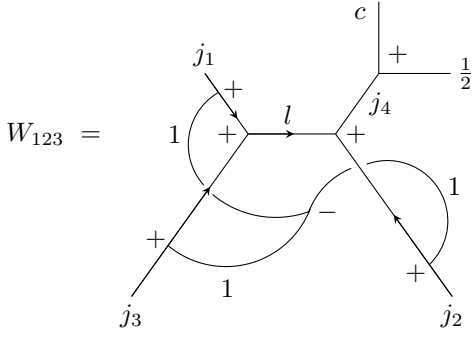
When we consider the volume operator acting on 4-valent nodes modified by a holonomy, we must account for the four possible ways in which $\{e_\alpha, e_\beta, e_\gamma\}$ can be chosen while neglecting the spin-1/2 link. Calling $W_{\alpha\beta\gamma}$ the action of $\hat{W}_{\{e_\alpha, e_\beta, e_\gamma\}}$ on the input spinnetwork up to prefactors, the action of \hat{Q} reads

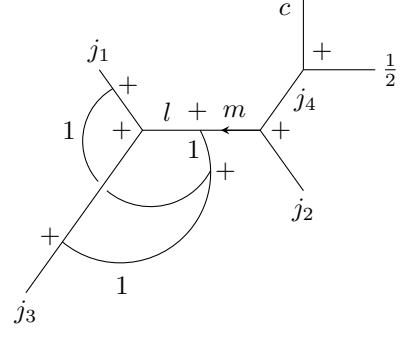


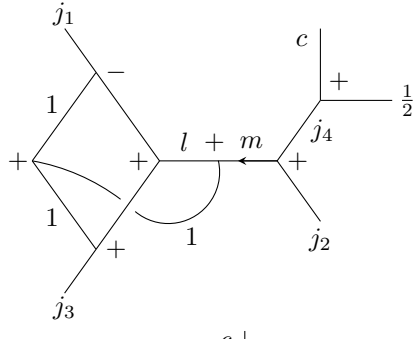
$$\frac{s}{\sqrt{6}} \hat{Q} = i\kappa_{123} L_{j_1} L_{j_2} L_{j_3} W_{123} - i\kappa_{134} L_{j_1} L_{j_3} L_c W_{134} - i\kappa_{124} L_{j_1} L_{j_2} L_c W_{124} - i\kappa_{234} L_{j_2} L_{j_3} L_c W_{234} \quad (81)$$

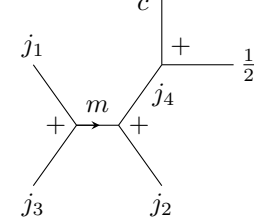
In this equation, the dotted ellipsis serves a mere illustrative purpose, crossing the links that can be acted upon by the grasps. We have used the notation $L_j = \sqrt{j d_{j/2} d_j}$ and $\kappa_{\alpha\beta\gamma} = \kappa(\{e_\alpha, e_\beta, e_\gamma\})/6$ (with $\kappa_{123} = \kappa_{134} = -1$ and $\kappa_{234} = \kappa_{124} = 1$). We initially consider any trio of links to be mutually perpendicular, so that a particularized discussion including embedding or other geometric arrangements implies neglecting some of these terms or introducing geometric prefactors.

The first contribution to the right-hand side of Eq. (81) is



$$W_{123} = (-1)^{2l} \sum_m (-1)^{1-j_4+j_2+l} d_m \begin{Bmatrix} 1 & l & m \\ j_4 & j_2 & j_2 \end{Bmatrix} (-1)^{1+2j_2} (-1)^3$$


$$= (-1)^{1+2j_1} (-1)^{1+2j_3} \sum_m (-1)^{1-j_2-j_4-l} d_m \begin{Bmatrix} 1 & l & m \\ j_4 & j_2 & j_2 \end{Bmatrix}$$


$$= \sum_m d_m (-1)^{1+2j_1-j_2+2j_3-j_4-l+2m} \begin{Bmatrix} 1 & l & m \\ j_4 & j_2 & j_2 \end{Bmatrix} \begin{Bmatrix} l & 1 & m \\ j_1 & 1 & j_1 \\ j_3 & 1 & j_3 \end{Bmatrix}$$


Note that, given our choice of labels for the links of the spinnetwork, the grasps for the links of spins j_2 and j_3 have to be braided, causing the node that joins the grasps to have a negative or clock-wise cyclicity. Braiding the spin-1 link around the spin- j_2 one (around the node joining the spins $\{1, j_2, j_2\}$, where the second grasp has been attached) gives a phase factor of $(-1)^{1+2j_2}$ and allows us to use Eq. (20) along the link containing $\epsilon^{(j_2)}$ to obtain the spinnetwork in the second row of Eq. (82). Simultaneously, we can use Eq. (10) in the node of spins $\{j_1, j_3, l\}$ to transfer the arrows to the spin- l link, and then remove its doubled $\epsilon^{(l)}$ via Eq. (5). We also change the cyclic orientation of the other two nodes where the other grasps were attached. Using the resolution of the identity [Eq. (A1) in Appendix A], we can factor out the additional structures in the penultimate row of Eq. (82), obtaining the result in the last row, where the input spinnetwork graph is recovered.

The second contribution, W_{134} , contains a grasp in the spin- c link, which, as previously explained, has its Wigner matrix oriented outwards from its node, since the spin- j_4 link has a Wigner matrix oriented toward the node of spins $\{l, j_2, j_4\}$. The corresponding contribution reads

$$\begin{aligned}
W_{134} &= \text{Diagram 1} \\
&= (-1)^{2l} (-1)^{1+4c} \sum_k d_k (-1)^{c-j_4+1+\frac{1}{2}} \left\{ \begin{matrix} c & \frac{1}{2} & k \\ j_4 & 1 & c \end{matrix} \right\} \text{Diagram 2} \\
&= \sum_k d_k (-1)^{2l+c-j_4+\frac{1}{2}} \left\{ \begin{matrix} c & \frac{1}{2} & k \\ j_1 & 1 & c \end{matrix} \right\} \sum_m d_m (-1)^{l-p+j_2+1} \left\{ \begin{matrix} l & 1 & m \\ k & j_2 & j_4 \end{matrix} \right\} + \text{Diagram 3} \\
&= \sum_{m,k} d_m d_k (-1)^{2j_1+j_2+2j_3+j_4+\frac{1}{2}+c+k-m} \left\{ \begin{matrix} c & \frac{1}{2} & k \\ j_4 & 1 & c \end{matrix} \right\} \left\{ \begin{matrix} l & 1 & m \\ k & j_2 & j_4 \end{matrix} \right\} \left\{ \begin{matrix} l & 1 & m \\ j_1 & 1 & j_1 \\ j_3 & 1 & j_3 \end{matrix} \right\} \text{Diagram 4}
\end{aligned} \tag{83}$$

Between the first and second rows of Eq. (83), we have braided the spin-1 link around the spin- c one [cf. Eq. (9)], while also employing Eqs. (10) and (5) to move $\epsilon^{(c)}$ to the links connected with it through the node of spins $\{c, c, 1\}$, picking up a phase [namely, $(-1)^{1+c+c}$ from the braiding and $(-1)^{2c}$ from the cancellation of a doubled arrow]. Equation (20) then allows us to move leftward the attachment point of the spin-1 link related to the rightmost grasp. A similar combination of Eqs. (10) and (5) applied to the node joining the spins $\{l, j_1, j_3\}$ converts $\epsilon^{(j_1)}$, $\epsilon^{(j_3)}$ and $\epsilon^{(l)}$ into a phase factor of $(-1)^{2l}$. These operations lead to the spinnetwork in the second row of Eq. (83). Using Eq. (10) to convert $\epsilon^{(k)}$ and $\epsilon^{(1)}$ into $\epsilon^{(j_4)}$, a second application of Eq. (20) on the spin- j_4 link, followed by a swap of cyclic order in the node of spins $\{j_1, 1, j_1\}$ and braids on the other two spin-1 links, gives the third row of the equation. Finally, Eq. (A2) allows us to factor out a term of the form (19), and flipping $\epsilon^{(m)}$ results in the last row of Eq. (83).

The next term is given by

$$\begin{aligned}
W_{124} &= \text{Diagram 1} \\
&= (-1)^{1+2c} (-1)^{1+2j_1} \sum_k d_k (-1)^{j_4 - c + \frac{1}{2} + 1} \left\{ \begin{matrix} j_4 & 1 & k \\ c & \frac{1}{2} & c \end{matrix} \right\} \text{Diagram 2} \\
&= \sum_k d_k (-1)^{j_4 + c - \frac{1}{2} + 2j_1} \left\{ \begin{matrix} j_4 & 1 & k \\ c & \frac{1}{2} & c \end{matrix} \right\} \sum_m d_m (-1)^{1 - j_3 + j_1 + l} \left\{ \begin{matrix} 1 & l & m \\ j_3 & j_1 & j_1 \end{matrix} \right\} \text{Diagram 3} \\
&= \sum_{k,m} d_k d_m (-1)^{-j_1 + 2j_2 - j_3 + 2j_4 + \frac{1}{2} + l + k + c} \left\{ \begin{matrix} j_4 & 1 & k \\ c & \frac{1}{2} & c \end{matrix} \right\} \left\{ \begin{matrix} 1 & l & m \\ j_3 & j_1 & j_1 \end{matrix} \right\} \left\{ \begin{matrix} l & 1 & m \\ j_2 & 1 & j_2 \\ j_4 & 1 & k \end{matrix} \right\} \text{Diagram 4}
\end{aligned} \tag{84}$$

As in Eq. (83), the passage from the first to the second row of Eq. (84) involves a braiding of the spin-1 link around the spin- c one [cf. Eq. (9)], picking up a phase $(-1)^{1+c+c}$, followed by the application of Eqs. (10) and (4) to move $\epsilon^{(c)}$ to the links connected with it through the node of spins $\{c, c, 1\}$. Equation (20) permits us to reallocate the corresponding spin-1 link. Analogously, braiding the spin-1 link around the spin- j_1 one gives a phase $(-1)^{1+j_1+j_1}$. The resulting spinnetwork is given in the second row of Eq. (84). We can then use Eq. (20) on the link containing

$\epsilon^{(j_1)}$ and combine $\epsilon^{(j_2)}$ and $\epsilon^{(l)}$ into $\epsilon^{(j_4)}$ employing Eq. (10) (this gathers the arrows on a single node, allowing them to be effectively removed). The spinnetwork in the third row is then obtained after performing a braiding at the node joining the spins $\{j_4, k, 1\}$. The final expression is reached by factoring out a term of the form (19) by employing Eq. (A2), recovering in this way the input spinnetwork graph.

The last contribution to the action of \hat{Q} on the modified 4-valent nodes is

$$\begin{aligned}
 W_{234} &= \text{Diagram 1} \\
 &= \sum_m d_m (-1)^{j_3 - l + 1 + j_1} \left\{ \begin{matrix} j_3 & j_1 & m \\ l & 1 & j_3 \end{matrix} \right\} (-1)^{1+2c} (-1)^3 \text{Diagram 2} \\
 &= \sum_m d_m (-1)^{j_1 + j_3 - l + 1 + 2c} \left\{ \begin{matrix} j_3 & j_1 & m \\ l & 1 & j_3 \end{matrix} \right\} \\
 &\quad \times \sum_k d_k (-1)^{j_4 - c + \frac{1}{2} + 1} \left\{ \begin{matrix} j_4 & 1 & k \\ c & \frac{1}{2} & c \end{matrix} \right\} (-1)^{2m + (m+l+1)} \text{Diagram 3} \\
 &= \sum_{m,k} d_m d_k (-1)^{j_1 + 2j_2 + j_3 + 2j_4 - \frac{1}{2} + c + k - m} \left\{ \begin{matrix} j_3 & j_1 & m \\ l & 1 & j_3 \end{matrix} \right\} \left\{ \begin{matrix} j_4 & 1 & k \\ c & \frac{1}{2} & c \end{matrix} \right\} \left\{ \begin{matrix} l & 1 & m \\ j_2 & 1 & j_2 \\ j_4 & 1 & k \end{matrix} \right\} \text{Diagram 4}
 \end{aligned}
 \tag{85}$$

Between the first and second rows of Eq. (85), we have performed a braiding of the spin-1 link around the

spin- c one [cf. Eq. (9)], followed by the application of Eqs. (10) and (4) to move $\epsilon^{(c)}$ to the links connected with it through the node of spins $\{c, c, 1\}$, picking up a phase $(-1)^{1+c+c}$. We have used Eq. (20) on the link containing $\epsilon^{(j_3)}$ and combined $\epsilon^{(j_2)}$ and $\epsilon^{(l)}$ into $\epsilon^{(j_4)}$ by means of Eq. (10). Inverting the cyclic order around the node connecting the grasps gives a -1 prefactor. This has led to the expression in the second row of Eq. (85). We have then applied Eq. (20) to the link containing $\epsilon^{(c)}$ and performed braidings at the nodes joining the spins $\{j_4, k, 1\}$ and $\{m, l, 1\}$, flipping also $\epsilon^{(m)}$. The final expression has been derived by factoring out a term of the form (19) by means of Eq. (A2), a procedure that allows us to recover the input spinnetwork graph.

Normalization of spinnetworks results in the change $d_m d_k \rightarrow \sqrt{d_l d_{j_4} d_m d_k}$ in Eqs. (82)-(85). Once these equations have been introduced into Eq. (81), the matrix elements of \hat{Q} can be calculated between spinnetworks with spins $\{l, j_4\}$ at the input and $\{m, k\}$ at the output, for every choice of these spins that fulfills triangularity with respect to the fixed ‘‘external’’ spins j_1, j_2, j_3 and c . Since $c = j_4 \pm 1/2$, its value also determines the admissible values for k when the Wigner 6j symbols are taken into account. In more detail, since both $\{k, 1, j_4\}$ and $\{c, 1/2, k\}$ must fulfill triangularity, $c = j_4 \pm 1/2$ implies that $k \in \{j_4, j_4 \pm 1\}$ (the choice of plus or minus is fixed by the value of c). There are, therefore, two choices of k for each c . The values that m can assume depend on the spins $\{j_1, j_2, j_3, j_4, k\}$, but since k can take different values on its own, we consider $|j_1 - j_3| \leq m \leq j_1 + j_3$, what gives $2 \min\{j_1, j_3\} + 1$ possible values. The matrix representing \hat{Q} has therefore dimension $2(2 \min\{j_1, j_3\} + 1)$. Once the i factor is included, this matrix can be diagonalized to give a matrix of purely real eigenvalues. The square root of their absolute values gives the volume matrix when the inverse diagonalizing unitaries are used.

Since we are also interested in the expectation values of the volume operator, we still need to calculate its action on spinnetworks that have not been modified by holonomies. For the 3-valent case [as in Eq. (32)], it is easy to show that the volume operator always gives zero [18, 32]. When the volume operator is applied on spinnetworks of the form (34), however, it acts in a non-trivial manner that differs both from Eqs. (79) and (81), because now all of the four links connected with the intertwiner can be grasped (as long as they are mutually perpendicular). In terms of the spinnetwork (34), only the links of spins j_1, a, b and j_4 will be grasped, because the two 3-valent nodes give zero contributions to the volume. The action of the volume operator can be derived in a similar manner to what was done in Eqs. (81)-(85), having four grasp arrangements when 4-valent nodes are considered. A much simpler derivation, however, can be obtained by setting the spin of the temporary link in the spinnetwork on the left-hand side of Eq. (81) to zero and using Eq. (11) [39]. Therefore, we omit the re-derivation of the action of the volume operator for a 4-valent intertwiner. A general derivation of the action of the volume

operator on vertices of arbitrary valency can be found in Ref. [23], and its spectral analysis when acting on nodes of valency up to 7 can be found in Ref. [40].

IX. NUMERICAL IMPLEMENTATION OF THE SCALAR CONSTRAINT AND THE VOLUME OPERATOR

The analytical discussion presented in Secs. VI and VII shows the complexity of the action of the scalar constraint on spinnetworks. Even though this action is confined to the vicinity of the nodes of the spinnetworks, the changes it induces forces us to consider a rapidly growing set of spinnetworks with different graph structures and different spin attributions to their links. It is well known that these complications render the study of the scalar constraint in LQG almost unfeasible with currently available analytical and numerical tools [27]. As a consequence, many questions still remain open in the field. As a remedy, approximations like the graph-preserving ones have been proposed, yet the regime of validity of most of these approximations (or even their validity overall) remains obscure.

As an effort to understand the graph-changing properties of Eq. (1) and to overcome some of the problems imposed by its action on spinnetworks, we develop here a new numerical approach that allows us to apply Eq. (1) on 3-valent and 4-valent spinnetworks without resorting to approximations. With this aim, we have implemented this new numerical framework as a code in Mathematica (available in Ref. [41]), but we believe that it can similarly be implemented (and potentially further optimized) in other programming languages and computational softwares.

A key idea of our approach is encoding spinnetworks in a way that numerical tools can easily understand and process. Graphical input and output are rather unpractical and resource consuming, yet we must store information not only about spins assigned to links, but also about the (constantly changing) arrangement of these links on a substrate manifold (or, more generally, their adjacency relations). We therefore fix a certain valency, and consider either three or four external legs (the outermost links) such that their internal structures can accommodate a, in principle, arbitrarily large number of inner loops ordered in terms of proximity to the central virtual link. This spin and location information is stored as ordered lists, each being in one-to-one relation (up to a padding of zeros) with a given spinnetwork (see further discussion for details). Spanning a vector space out of these lists is, however, not possible in a direct manner, and for this reason we instead adopt a vector space of functions for which the arguments are these lists. The functions are never truly defined (i.e., at no point during the computation they are assigned a functional form), and for this reason we call them ghost functions. All needed information for

the computation is stored in the arguments of ghost functions. These arguments can have arbitrary sizes and the orthogonality relations of ghost functions are only based on whether their arguments coincide. If $s_i = \{s_{i,1}, s_{i,2}, \dots\}$ denotes lists encoding the spin and structural information of distinct (normalized) spinnetworks, the inner product I on functions $f(s_i)$ is defined so that $I[f(s_i)|f(s_j)] = \delta_{i,j}$. The scalar constraint is then included in our code as a linear functional C_s that acts on the ghost functions by reading and manipulating their arguments, i.e., $C_s[f(s_i)] = \sum_j c_j(s_i)f(s_j)$ for coefficients c_j taken from Eqs. (49) or (77) and (78) for 3-valent or 4-valent spinnetworks, respectively. Linearity implies then that $C_s[\sum_i c_i f(s_i)] = \sum_i c_i C_s[f(s_i)]$, so that the constraint functional can be used recursively, e.g., to generate perturbative outputs.

Let us start with the discussion of the functional for 4-valent spinnetworks, since this is the most relevant and intricate case. We do not constrain ourselves to the consideration of structures of the form (34), but instead assume that we start with a spinnetwork with four external legs, an inner virtual link and an arbitrary number of inner loops. The inner loops can be arranged in six different ways, by connecting links belonging to each possible pair of directions (say, p_1, p_2, p_3 or p_4 according to our previous notation). We label the locations of such inner loops from 1 to 6, corresponding to inner loops connecting the links along the pairs of directions $\{p_1, p_3\}$, $\{p_2, p_3\}$, $\{p_2, p_4\}$, $\{p_1, p_4\}$, $\{p_1, p_2\}$ and $\{p_3, p_4\}$, respectively [cf. Fig. 2(a)]. One important thing is that the presence of certain inner loops affects the ways in which Eq. (1) can attach new inner loops. If a loop is present in location 1 (placed between directions p_1 and p_3), for example, the scalar constraint attaches a new loop in the same location by coupling its holonomies with the already existing loop links, leading to no change in the graph structure, but changing the spins attributed to these links (unless the spin of the connecting link is reduced to zero, which effectively changes the graph by removing the loop). On top of that, the Hamiltonian also applies holonomies to form inner loops in the locations 2, 3, 4, 5 and 6, but the presence of a loop in location 1 means that loops in locations 2, 4, 5 and 6 (which share a common link with loop 1) would have to be introduced further inwards (or closer to the node) relative to the location-1 loop, while the introduction of a loop in location 3 is completely unaffected by this subtlety. A diagrammatic representation of these loop-attachment relations is shown in Fig. 2(b) in the form of a pseudocode, which also summarizes our implementation of C_s . As a consequence of these relations, recursive application of Eq. (1) leads to structures with increasingly deeper inner loops, with depths that depend on the positions of outer loops.

We choose our spinnetwork encoding lists to have the first four entries representing the spins of the four outermost links: j_1, j_2, j_3 and j_4 , following the convention of Eq. (34). These values are fixed and unaffected by the functional C_s , but should be stored in the list for the pur-

pose of normalization after Eq. (1) is applied a desired number of times. The next four entries in the list are the four innermost spins adjacent to the central virtual link along directions p_1, p_2, p_3 and p_4 , which will be affected by the scalar constraint [e.g., j_1, b, a and j_4 in Eq. (34)]. The 9th entry is the spin of the central virtual link. If the spinnetwork has no inner loops, all remaining entries in the list are zero. For spinnetworks containing inner loops, the innermost loop will occupy the next four entries of the list, and every following loop, in decreasing order of depth, will be described by four additional entries. From each such quadruple of entries, the first two store the location of the loop and the spin of the connecting link of the loop, while the other two store the spins adjacent to the loop along the directions that the loop connects [e.g., $2, \varepsilon, j_2$ and j_3 for the loop in Eq. (34)]. The spinnetwork (34) would therefore correspond to the list $\{j_1, j_2, j_3, j_4, j_1, b, a, j_4, i, 2, \varepsilon, j_2, j_3, 0, \dots, 0\}$, where the zero padding should be chosen in such a way as to accommodate as many inner-loop entries as one intends to recursively apply the Hamiltonian constraint. The size of the lists should be fixed prior to any calculations, so that orthogonality relations can be properly applied.

The action of the functional C_s reorganizes the lists contained as arguments in the ghost functions according to all p_i -direction permutations of Eqs. (77) and (78). When it creates a new inner loop, it effectively moves all list entries from 10th onward to the right by four entries, so that entries corresponding to inner loops are now moved down in depth order for the data corresponding to a new loop to be included. The new spins immediately adjacent to the central nodes are encoded in entries 5 to 8, and the new central spin becomes the 9th entry. Entries 10 to 13 receive the information about the added innermost loop, according to our loop-description convention. In this manner, the zero padding in the lists is gradually filled from the left with inner-loop information as new loops are included in the spinnetwork by the action of the scalar constraint. As an example, if we add a new loop in location 1 to the spinnetwork (34), its list will change to $\{j_1, j_2, j_3, j_4, c, b, d, j_4, k, 1, \gamma, j_1, a, 2, \varepsilon, j_2, j_3, 0, \dots, 0\}$, where c and d are the new innermost spins along directions p_1 and p_3 , respectively, k is the new central spin and γ is the connecting spin of the new loop at location 1. Although the spinnetworks and their encoding lists become increasingly complicated with each application of Eq. (1), only the two deepest inner loops of a 4-valent node-like spinnetwork are acted upon by the Hamiltonian. Since in our encoding the information about these two loops is stored between the 5th and 17th entries of the list, the coefficients $c_j(s_i)$ in $C_s[f(s_i)] = \sum_j c_j(s_i)f(s_j)$ depend only on these entries of the input ghost-function argument, avoiding the search for entries scattered among large lists (in fact, the size of the list does not affect the Hamiltonian functional).

It turns out that the constraint functional might output the same spinnetwork with different coefficients as independent terms in a linear combination, what slows re-

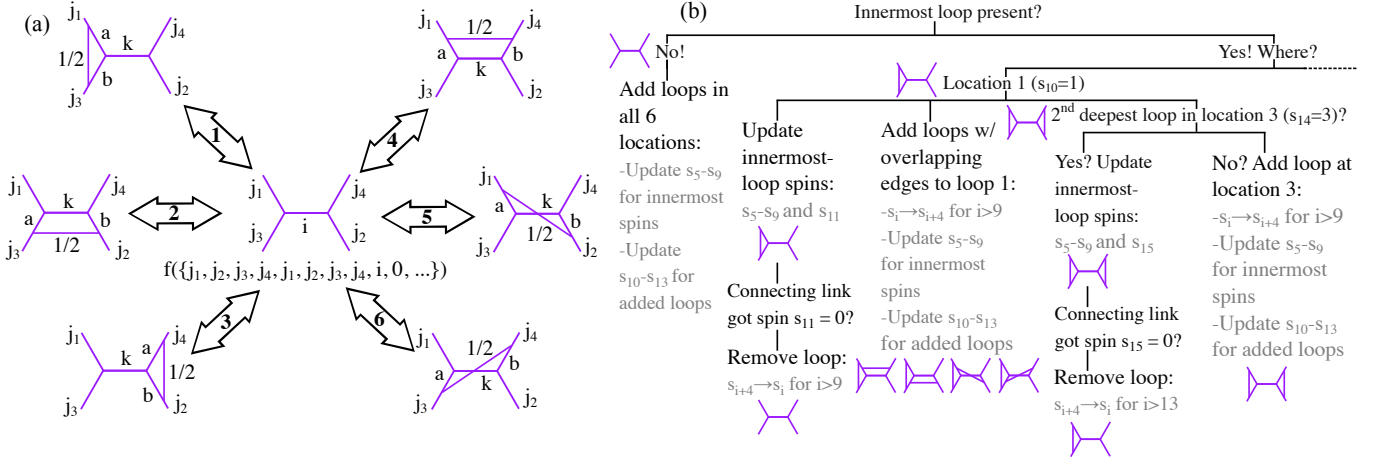


FIG. 2. (a) Schematic representation of the graphical changes introduced by the Hamiltonian constraint on 4-valent node-like spinnetworks. The central spinnetwork contains its encoding function represented below. The rest of spinnetworks, differing from the central one by the addition of an inner loop at the location indicated within the arrows, are represented by the functions $f(\{j_1, j_2, j_3, j_4, a, j_2, b, j_4, k, 1, 1/2, j_1, j_3, 0, \dots, 0\})$, $f(\{j_1, j_2, j_3, j_4, j_1, b, a, j_4, k, 2, 1/2, j_2, j_3, 0, \dots, 0\})$, $f(\{j_1, j_2, j_3, j_4, j_1, b, j_3, a, k, 3, 1/2, j_2, j_4, 0, \dots, 0\})$, $f(\{j_1, j_2, j_3, j_4, a, j_2, j_3, b, k, 4, 1/2, j_1, j_4, 0, \dots, 0\})$, $f(\{j_1, j_2, j_3, j_4, a, b, j_3, j_4, k, 5, 1/2, j_1, j_2, 0, \dots, 0\})$ and $f(\{j_1, j_2, j_3, j_4, j_1, j_2, a, b, k, 6, 1/2, j_3, j_4, 0, \dots, 0\})$, respectively for loop insertions at positions 1, 2, 3, 4, 5 and 6. (b) Pseudocode for the Hamiltonian implementation. The code checks whether an inner loop is present. If absent, it introduces inner loops in all six locations, with spin $1/2$ on the newly created link. If present, for each possible location, a series of steps are followed. The case for location 1 is shown, while for other locations the dashed-line continuation of the diagram implies the presence of similar rules not shown. The corresponding innermost loop has its spins shifted by all allowed values without graph changes, and if the connecting link reaches spin 0, it is removed, and the inner-loop data in the corresponding list is shifted to the left by four entries. Additionally, inner loops are added to all other positions, but if a loop was added at position 3 right before adding one at position 1 (these loops share no links), it is again possible to remove its extra link or simply change its spin. The diagram contains examples for the simplest spinnetworks for which the rules apply.

cursive application of the Hamiltonian by forcing its functional to evolve the same spinnetwork multiple times. To remedy that, consecutive applications of the constraint functional are intercalated by a “collector” functional (inbuilt in Mathematica as “Collect[]” command) that collects all coefficients of the same spinnetwork into one.

The Hamiltonian acts on and also generates non-normalized spinnetworks, so normalization takes place after C_s has been recursively applied a number of times, and denormalization is employed prior to any calculations if one decides to start with normalized spinnetworks. We have developed a “normalizer” functional, which linearly implements the normalization discussed in Sec. V according to the formula $f(s_i) \rightarrow [d_{j_1} d_{j_2} d_{j_3} d_{j_4} \prod_k d_k^{-1}] f(s_i)$, where d_{j_i} is associated with the outermost legs and k runs over the spins of all links in the spinnetwork, including the outermost ones (so that they effectively cancel out from the normalization factor). To achieve this, the normalizer reads the first six entries of each ghost-function argument list, as well as the j -th, $(j-1)$ -th and $(j-2)$ -th entries for $j = 4n + 9$ ($n \in \mathbb{N}$). Note that the zero padding does not contribute since $d_0 = 1$. Similarly, a “denormalizer” functional has been implemented to perform the inverse of the normalizer functional.

After normalization has been performed, one can either calculate inner products or act with observables on

the output states in order to estimate expectation values. As key observable of our work, we have implemented a quantum-volume functional, which generates matrices depending on the input spinnetworks. Note that the volume operator only sees the innermost spins in the spinnetwork, i.e., those closest to the node. These spins determine the size of the matrix \hat{Q} generated by the volume operator. Since the volume operator maps a 4-valent spinnetwork with central spin i to a linear combination of 4-valent spinnetworks with all possible central spins, the size of the matrix it generates runs from $|j'_1 - j'_3|$ to $j'_1 + j'_3$ (for innermost spins j'_1, j'_2, j'_3 and j'_4), and the indices are the input and output spin values of the central link. Note that this is equivalent to considering the range of spins from $\max\{|j'_1 - j'_3|, |j'_2 - j'_4|\}$ to $\min\{j'_1 + j'_3, j'_2 + j'_4\}$, since for $|j'_1 - j'_3| < |j'_2 - j'_4|$ and/or $j'_1 + j'_3 > j'_2 + j'_4$ the matrix we generate contains the actual volume matrix as a block, and the remaining elements are all zero. Following the calculations in Sec. VIII, the \hat{Q} matrix is generated according to Eq. (81), and the resulting matrix is diagonalized, so that the square root of the absolute value of its entries can be taken before applying the inverse of the diagonalizing transformation. The resulting matrix is the volume operator in a basis of 4-valent spinnetwork states, and can be turned into a linear functional V by using its matrix elements as coefficients of the output linear combination, $V[f(s_i)] = \sum_j V_{j,i} f(s_j)$.

Finally, the inner product is introduced as a functional I that is antilinear in its first argument and linear in its second one,

$$I\left[\sum_i c_i f(s_i), \sum_j d_j f(s_j)\right] = \sum_{i,j} c_i^* d_j I[f(s_i), f(s_j)]. \quad (86)$$

Once two (linear combinations of) normalized spinnetworks are given in the form of ghost functions with suitable list arguments, the inner-product functional evaluates the orthonormality based on the criterion of whether the lists in the arguments of the functions are the same (i.e., $I[f(s_i), f(s_j)] = \delta_{i,j}$, as defined above).

For 3-valent node-like spinnetworks, we use a similar scheme for encoding graphs and spins as lists. The first three entries of the list carry the information about the spins of the outermost links of the spinnetwork following counter-clockwise order starting from the top [e.g., for the spinnetwork (32) these would be j_1, j_2 and j_3]. The following three entries correspond to the counter-clockwise ordered innermost spins [once again, for the spinnetwork (32) these would be j_1, a and b]. For each inner loop in descending order of depth we assign groups of four entries, starting at position 7 in the ordered list. In each of these quadruples, the first entry indicates the position of the inner loop (1 for upper left, 2 for bottom and 3 for upper right). The second entry stores the spin of the bridging link in this loop and the remainder entries give the spins of the links adjacent to (but not included in) the loop. The scheme is similar to the one introduced for 4-valent node-like spinnetworks, and allows us to implement the scalar constraint as a functional acting on the arguments of ghost functions. When it creates a new inner loop, it effectively moves all list entries from 7th onward to the right by four entries, so that entries corresponding to inner spins are now moved down in depth for the data corresponding to a new loop to be included. The new spins immediately adjacent to the node are encoded in entries 4 to 6, while entries 7 to 10 receive the information about the new innermost loop.

X. RESULTS

Our numerical approach allows us to investigate a variety of properties of the scalar constraint. One of the open questions regarding the operator (1) is finding its zero-eigenvalue eigenstates, since these ultimately span the space of physical states in LQG. A solution to Eq. (1) was given in Ref. [26], although the corresponding derivation was based on an incomplete application of the scalar constraint on 4-valent spinnetworks. In Ref. [42] it was shown that, in the cosmological symmetry-reduced case where a massless scalar field serves as relational clock variable, solutions to the scalar constraint of the joint matter and gravitational fields in a certain region of phase space can be given by cylindrical functions generated from transformed wave functions depending solely

on the Ashtekar-Barbero one-form. Furthermore, in Ref. [43] it was shown that when the quantum-deformed Temperley-Lieb algebra is considered, certain states generated through transforms with a Chern-Simons kernel are eigenstates of the (deformed) Thiemann's Hamiltonian constraint. Using our code, which allows to implement the scalar constraint acting on spinnetworks of the forms (32) and (34) with arbitrary spins assigned to their links, we have searched for zero-eigenvalue solutions of Eq. (1). Our protocol is based on “For” loops (a routine that runs a section of code repeatedly while varying some parameters) covering all possible spin values within a certain range on each of the links besides the one containing a Wigner matrix, for which the spin is fixed at zero. States that are not gauge invariant are excluded from the search, since they violate one of the LQG constraints. Whenever $C_s[f(s_i)] = 0$ for a certain s_i within the search range, our protocol prints the corresponding spin assignments that led to this result. For spinnetworks of the form (32), we vary each of the spins $j_1, j_2, j_3 \in \mathbb{N}/2$ from 0 to $7/2$ while keeping $\varepsilon = 0$ (therefore $a = j_2$ and $b = j_3$). The only spin values for which the condition $C_s[f(s_i)] = 0$ is fulfilled are $j_1 = j_2 = j_3 = 0$. Additional numerical data for spinnetworks with more inner loops suggest that any spinnetwork with zero innermost spins connected to the 3-valent intertwiner is also an eigenstate of Eq. (1) with null eigenvalue. By inspecting Eq. (49) we can easily understand and generalize these results. If we set, e.g., $j_1 = a = b = 0$ for the input (32), we see that the two terms within square brackets in that equation turn out to be equal and cancel out [cf. also Eq. (21)]. The \mathcal{C}_3 rotational symmetry at the innermost-node level assures that the result extends to the three possible ways of inserting an inner loop.

Running the search protocol on spinnetworks of the form (34) with no embedding and $\varepsilon = 0$ (i.e., allowing for all possible terms derived in Sec. VII) reveals that the same single family of eigenstates of the Hamiltonian with $j_1 = j_2 = j_3 = j_4 = i = 0$ can be found. Not surprisingly, when we assume that the link along the direction p_4 does not participate in the action of the Hamiltonian [i.e., considering a (re-)embedding of the spinnetwork in a 3D manifold that does not include the direction p_4], we get the same zero-eigenvalue family of eigenstates of the Hamiltonian. These eigenstates have no volume, since their innermost spins are all zero, yet, due to their possible “shielding” by inner loops with nontrivial spins, they can still have nonzero areas, and hence these eigenstates might potentially serve as boundaries.

When acting on any single spinnetwork or on a linear combination of spinnetworks that cannot be generated from one another by inner-loop couplings, the Hamiltonian generates a linear combination of spinnetworks that has no overlap with the input state. In fact, starting from a certain $|s_0\rangle$ for which $\hat{C}_s|s_0\rangle = c_1^*|s_1\rangle$ (e.g., a state from which one cannot remove inner loops), if we denote the (normalized linear combinations of) states generated by i loop insertions as $|s_i\rangle$, with $\langle s_i|s_j\rangle = \delta_{i,j}$, we

have $\hat{C}_s|s_i\rangle = c_i|s_{i-1}\rangle + c_{i+1}^*|s_{i+1}\rangle = \langle s_{i-1}|\hat{C}_s|s_i\rangle|s_{i-1}\rangle + \langle s_{i+1}|\hat{C}_s|s_i\rangle|s_{i+1}\rangle$. From this relation and any suitable

$|s_0\rangle$, containing intertwiners of any valency, we can generate the following solution of the Hamiltonian constraint:

$$|E_0\rangle = |s_0\rangle - \frac{\langle s_1|\hat{C}_s|s_0\rangle}{\langle s_1|\hat{C}_s|s_2\rangle}|s_2\rangle + \frac{\langle s_1|\hat{C}_s|s_0\rangle\langle s_3|\hat{C}_s|s_2\rangle}{\langle s_1|\hat{C}_s|s_2\rangle\langle s_3|\hat{C}_s|s_4\rangle}|s_4\rangle + \dots = \sum_{i \text{ even}} (-1)^{i/2} \frac{\langle s_1|\hat{C}_s|s_0\rangle \dots \langle s_{i-1}|\hat{C}_s|s_{i-2}\rangle}{\langle s_1|\hat{C}_s|s_2\rangle \dots \langle s_{i-1}|\hat{C}_s|s_i\rangle} |s_i\rangle. \quad (87)$$

Although it is not clear whether this state can be normalized, it is easy to check that it is annihilated by the action of Eq. (1),

$$\hat{C}_s|E_0\rangle = \sum_{i \text{ even}} (\dots) \left[\frac{\langle s_{i-1}|\hat{C}_s|s_{i-2}\rangle}{\langle s_{i-1}|\hat{C}_s|s_i\rangle} \langle s_{i+1}|\hat{C}_s|s_i\rangle |s_{i+1}\rangle - \frac{\langle s_{i-1}|\hat{C}_s|s_{i-2}\rangle \langle s_{i+1}|\hat{C}_s|s_i\rangle}{\langle s_{i-1}|\hat{C}_s|s_i\rangle \langle s_{i+1}|\hat{C}_s|s_{i+2}\rangle} \langle s_{i+1}|\hat{C}_s|s_{i+2}\rangle |s_{i+1}\rangle \right] = 0. \quad (88)$$

The idea underlying the construction of the solution $|E_0\rangle$ is that two consecutive terms on the right-hand side of Eq. (87) differ by two loop insertions, and applying the Hamiltonian constraint converts them into the same linear combination of spinnetworks (inserting loops on one and removing loops from another) with opposite prefactors. Furthermore, although Eq. (87) holds for entire spinnetworks if the values of the lapse contained in \hat{C}_s are the same at all nodes, if one allows different values at each node, one needs to build NLSN solutions via Eq. (87) for each “building block” of the the spinnetwork and then contract these NLSN solutions to create a full spinnetwork solution. This construction assures that $|E_0\rangle$ remains independent from the values of the lapse [note the mutual cancellation of these values between numerators and denominators in the coefficients in Eq. (87)]. Put simply, breaking a large spinnetwork into NLSNs and using Eq. (87) on each of them before reassembling a spinnetwork assures that Eq. (88) is fulfilled at each spinnetwork node, since the action of the Hamiltonian on the entire spinnetwork is the sum of its action at each node. It would be interesting to analyze whether diffeomorphism averaging can be related or made compatible with this result [44].

Another interesting open question in LQG is the regime of validity of some commonly used approximations, such as the assumption that the graph does not change. A hypothesis that is frequently employed to support this assumption is that a coarse-grained triangulation of a manifold might produce a spinnetwork capturing the key features of the quantum geometry and such that its dynamics effectively leaves the graph unaffected [45]. One can indeed see that a first application of Eq. (34) on a spinnetwork implements a graphical change, but a consecutive application of the constraint should recover the “original” spinnetwork. Nonetheless, as our discussion in Secs. VI and VII shows, while the scalar constraint is Hermitian and maps output into input once applied a second time, it also maps these “1st-order” output states into a new family of spinnetworks with even larger graphical changes relative to the input spinnetwork. If Eq. (1) is recursively applied many times, the number of spinnet-

works with graphs that depart from the starting spinnetwork structure increases drastically. It is therefore unclear whether such changes can be effectively absorbed into a coarse-grained spinnetwork with graph-preserving dynamics.

To investigate the validity of this graph-preserving approximation, in the rest of this section we are going to discuss the transformation properties of some fiducial spinnetworks up to a certain order in perturbation theory, which corresponds to applying Eq. (1) recursively up to a fixed number of times. More concretely, we are going to study how the expectation value of the volume operator varies when comparing graph-changing and graph-preserving dynamics. The choice of the volume operator as the figure of merit is based on the central role that this operator plays in the dynamics (since it is present in the Hamiltonian) and in the conceptual foundations of LQG (it is one of the key observables of LQG and also leads to rather drastic and distinct quantum consequences, such as the discretization of spacetime geometry).

The Hamiltonian constraint obtained after quantization of the Ashtekar-Barbero variables should in principle be integrated over the volume of a 3D manifold, smeared by a distribution corresponding to the (time) lapse. When a regularization protocol is adopted to allow for a description of the constraint in terms of observables acting locally at spinnetwork nodes, as in Eq. (1), the lapse distribution is reduced to a set of parameters N_\square , each of which is related to one of the nodes of the spinnetwork, appearing as a summand in Eq. (1). When considering only a spinnetwork node [so that the sum in Eq. (1) disappears], the single parameter $N = N_\square$ plays a role similar to time in the standard unitary description of quantum mechanics (in the absence of time ordering). Following this similarity, we choose to treat N as our perturbation parameter. Our objective is to construct the unitary operator generated by the Hamiltonian constraint, $\hat{U} = \exp(-i\hat{C}_s[N])$ [46], and expand it as a series in our perturbation parameter up to a specific desired order, acting with it on a given spinnetwork and then estimating the expectation value of the volume with respect to the resulting transformed state.

For the consideration of the (non-embedded) graph-changing constraint acting on NLSNs with legs that are all assumed mutually perpendicular (i.e., $p_1 \perp p_2 \perp p_3 \perp p_4$, making the action of the constraints effectively “topological”), we are going to compute terms only up to 3rd order in perturbation theory. The reason is that, in this case, the number of considered possibilities is rather large, and therefore also the computation times (cf. Table II). In contrast, when taking into account the (re-)embedding in 3D to effectively disregard the NLSN links along p_4 , we are going to include terms up to 4th order. On the other hand, the considered graph-preserving constraint is going to act on three different spinnetwork structures [see Figs. 4(a), 4(b) and 4(c)] by inserting extended loops solely between neighboring intertwiners, and the perturbative expansion of the unitary transformation in these cases is going to be truncated at 4th order.

It is worth noting that 3rd- and general odd-order contributions to the expectation values are absent in all calculations, but the reasons for this differ between graph-preserving and graph-changing dynamics. Since, under the action of the graph-changing constraint, any spinnetwork graph can only be recovered after applying the constraint an even number of times, while the volume operator does not change the graph, but rather shuffles spin assignments, any term of the form $\langle \hat{C}_s^n \hat{V} \hat{C}_s^m \rangle$ in which n is even and m is odd, or vice versa, gives zero whenever one starts from a single spinnetwork. This is also true for matrix elements of the Hamiltonian itself, with $\langle \hat{C}_s^m \rangle = 0$ for m odd (since the structures generated by \hat{C}_s^m starting from any spinnetwork differ graphically from that of the starting spinnetwork). For the case of fixed graph structures, however, a certain spinnetwork can in general be recovered also after an odd number of applications of the Hamiltonian constraint, as is the case for ladder-like spinnetworks [cf. Fig. 4(c)] if one couples loops not only between each pair of intertwiners, but also from the “sides” of the ladder structure (which is closed via contraction of the lower legs of the bottommost intertwiner to the upper legs of the uppermost intertwiner, making the ladder into a ring). If such spinnetwork is composed of an odd number m of intertwiners, m different loops coupled between intertwiners with two additional side loops suffice to recover the initial spinnetwork, leading to $\langle \hat{C}_s^{m+2} \rangle \neq 0$. As a consequence, the terms of odd order in the expectation value of the transformed volume can fail to cancel out in general. But, since “side” loops are neglected in our discussion (the expressions for their couplings depend on the specific number of intertwiners in the entire spinnetwork), we observe no such behavior in our graph-preserving plots.

The volume expectation value, as a function of the (perturbative) lapse parameter for two fiducial NLSNs, is shown in Fig. 3 for the non-embedding (up to 3rd order) and embedding (up to 4th order) cases, respectively. Note that, when (re-)embedding is considered, since the edge of spin j_4 is effectively disregarded in the transfor-

mation, inner loops can only appear in locations 1, 2 and 5 (nonetheless, the same volume operators are used as in the general graph-changing case). We choose NLSNs of the form (34) with $j_1 = j_2 = j_3 = j_4 = 1/2$, $\varepsilon = 0$, and $i = 0$ (green curves) or $i = 1$ (red curves). The choice of spin assignments for the considered spinnetworks aims at minimizing the computational times, since higher spins also imply an increase in the time cost of computations, as shown in Table I.

$\{j_1, j_2, j_3, j_4, i\}$	Time (seconds)
$\{1/2, 1/2, 1/2, 1/2, 0\}$	168.8
$\{1/2, 1/2, 1/2, 1/2, 1\}$	187.5
$\{1, 1/2, 1/2, 1, 1/2\}$	668.8
$\{1, 1/2, 1/2, 1, 3/2\}$	687.9
$\{1/2, 1, 1/2, 1, 0\}$	822.4
$\{1/2, 1, 1/2, 1, 1\}$	826.0
$\{1, 1, 1, 1, 0\}$	6543.8
$\{1, 1, 1, 1, 1\}$	6744.7
$\{1, 1, 1, 1, 2\}$	6482.7

TABLE I. Computational times for the application of the Hamiltonian constraint, Eq. (1), on node-local spinnetworks without inner loops [Eq. (34) for $\varepsilon = 0$, $\alpha = j_3$ and $\beta = j_2$] for several choices of link spins. As higher spins are chosen, the computational times rise considerably. We estimate that the time T scales as $T \sim 2^4 j_1 j_2 j_3 j_4 \max\{i\} T_0$, where $\max\{i\}$ is the maximum value of the spin i allowed by the Clebsch-Gordan conditions and T_0 is the time cost of the lowest spin choice, $\{1/2, 1/2, 1/2, 1/2, 0\}$. Times were recorded on a MacBook Pro with M1 chip.

For comparison, we also show in Fig. 3 the volume for the ladder-like spinnetworks transformed under graph-preserving dynamics [represented in Fig. 4(c)], expanded up to 4th order in N . Since graph-preserving calculations depend on specificities of the choice of spinnetwork, we provide in Fig. 4(d) additional data to compare the behaviors of three spinnetwork structures with different modular “patches”, shown in Figs. 4(a)-4(c). This additional comparison supports the choice of the spinnetwork displayed in Fig. 4(c) as a reference to study the deviations between graph-changing and graph-preserving dynamics. Indeed, the spinnetworks in Figs. 4(b) and 4(c) seemingly have very close volume profiles, possibly indicating that other more complicated spinnetworks could have volumes not so far from those plotted in Fig. 4(d) when graph-preserving dynamics is implemented. To that extent, we may regard this ladder-like spinnetwork as a good representative for the study of graph-preserving dynamics. It is worth noting that the “bubble-like” spinnetworks shown in Fig. 4(a) are eigenstates of the graph-preserving Hamiltonian, therefore their volume and volume variance remain equal to zero.

Functional	$\{j_1, j_2, j_3, j_4, i\}$	Time (seconds)				
		1	C_s	C_s^2	C_s^3	C_s^4
Hamiltonian	$\{1/2, 1/2, 1/2, 1/2, 0\} _{\text{gc}}$	NA	168.8	10058.5	10^6	NA
	$\{1/2, 1/2, 1/2, 1/2, 1\} _{\text{gc}}$	NA	187.5	10438.1	10^6	NA
	$\{1/2, 1/2, 1/2, 1/2, 0\} _{\text{gc}}^e$	NA	44.8	1048.1	9793.3	85985.6
	$\{1/2, 1/2, 1/2, 1/2, 1\} _{\text{gc}}^e$	NA	42.0	1054.0	10230.4	85636.3
	$\{1/2, 1/2, 1/2, 1/2, 0\} _{\text{gp}}^o$	NA	70.1	1057.7	7282.4	21233.1
	$\{1/2, 1/2, 1/2, 1/2, 1\} _{\text{gp}}^o$	NA	71.2	1054.0	6141.1	21196.5
	$\{1/2, 1/2, 1/2, 1/2, 0\} _{\text{gp}}^\Delta$	NA	69.8	1212.1	7070.1	32628.2
	$\{1/2, 1/2, 1/2, 1/2, 1\} _{\text{gp}}^\Delta$	NA	69.9	1177.0	7650.5	33529.5
	$\{1/2, 1/2, 1/2, 1/2, 0\} _{\text{gp}}^\square$	NA	35.4	746.7	11562.7	59017.1
	$\{1/2, 1/2, 1/2, 1/2, 1\} _{\text{gp}}^\square$	NA	69.7	2203.7	22876.1	96747.7
Collector	$\{1/2, 1/2, 1/2, 1/2, 0\} _{\text{gc}}$	NA	0.009	11.06	NA	NA
	$\{1/2, 1/2, 1/2, 1/2, 1\} _{\text{gc}}$	NA	0.008	11.66	NA	NA
	$\{1/2, 1/2, 1/2, 1/2, 0\} _{\text{gc}}^e$	NA	0.002	0.44	147.7	NA
	$\{1/2, 1/2, 1/2, 1/2, 1\} _{\text{gc}}^e$	NA	0.002	0.43	157.1	NA
	$\{1/2, 1/2, 1/2, 1/2, 0\} _{\text{gp}}^o$	NA	0.001	0.04	0.9	22.4
	$\{1/2, 1/2, 1/2, 1/2, 1\} _{\text{gp}}^o$	NA	0.001	0.03	1.1	23.9
	$\{1/2, 1/2, 1/2, 1/2, 0\} _{\text{gp}}^\Delta$	NA	0.001	0.06	2.5	114.5
	$\{1/2, 1/2, 1/2, 1/2, 1\} _{\text{gp}}^\Delta$	NA	0.001	0.07	2.6	111.7
	$\{1/2, 1/2, 1/2, 1/2, 0\} _{\text{gp}}^\square$	NA	0.001	0.09	5.4	375.9
	$\{1/2, 1/2, 1/2, 1/2, 1\} _{\text{gp}}^\square$	NA	0.005	0.25	19.8	NA
Normalizer	$\{1/2, 1/2, 1/2, 1/2, 0\} _{\text{gc}}$	0.00010	0.0013	0.617	24.982*	NA
	$\{1/2, 1/2, 1/2, 1/2, 1\} _{\text{gc}}$	0.00009	0.0021	0.408	7.30692*	NA
	$\{1/2, 1/2, 1/2, 1/2, 0\} _{\text{gc}}^e$	0.00010	0.0014	0.053	2.270	10.14*
	$\{1/2, 1/2, 1/2, 1/2, 1\} _{\text{gc}}^e$	0.00011	0.0006	0.026	1.346	9.95*
	$\{1/2, 1/2, 1/2, 1/2, 0\} _{\text{gp}}^o$	0.00083	0.0004	0.001	0.002	0.43
	$\{1/2, 1/2, 1/2, 1/2, 1\} _{\text{gp}}^o$	0.00011	0.0005	0.001	0.003	0.47
	$\{1/2, 1/2, 1/2, 1/2, 0\} _{\text{gp}}^\Delta$	0.00083	0.0010	0.003	0.003	2.38
	$\{1/2, 1/2, 1/2, 1/2, 1\} _{\text{gp}}^\Delta$	0.00003	0.0004	0.001	0.002	2.34
	$\{1/2, 1/2, 1/2, 1/2, 0\} _{\text{gp}}^\square$	0.00005	0.0042	0.002	0.010	9.47
	$\{1/2, 1/2, 1/2, 1/2, 1\} _{\text{gp}}^\square$	0.00024	0.0009	0.003	1.103	7.33*
Volume	$\{1/2, 1/2, 1/2, 1/2, 0\} _{\text{gc}}$	0.092	1.39	27.8	NA	NA
	$\{1/2, 1/2, 1/2, 1/2, 1\} _{\text{gc}}$	0.086	1.40	27.7	NA	NA
	$\{1/2, 1/2, 1/2, 1/2, 0\} _{\text{gc}}^e$	0.091	0.81	7.6	NA	NA
	$\{1/2, 1/2, 1/2, 1/2, 1\} _{\text{gc}}^e$	0.096	0.85	8.3	NA	NA
	$\{1/2, 1/2, 1/2, 1/2, 0\} _{\text{gp}}^o$	0.085	0.37	1.5	NA	NA
	$\{1/2, 1/2, 1/2, 1/2, 1\} _{\text{gp}}^o$	0.095	0.38	1.6	NA	NA
	$\{1/2, 1/2, 1/2, 1/2, 0\} _{\text{gp}}^\Delta$	0.094	0.47	2.0	NA	NA
	$\{1/2, 1/2, 1/2, 1/2, 1\} _{\text{gp}}^\Delta$	0.081	1.38	8.7	NA	NA
	$\{1/2, 1/2, 1/2, 1/2, 0\} _{\text{gp}}^\square$	0.090	0.46	3.2	NA	NA
	$\{1/2, 1/2, 1/2, 1/2, 1\} _{\text{gp}}^\square$	0.094	0.82	5.3	NA	NA

TABLE II. Computational times for the application of several functionals at different perturbative levels on node-local spinnetworks (NLSNs) given by Eq. (34) for $\varepsilon = 0$, $\alpha = \beta = j_1 = j_2 = j_3 = j_4 = 1/2$ and $i = 0, 1$. Subscripts gc and gp denote NLSNs transformed under graph-changing or graph-preserving constraints, respectively. Superscripts e refer to embedding, while o, Δ, \square represent the spinnetwork structures depicted respectively in Figs 4(a), 4(b) and 4(c). The number of recursive applications of the Hamiltonian constraint is labeled by the exponent n in C_s^n , with the unit 1 representing no application. In the Hamiltonian rows, the entries correspond to times consumed when applying the constraint the n -th time. The other considered functionals are generally applied afterwards. However, in the case of the normalizer and volume functionals, they are also applied on the initial spinnetworks. Therefore, they possess entries at the column labeled by 1, corresponding to the level prior to the first application of the Hamiltonian. Normalization times marked with an asterisk were recorded without using the collector functional before, since for very large linear combinations of ghost functions the collector offers no time advantage relative to a direct application of the normalizer. Not every functional needs to be applied to every output NLSN superposition to calculate the volume expectation value, therefore some entries are marked as “non applicable” (NA). Times were recorded on a MacBook Pro with M1 chip.

The results displayed in the figures indicate that the graph-preserving approximation leads to a misestimation of the geometric observables of the system by nearly one order of magnitude at moderate values of the lapse. As discussed previously, the fact that $\langle \hat{C}_s^m \rangle$ can be different from zero for m odd in the graph-preserving scenario (assuming one allows for all possible loop-coupling locations) also shows that the dynamics of the constraint is affected by this approximation. Although computational-time limitations have prevented us from completing the graph-changing calculations at 4th order, the results for graph-changing dynamics of NLSNs (re-)embedded in 3D indicate that the volume tends to increase for $N \gtrsim 3/4$ under graph-changing dynamics, even somewhat higher than the volume increase for $N \gtrsim 1/2$ observed under graph-preserving dynamics [47]. The behaviors of two (out of the three) investigated spinnetwork graphs for the graph-preserving dynamics are qualitatively similar to the (re-)embedded graph-changing case. For the considered NLSNs, the 4th-order contributions to the volume under graph-changing dynamics only become comparable to the 2nd-order ones at $N \sim 10/9$, while this happens at $N \sim 4/5$ in the graph-preserving case. This fact supports the idea that the graph-changing perturbative results are more reliable than the graph-preserving ones. Furthermore, within the range of positivity of the variance, which provides an estimate of the maximum value of the lapse for which perturbation theory is acceptable, the two NLSNs transformed under graph-changing dynamics have the same volume profile, in contrast to what we see in the graph-preserving case.

Although consideration of only two spinnetworks does not provide a proof that the graph-preserving approximation leads to a considerable departure from the graph-changing dynamics, the presented numerical data serves as the first evidence that this might indeed be the case. Further scrutinization of the different behavior of the volume expectation value between the graph-changing and graph-preserving scenarios is still needed, as well as consideration of other figures of merit beyond the volume operator and the diagonal matrix elements $\langle \hat{C}_s^m \rangle$.

XI. CONCLUSIONS AND OUTLOOK

In the first part of our work, we have made use of the modern conventions in recoupling theory to fully derive the action of the LQG Euclidean scalar constraint around 3-valent and 4-valent nodes of spinnetworks. These results represent an update, as well as an extension, of previous derivations [23–26]. Our discussion shows how reversibility and self-adjointness can be directly visualized in the spinnetworks acted upon by the Hamiltonian constraint: inner loops can both be added or removed around the intertwiner. In fact, we show that, when acting on spinnetworks with inner loops, possible outcomes of the scalar constraint are spinnetworks with the same graph, but with different spin assignments on the bridge-

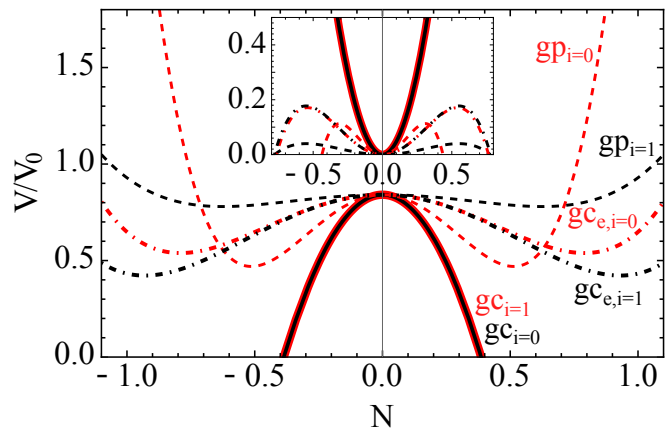


FIG. 3. Variation of the dimensionless volume expectation value with respect to the lapse under different scenarios. The curves correspond to two fiducial spinnetworks with $j_1 = j_2 = j_3 = j_4 = 1/2$, $\varepsilon = 0$ and $i = 0$ (red) or $i = 1$ (black). We compare graph-changing dynamics with (dot-dashed lines) and without (solid lines) (re-)embedding, as well as a graph-preserving transformation of the spinnetwork shown in Fig. 4(c) (dashed lines). Unitary transformations are expanded up to 3rd order in N for the full graph-changing case, and 4th order otherwise. Note that, as expected from our discussion in the main text, the 3rd-order contributions to the volume vanish. It is possible to see that the graph-preserving dynamics misestimates the volume expectation value both in absolute value and in the location of its minima. The graph-preserving dynamics also violates the equality between volume profiles observed for the two choices of inner virtual spins, $i = 0$ and $i = 1$. The input spinnetworks employed in the calculations are normalized. The inset gives the corresponding curves for the variance, $(\langle \hat{V}^2 \rangle - \langle \hat{V} \rangle^2)/V_0^2$. Recall that V_0 is the global constant factor introduced in our definition of the volume operator

ing link of the inner loops. We derive this “loop-coupling” mechanism using the tools from recoupling theory, something so far not yet presented in the literature. These calculations should serve as a reference for future studies of the full Euclidean Hamiltonian constraint in the graph-changing regime.

We have then introduced a novel numerical approach that enables us to encode spinnetworks and implement the action of the Hamiltonian constraint on them. The code allows us to explore the effects of the graph-changing behavior of the scalar constraint on the expectation value of the volume operator and even compare them to the approximated, graph-preserving constraint. Our results for spinnetworks of low spins show the first concrete evidence that the assumption that the dynamics can be properly approximated by a graph-preserving Hamiltonian might not be firmly justified. In addition to this analysis, we have also managed to determine with our numerical methods two families of solutions of the Euclidean Hamiltonian. It is worth noting, however, that, as we showed in our time-cost analysis, computations on

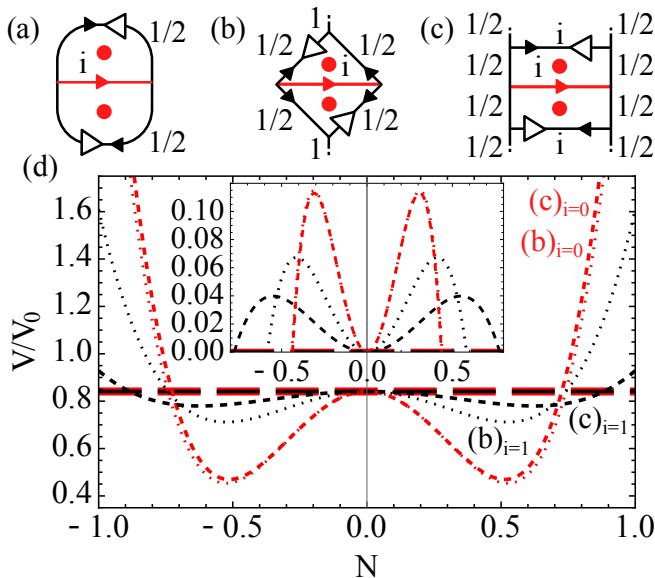


FIG. 4. (a)-(c) Three different choices of spinnetworks, selected for the study of graph-preserving dynamics. Structures (b) and (c) are modular, as implied by the dotted links above and below. The red dots mark locations where loops can be coupled (note the absence of loops coupled from the sides of the spinnetworks, even though this is technically possible). The loops extend along the entire perimeter of the regions marked by these red dots. The red link represents the sole intertwiner acted upon by the graph-preserving Hamiltonian, and its spin takes values $i = 0$ or $i = 1$, each corresponding to red or black volume profiles in (d), respectively. (d) Variation of the dimensionless volume expectation value with respect to the lapse N for the three different choices of spinnetworks. The unitary transformation is expanded up to 4th order in N . Volumes of spinnetworks (a), (b) and (c) are represented by long-dashed, dotted and dashed lines, respectively. Note the similarity of the results for spinnetworks (b) and (c), particularly when $i = 0$. The inset shows the corresponding curves for the variance, $(\langle \hat{V}^2 \rangle - \langle \hat{V} \rangle^2)/V_0^2$, where V_0 is the global constant factor introduced in our definition of the volume operator.

a single computer are expectedly demanding and processing times increase rapidly both with the number of recursive applications of the Hamiltonian and with the spins involved. Therefore, it would be interesting to explore the potential to run these calculations in a computational cluster.

Our work is a thorough study of the graph-changing aspects of the Euclidean scalar constraint, both analytically and numerically, and introduces a new tool to further explore its action on spinnetworks. These contributions should seed new developments in the field of LQG, pushing the limits of what was previously assumed to be

numerically intangible results. We expect future works on LQG to further use and build on our numerical approach and therewith extend our results to a wider domain of validity, potentially also unveiling new families of eigenstates and new phenomenology in LQG. In particular, it would be interesting to discuss how precise LQG formulations would affect relevant semi-classical results such as the black-to-white-hole tunneling [48], the potential tiny-white-hole nature of dark matter [49] or the black-hole halos potentially left from past universes through bounces [50].

ACKNOWLEDGMENTS

The authors are grateful for discussions with and suggestions by Ilkka Mäkinen, Jorge Pullin, Carlo Rovelli and Etera Livine. This work is supported by the ID# 62312 grant from the John Templeton Foundation, as part of the project “The Quantum Information Structure of Spacetime” (QISS).

TLMG and MM acknowledge support by the ERC Starting Grant QNets through Grant Number 804247, and the European Union’s Horizon Europe research and innovation program under Grant Agreement Number 101114305 (“MILLENION-SGA1” EU Project) and under Grant Agreement Number 101046968 (BRISQ). MM furthermore acknowledges support by the Deutsche Forschungsgemeinschaft (DFG, German Research Foundation) under Germany’s Excellence Strategy ‘Cluster of Excellence Matter and Light for Quantum Computing (ML4Q) EXC 2004/1’ 390534769. This research is also part of the Munich Quantum Valley (K-8), which is supported by the Bavarian state government with funds from the Hightech Agenda Bayern Plus.

FV’s research at Western University is supported by the Canada Research Chairs Program and by the Natural Science and Engineering Council of Canada (NSERC) through the Discovery Grant “Loop Quantum Gravity: from Computation to Phenomenology.” FV acknowledges support from the Perimeter Institute for Theoretical Physics through its affiliation program. Research at Perimeter Institute is supported by the Government of Canada through Industry Canada and by the Province of Ontario through the Ministry of Economic Development and Innovation. FV acknowledges the Anishinaabek, Haudenosaunee, Lūnaapéewak, Attawandaron, and neutral people, on whose traditional lands Western University and the Perimeter Institute are located.

GAMM acknowledges support by MCIN/AEI/10.13039/501100011033/FEDER from Spain under the Grant Number PID2020-118159GB-C41 and also partly by the Grant Number PID2023-149018NB-C41, funded by MCIU/AEI/10.13019/501100011033 and by FSE+.

Appendix A: Additional formulas from recoupling theory

One important point for the derivation of the action of the scalar constraint (1) on 4-valent NLSNs is how to factor out diagonal inner links. The relation that allows this requires the use of several expressions from Sec. IV. For this reason, we include its derivation here. The idea is that one uses a double braid operation (namely on the nodes of spins $\{a, j_3, 1/2\}$ and $\{j_3, j_1, p\}$) to convert the spinnetwork into a more tractable form while picking up a phase from these braidings [cf. Eq. (9) and the discussion thereafter]. One then uses Eq. (10) to introduce arrows on the four links connected to the intertwiner. This permits us to use Eq. (20) on the links with spins j_3 and q . The double Pachner move combined with the removal of three arrows at the node $\{p, o, 1/2\}$ [which requires flipping $\epsilon^{(p)}$ and therefore contributes with a phase factor $(-1)^{(2p)}$], gives the expression in the second row of Eq. (A1). We are required to flip the cyclicity of the node $\{p, o, 1/2\}$ to allow for the use of Eq. (13), which factors out the inner ‘‘bubble’’ loop and removes a prefactor of d_n . Flipping both $\epsilon^{(j_1)}$ and $\epsilon^{(j_2)}$ leads to the expression in the third row of the equation. Finally, since $(-1)^{(2j_3)} = (-1)^{(2a+1)}$ and $(-1)^{(2n)} = (-1)^{(2j_2+2m)}$ (note the triangularity conditions imposed by the Wigner 6j symbols), we can rewrite the final expression in the form given in the last row of Eq. (A1) (using the symmetry of the Wigner 6j symbols).

$$\begin{aligned}
 & \begin{array}{c} j_1 \\ \diagdown \\ + \\ \diagup \\ a \end{array} \begin{array}{c} \xrightarrow{p} \\ + \\ \xleftarrow{q} \\ \end{array} \begin{array}{c} \xrightarrow{\frac{1}{2}} \\ + \\ \xrightarrow{m} \end{array} = (-1)^{(j_1+j_3+p)+(a+1/2+j_3)} \begin{array}{c} a \\ \diagdown \\ + \\ \diagup \\ j_1 \end{array} \begin{array}{c} \xrightarrow{p} \\ + \\ \xleftarrow{q} \\ \end{array} \begin{array}{c} \xrightarrow{\frac{1}{2}} \\ + \\ \xrightarrow{m} \end{array} \\
 & = (-1)^{j_1+2j_3+a-p+1/2} \sum_{n,o} d_n d_o (-1)^{(1/2-j_1+a+p)+(m-p+1/2+j_2)} \left\{ \begin{array}{ccc} 1/2 & p & n \\ j_1 & a & j_3 \end{array} \right\} \left\{ \begin{array}{ccc} m & j_2 & o \\ p & 1/2 & q \end{array} \right\} \begin{array}{c} a \\ \diagdown \\ + \\ \diagup \\ j_1 \end{array} \begin{array}{c} \xrightarrow{n} \\ + \\ \xrightarrow{p} \end{array} \begin{array}{c} \xrightarrow{1/2} \\ + \\ \xrightarrow{o} \end{array} \begin{array}{c} \diagup \\ + \\ \diagdown \\ j_2 \end{array} \\
 & = \sum_n d_n (-1)^{-j_1-j_2+2j_3-a+m+2n} \left\{ \begin{array}{ccc} 1/2 & p & n \\ j_1 & a & j_3 \end{array} \right\} \left\{ \begin{array}{ccc} m & j_2 & n \\ p & 1/2 & q \end{array} \right\} \begin{array}{c} j_1 \\ \diagdown \\ + \\ \diagup \\ a \end{array} \begin{array}{c} \xrightarrow{n} \\ + \\ \xrightarrow{p} \end{array} \begin{array}{c} \diagup \\ + \\ \diagdown \\ j_2 \end{array} \\
 & = \sum_n d_n (-1)^{-j_1+j_2+a+1-m} \left\{ \begin{array}{ccc} a & j_1 & n \\ p & 1/2 & j_3 \end{array} \right\} \left\{ \begin{array}{ccc} p & 1/2 & n \\ m & j_2 & q \end{array} \right\} \begin{array}{c} j_1 \\ \diagdown \\ + \\ \diagup \\ a \end{array} \begin{array}{c} \xrightarrow{n} \\ + \\ \xrightarrow{p} \end{array} \begin{array}{c} \diagup \\ + \\ \diagdown \\ j_2 \end{array} .
 \end{aligned} \tag{A1}$$

Another important relation appears in the derivation of the action of the volume operator (or, more precisely, in the action of \hat{W}). We use Eq. (28) to introduce the resolution of the identity in such a way that it isolates the spin-1 links, i.e., it ‘‘splits’’ the links of spins j_1 , j_3 and m . The factored term forms a hexagonal spinnetwork that corresponds to

the Wigner 9j symbol [cf. Eq. (19)],

Equation (A2) shows a tetrahedral spinnetwork on the left, which is equal to a 6j symbol in the middle and a 3j symbol on the right. The tetrahedron has edges labeled a, b, c, l, m, p and spins j_1, j_2, j_3 . The 6j symbol is a hexagon with edges labeled a, b, c, l, m, p and spins j_1, j_2, j_3 . The 3j symbol is a triangle with edges labeled a, b, c and spins j_1, j_2, j_3 .

We now show a simple example of how the arrows within a tetrahedral spinnetwork of the form (18) can be rearranged using Eq. (10) to give similar structures, all of which correspond to the Wigner 6j symbol up to varying phase factors. In the concrete example below, we introduce three arrows on the node joining the spins $\{k_3, k_1, j_3\}$, and use Eqs. (4) and (5) to remove doubled arrows, obtaining a phase,

Equation (A3) shows a sequence of three tetrahedral spinnetworks. The first has arrows on edges k_1, k_2, k_3 . The second has arrows on edges k_1, k_2, k_3 and j_1 . The third has arrows on edges k_1, k_2, k_3 and j_1 , with a phase factor $(-1)^{2k_2}$ in front.

Expressions like the one on the right-hand side are often factored out in the equations of Secs. VI and VII.

Finally, the 2-2 Pachner move can be derived by means of a braid, Eq. (17) and another braid, in the following sequence:

Equation (A4) shows a sequence of three equations. The first is a braid relation involving spins j_1, j_2, j_3, j_4 and edge l . The second is a similar braid relation with a phase factor $(-1)^{2l+k+j_1+j_2+j_3+j_4}$ and a 6j symbol. The third is a similar braid relation with a phase factor $(-1)^{j_1-j_2+j_3+j_4}$ and a 6j symbol.

Note that, in the last row of this equation, the intertwiner has been rotated clockwise by $\pi/2$. Furthermore, the (Clebsch-Gordan) relation $(-1)^{2l+2j_2+2j_4} = 1$ has been employed in the phase factor.

Appendix B: Temperley-Lieb algebra

Equation (B1) shows a Temperley-Lieb algebra relation: a crossing of two lines with spins a, b, c, d and j is equal to a sum over i of a product of two crossings with spins a, b, c, d and i .

Instead of using the modern orthonormalized spinnetworks as quantum states in our description, we will use here the old-fashioned, yet more graphically intuitive description of such systems in terms of Temperley-Lieb tangles [19]. We introduce below the main working tools from recoupling theory with Temperley-Lieb algebra, that will be needed to follow the following derivations (note the difference from what was introduced in Sec. IV),

Equation (B2) shows a Temperley-Lieb algebra relation: a crossing of two lines with spins a, b, c, d and i is equal to a fraction of two crossings with spins a, b, c, d and i .

$$\begin{array}{c} i \\ \square \\ \square \end{array} = (-1)^i (i+1), \quad (\text{B3})$$

$$\frac{a}{\frac{b}{c}} = (-1)^{\frac{a+b+c}{2}} \frac{(\frac{a+b+c+2}{2})! (\frac{a+b-c}{2})! (\frac{a-b+c}{2})! (\frac{-a+b+c}{2})!}{a!b!c!}, \quad (\text{B4})$$

$$n \parallel m = \sum_i \frac{\begin{array}{c} i \\ \square \\ \square \end{array}}{m} \frac{\begin{array}{c} n \ m \\ \diagdown \ / \\ i \end{array}}{n \ m}, \quad (\text{B5})$$

$$\begin{array}{c} a \\ \diagdown \ / \\ r \ s \\ b \ c \end{array} = \frac{\begin{array}{c} r \ t \\ \diagdown \ / \\ b \ c \end{array}}{\frac{a}{c}} \begin{array}{c} a \ a \\ \diagdown \ / \\ b \ c \end{array}, \quad (\text{B6})$$

$$\begin{array}{c} a \\ | \\ b \circ c \\ | \\ d \end{array} = \delta_{ad} \frac{\frac{a}{b}}{c} \begin{array}{c} a \\ \square \\ \square \end{array} \Big| a, \quad (\text{B7})$$

$$\begin{array}{c} a \ b \\ \diagdown \ / \\ \circ \\ | \\ c \end{array} = \lambda_c^{a,b} \begin{array}{c} a \ b \\ \diagdown \ / \\ c \end{array} \equiv (-1)^{[a(a+3)+b(b+3)-c(c+3)]/2} \begin{array}{c} a \ b \\ \diagdown \ / \\ c \end{array}. \quad (\text{B8})$$

The labels $(a, b, c, d, i, j, m, n, r, s, t)$ used in Eqs. (B1)-(B8) are “colors”, corresponding to twice the spins. Equation (B1) represents a so-called 2-2 Pachner move [19]. The coefficient in the summand of Eq. (B1), related through Eq. (B2) to other commonly occurring symbols in recoupling theory, is the 6j symbol in the Temperley-Lieb normalization. The tetrahedral net symbol with inputs (a, b, c, d, i, j) on the (numerator on the) right-hand side of Eq. (B2) will regularly appear throughout the following calculations. Its formula [51] can be found in Sec. 9.11 of Ref. [19], but we will often convert it to the most widely used 6j symbol with spin entries rather than colors [52], often encountered in mathematical softwares [e.g., the “SixJSymbol” function

in Mathematica] and represented here in parentheses,

$$\left(\begin{array}{ccc} a/2 & b/2 & i/2 \\ c/2 & d/2 & j/2 \end{array} \right) = \frac{\begin{array}{c} b \ j \ c \\ \diagdown \ / \\ a \ d \end{array} \Big| i}{\sqrt{\frac{a}{d} \frac{b}{c} \frac{a}{b} \frac{c}{j}}}. \quad (\text{B9})$$

It is worth noting that the tetrahedral net symbol is invariant with respect to the following permutations of arguments: (a, b, i, c, d, j) , (b, a, i, d, c, j) , (a, i, b, c, j, d) , (a, d, j, c, b, i) , (c, d, i, a, b, j) and (c, b, j, a, d, i) . Another important property of this function is its triangularity, i.e., it only assumes nonzero values if the triples (a, b, i) , (i, c, d) , (d, j, a) and (c, b, j) simultaneously fulfil the triangle/Clebsch-Gordan conditions for all (permutations of) its entries. Equation (B5) is a symbolic representation of the Clebsch-Gordan spin coupling, with the colors n and m summing up to all allowed values i such that $|m - n| \leq i \leq m + n$, with the additional (gauge-invariance) constraint $m + n + i = 2k$ ($k \in \mathbb{N}$), referred to as the Clebsch-Gordan or triangle conditions. One interesting aspect of the Temperley-Lieb algebra is the fact that the geometric arrangement of colors in Eq. (B9) differs from that in Eq. (18), resulting in different predictions for the two approaches considered. The single loop in Eq. (B3) represents, up to a possible -1 factor, the dimension of the color- i representation (i.e., for $i = 2j$, $d = 2j + 1$) and results from summing over all tangle permutations (the permutation is represented by a white square). The remaining equations are mostly used for the purpose of renormalization of virtual edges (edges added to the spinnetwork through manipulations). Making use of those equations we will proceed with the derivation of the action of the scalar constraint on general spinnetworks.

We start with a generic collection of three mutually perpendicular edges attached to a common vertex of valency 3. We label their colors as r , p and q . Following Refs. [24, 25], both the edges and the paths of the holonomies in Eq. (1) are oriented towards the vertex (inverse holonomies are therefore associated with segments oriented away from the vertex). Whenever necessary, the orientation of edges and holonomies will be indicated by an arrow. The orientation is important, since the consecutive application of the holonomies in Eq. (1) should follow a cyclic orientation closed by the trace (i.e., two holonomies connected by a virtual 2-valent vertex should not be simultaneously oriented towards this vertex).

We proceed with the application of the first holonomy of the first term on the right-hand side of Eq. (1) to the three fiducial edges from the same vertex. At first, we consider the action of $\hat{h}^{-1}[p_k]$ only along the path p_r

parallel to the edge labelled by r , i.e.,

$$\hat{h}^{-1}[p_r] \begin{array}{c} r \\ | \\ p \text{---} \text{---} q \\ \diagup \quad \diagdown \end{array} \equiv \begin{array}{c} r \\ \parallel \\ 1 \\ | \\ p \text{---} \text{---} q \\ \diagup \quad \diagdown \end{array} = \sum_c \frac{\begin{array}{c} c \\ \circ \\ 1 \\ \circ \\ r \\ c \end{array}}{\begin{array}{c} r \\ \circ \\ 1 \\ \circ \\ r \\ c \end{array}} \begin{array}{c} r \\ \rightarrow 1 \\ | \\ c \\ | \\ p \text{---} \text{---} q \\ \diagup \quad \diagdown \end{array}. \quad (\text{B10})$$

The action of the holonomies $\hat{h}^{-1}[p_p]$ and $\hat{h}^{-1}[p_q]$ along the edges p and q follow analogous relations with permuted labels. Note that the holonomy $\hat{h}^{-1}[p_r]$ is represented as an arrow of color 1 [the fundamental representation of the SU(2) group] with orientation opposite to its adjacent edge, with label given by r . Using Eq. (B5), the two parallel segments with labels r and 1 (i.e., the edge and the holonomy) can be coupled, with their combined colors/spins assuming all values c allowed by the Clebsch-Gordan conditions, namely $c = r + \epsilon$ with $\epsilon = \pm 1$. The use of Eq. (B5) automatically results in a trivalent decomposition, with the small r -colored segment attached to the original vertex being actually virtual (i.e., it has no physical extension in the manifold), so that this vertex becomes effectively 4-valent with edges p , q , c and 1. The increased valency of the original vertex, however, is not permanent, since the new inwards-oriented edge of color 1 is supposed to be tied to the other holonomies in Eq. (1), in a similar way to how the indices of a product of matrices have to be contracted pairwise (and there-

fore no free indices are left after a trace is applied). The same holds for the oriented edge of color 1 created on the upper-most virtual vertex.

The considered spinnetworks, and therefore also their corresponding tangles, are eigenstates of the volume operator. This operator acts on the (physical) vertices of the graph, giving zero contribution from vertices with valency below 4, while higher-valency vertices have a contribution defined by the colors of the edges attached to them. In practice, $\hat{V} \equiv \frac{l_0^3}{4} \sqrt{|i\hat{W}_{[p,q,c]}^{(4)}|}$ is defined in terms of the Planck length l_0 and the operator $\hat{W}_{[p,q,c]}^{(4)}$. Applying $\hat{W}_{[p,q,c]}^{(4)}$ on the right-hand side of Eq. (B10), which contains an effective 4-valent vertex with edges of colors p , q , c and 1 decomposed in a trivalent arrangement, leads to

$$\hat{W}_{[p,q,c]}^{(4)} \begin{array}{c} r \\ \rightarrow 1 \\ | \\ c \\ | \\ p \text{---} \text{---} q \\ \diagup \quad \diagdown \end{array} = \sum_{\beta} W_{[p,q,c]}^{(4)}(p, q, 1, c)_{r}^{\beta} \begin{array}{c} r \\ \rightarrow 1 \\ | \\ \beta \\ | \\ p \text{---} \text{---} q \\ \diagup \quad \diagdown \end{array}. \quad (\text{B11})$$

The matrix $W_{[p,q,c]}^{(4)}(p, q, 1, c)_{r}^{\beta}$ in Eq. (B11) is skew-symmetric and, with the exception of two entries, is composed of zeros. The two nonzero entries depend on the value of c : if $c = r + 1$, the entries with row $r - 2$ and column r , and vice versa, are nonzero, while if $c = r - 1$, the entries with row r and column $r + 2$, and vice versa, are nonzero instead [24, 25, 32]. These matrix elements read

$$W_{[p,q,c]}^{(4)}(p, q, 1, c)_{r}^{r\pm 2} = \pm (-1)^{(p+q+r+1\pm 1)/2} \times \left[\frac{1}{2^8} (p+q+r\pm 1+3)(1+p+q-r\mp 1)(1+p+r\pm 1-q)(1+q+r\pm 1-p) \right]^{1/2}. \quad (\text{B12})$$

While $W_{[p,q,c]}^{(4)}(p, q, 1, c)_{\alpha}^{\beta}$ is not diagonal, it can be easily diagonalized by a unitary matrix U . The two eigenvalues of $W_{[p,q,c]}^{(4,\text{diag})}(p, q, 1, c) = UW_{[p,q,c]}^{(4)}(p, q, 1, c)U^{\dagger}$ are $W_{[p,q,c]}^{(4)}(p, q, 1, c)_{r}^{r\pm 2}$ and $-W_{[p,q,c]}^{(4)}(p, q, 1, c)_{r}^{r\pm 2}$. The square root of the matrix $iW_{[p,q,c]}^{(4)}(p, q, 1, c)$ can be expanded to show that

$$\begin{aligned} & \sqrt{|iW_{[p,q,c]}^{(4)}(p, q, 1, c)|} \\ &= U^{\dagger} \sqrt{|iW_{[p,q,c]}^{(4,\text{diag})}(p, q, 1, c)|} U \\ &= U^{\dagger} \mathbb{1} \sqrt{|W_{[p,q,c]}^{(4)}(p, q, 1, c)_{r}^{r\pm 2}|} U \\ &= \mathbb{1} \sqrt{|W_{[p,q,c]}^{(4)}(p, q, 1, c)_{r}^{r\pm 2}|}. \end{aligned} \quad (\text{B13})$$

The matrix representation of the volume operator is therefore diagonal.

The next operator on the right-hand side of Eq. (1) is the holonomy $\hat{h}[p_k]$. For the specific case of the path p_r along the r -colored edge, $\hat{h}[p_r]$ is graphically represented by an arrow parallel, but oppositely oriented, to the arrow representing $\hat{h}^{-1}[p_r]$ in Eq. (B10). $\hat{h}[p_r]$ can be directly attached [53] to the loose end of the upper edge of color 1 on the right-hand side of Eq. (B10) to give

$$\hat{h}(p_r) \begin{array}{c} r \\ \rightarrow 1 \\ | \\ c \\ | \\ p \text{---} \text{---} q \\ \diagup \quad \diagdown \end{array} \equiv \begin{array}{c} 1 \\ \parallel \\ c \\ | \\ p \text{---} \text{---} q \\ \diagup \quad \diagdown \end{array} = \begin{array}{c} r \\ \parallel \\ 1 \\ | \\ c \\ | \\ p \text{---} \text{---} q \\ \diagup \quad \diagdown \end{array}. \quad (\text{B14})$$

The holonomies over the triangular loop, $\hat{h}[\alpha_{ij}] - \hat{h}[\alpha_{ji}]$, should be applied on the right-hand side of Eq. (B14) in such a way that the orientation of the sequentially coupled holonomies is preserved. Since α_{ij} and α_{ji} have opposite orientations, they are attached to the loose ends

of the two virtual edges of color 1 (which are physically at the same point of the manifold) in different ways. The presence of the trace in Eq. (1) enforces that all virtual edges should be tied together, such that no loose virtual edges remain. As a result,

$$\hat{h}(\alpha_{ij}) - \hat{h}(\alpha_{ji}) \equiv \text{Diagram 1} - \text{Diagram 2} \quad (\text{B15})$$

The effect of coupling holonomies (with color 1) to the edges of colors p and q can be accounted for by applying Eq. (B5) to each of those edges (i.e., a region of a spinnetwork around one of its vertices) on the right-hand side of Eq. (B15) this leads to

$$\text{Diagram 1} = \sum_{a,b} \frac{\text{Diagram 2}}{\text{Diagram 3}} \text{Diagram 4} \quad (\text{B16})$$

where $a = p + \epsilon'$ and $b = q + \epsilon''$ (with $\epsilon', \epsilon'' = \pm 1$ according to the Clebsch-Gordan conditions) and all virtual edges originating from holonomies have color 1 (this also applies for the following derivations). We can now use Eq. (B8) to rearrange the crossings of edges [54],

$$\text{Diagram 1} = \lambda_c^{1,r} \lambda_a^{1,p} \lambda_b^{1,q} \text{Diagram 2} \quad (\text{B17})$$

This operation is performed three times, once for each of

the original edges that we are considering. The virtual loops that appear on the right-hand side of Eq. (B17) can be renormalized with the aid of Eq. (B6) to give

$$\text{Diagram 1} = \frac{\text{Diagram 2} \text{Diagram 3}}{\text{Diagram 4} \text{Diagram 5}} \text{Diagram 6} \quad (\text{B18})$$

Similar operations can be performed on the second graph on the right-hand side of Eq. (B15).

After taking into account that the trace gives an additional -1 prefactor, Eqs. (B10)-(B17) synthesize the action of the first term of the Hamiltonian (1) on the fiducial three edges attached to the same vertex. The second term of the Hamiltonian, arising from the alternate order of operators in the anticommutator, has a similar effect, but since the holonomies $\hat{h}[\alpha_{ij}] - \hat{h}[\alpha_{ji}]$ are applied before the volume operator, the latter has instead the matrix elements

$$\frac{l_0^3}{4} \sqrt{|W_{[p+\epsilon', q+\epsilon'', c]}^{(4)}(p+\epsilon', q+\epsilon'', 1, c)_r^{\pm 2}|}.$$

Calling

$$K_{[p,q,c]}^{[a,b,c]} = \sqrt{|W_{[p,q,c]}^{(4)}(p, q, 1, c)_r^{\pm 2}|} + \sqrt{|W_{[a,b,c]}^{(4)}(a, b, 1, c)_r^{\pm 2}|} \quad (\text{B19})$$

the action of the Hamiltonian (1) can thus be written as

$$\begin{aligned}
\hat{C}_s \begin{array}{c} r \\ / \quad \backslash \\ p \quad q \end{array} &= \frac{il_0}{12} \sum_{a,b,c} \lambda_c^{1,r} \lambda_a^{1,p} \lambda_b^{1,q} \frac{\begin{array}{ccc} \textcircled{c} & \textcircled{a} & \textcircled{b} \\ \textcircled{r} & \textcircled{p} & \textcircled{q} \\ 1 & 1 & 1 \end{array}}{\left(\frac{\begin{array}{cc} \boxed{1 \ p \ r} & \boxed{c \ q \ 1} \\ \boxed{a \ \quad \quad} & \boxed{\quad \quad b} \end{array}}{\begin{array}{cc} \textcircled{c} & \textcircled{a} \\ \textcircled{q} & \textcircled{b} \end{array}} - \frac{\begin{array}{cc} \boxed{r \ q \ 1} & \boxed{1 \ p \ c} \\ \boxed{p \ \quad \quad} & \boxed{a \ \quad \quad} \end{array}}{\begin{array}{cc} \textcircled{b} & \textcircled{r} \\ \textcircled{c} & \textcircled{a} \end{array}} \right)} \\
&\times K_{[p,q,c]}^{[a,b,c]} \begin{array}{c} r \\ / \quad \backslash \\ a \quad b \\ \backslash \quad / \\ p \quad 1 \quad q \end{array} + \left\{ \frac{\begin{array}{cc} \boxed{1 \ r \ q} & \boxed{b \ p \ 1} \\ \boxed{c \ \quad \quad} & \boxed{\quad \quad a} \end{array}}{\begin{array}{cc} \textcircled{c} & \textcircled{q} \\ \textcircled{b} & \textcircled{a} \end{array}} - \frac{\begin{array}{cc} \boxed{q \ p \ 1} & \boxed{1 \ r \ b} \\ \boxed{r \ \quad \quad} & \boxed{c \ \quad \quad} \end{array}}{\begin{array}{cc} \textcircled{a} & \textcircled{q} \\ \textcircled{b} & \textcircled{a} \end{array}} \right\} K_{[r,p,b]}^{[c,a,b]} \begin{array}{c} r \\ / \quad \backslash \\ 1 \quad c \\ \backslash \quad / \\ p \quad a \quad q \end{array} \\
&+ \left\{ \frac{\begin{array}{cc} \boxed{1 \ q \ p} & \boxed{a \ r \ 1} \\ \boxed{b \ \quad \quad} & \boxed{b \ \quad \quad} \end{array}}{\begin{array}{cc} \textcircled{a} & \textcircled{b} \\ \textcircled{r} & \textcircled{c} \end{array}} - \frac{\begin{array}{cc} \boxed{p \ r \ 1} & \boxed{1 \ q \ a} \\ \boxed{q \ \quad \quad} & \boxed{b \ \quad \quad} \end{array}}{\begin{array}{cc} \textcircled{c} & \textcircled{p} \\ \textcircled{a} & \textcircled{b} \end{array}} \right\} K_{[q,r,a]}^{[b,c,a]} \begin{array}{c} r \\ / \quad \backslash \\ c \quad 1 \\ \backslash \quad / \\ p \quad b \quad q \end{array}. \tag{B20}
\end{aligned}$$

Since the Hamiltonian is Hermitian, if it takes an input spinnetwork $|A\rangle$ into an output spinnetwork $|B\rangle$, it should take $|B\rangle$ into $|A\rangle$ with equal probability, i.e., $\langle A|\hat{C}_s|B\rangle = \langle B|\hat{C}_s|A\rangle^*$. We apply our constraint operator on the first subgraph on the right-hand side of Eq. (B20) to check this condition. Similar arguments to those presented in the derivation of Eqs. (B10)-(B20) show that one of the terms resulting from the application of Eq. (1) on this subgraph introduces a triangular loop inside the previously added loop, i.e.

$$\begin{array}{c} r \\ / \quad \backslash \\ a \quad b \\ \backslash \quad / \\ p \quad 1 \quad q \end{array} \rightarrow \frac{\begin{array}{ccc} \textcircled{c} & \textcircled{d} & \textcircled{e} \\ \textcircled{c} & \textcircled{d} & \textcircled{e} \\ 1 & 1 & 1 \end{array}}{\left(\frac{\begin{array}{cc} \boxed{1 \ a \ r} & \boxed{c \ b \ 1} \\ \boxed{d \ \quad \quad} & \boxed{d \ \quad \quad} \end{array}}{\begin{array}{cc} \textcircled{d} & \textcircled{r} \\ \textcircled{c} & \textcircled{e} \end{array}} - \frac{\begin{array}{cc} \boxed{r \ b \ 1} & \boxed{1 \ a \ c} \\ \boxed{a \ \quad \quad} & \boxed{d \ \quad \quad} \end{array}}{\begin{array}{cc} \textcircled{e} & \textcircled{r} \\ \textcircled{c} & \textcircled{d} \end{array}} \right)} \begin{array}{c} r \\ / \quad \backslash \\ d \quad e \\ \backslash \quad / \\ p \quad 1 \quad q \end{array}, \tag{B21}$$

where the sum over ξ', ξ'', ϵ (with $d = a + \xi'$, $c = r + \epsilon$, $e = b + \xi''$ and $\xi', \xi'', \epsilon = \pm 1$), as well as the factor $\lambda_c^{1,r} \lambda_d^{1,a} \lambda_e^{1,b} K_{[a,b,c]}^{[d,e,c]}$, have been omitted. The two previously inexistent edges of color 1 in the subgraph on the right-hand side of Eq. (B21) can be combined with the help of relation (B5), which merges the two into a single

edge that can take the colors 0 or 2,

$$\begin{array}{c} r \\ / \quad \backslash \\ d \quad e \\ \backslash \quad / \\ p \quad 1 \quad q \end{array} = \sum_{l=0,2} \frac{\begin{array}{c} \textcircled{l} \\ \textcircled{1} \end{array}}{\begin{array}{c} \textcircled{1} \\ \textcircled{l} \end{array}} \begin{array}{c} r \\ / \quad \backslash \\ d \quad e \\ \backslash \quad / \\ p \quad l \quad q \end{array}. \tag{B22}$$

When the merging of the edges of color 1 leads to an edge of color 2, its attachments to the two previously existent edges can be renormalized by means of Eq. (B6) to remove the virtual triangles. When this merging process results in no edge ($l = 0$), the coefficient on the right-hand side in Eq. (B22) becomes $-1/2$ and the remaining "loop" in two of the edges can be removed with the aid of Eq. (B7), recovering the original subgraph (with no added triangular loops) with an overall coefficient $\lambda_c^{1,r} \lambda_p^{1,a} \lambda_q^{1,b} K_{[a,b,c]}^{[p,q,c]}/2 (= \lambda_c^{1,c} \lambda_a^{1,p} \lambda_b^{1,q} K_{[p,q,c]}^{[a,b,c]}/2)$ multiplied by

$$\begin{array}{c}
\begin{array}{c} c \\ \circ \\ c \\ r \\ 1 \end{array}
\left(
\begin{array}{c}
\begin{array}{c} 1 \quad a \quad r \\ \diagdown \quad \diagup \\ p \quad b \end{array}
\quad c \quad
\begin{array}{c} c \quad b \quad 1 \\ \diagdown \quad \diagup \\ p \quad q \end{array}
\quad r \\
\hline
\begin{array}{c} p \quad r \\ \circ \quad \circ \\ c \quad p \\ b \quad q \end{array}
\quad - \quad
\begin{array}{c} r \quad 1 \quad c \\ \diagdown \quad \diagup \\ a \quad q \end{array}
\quad c \quad
\begin{array}{c} 1 \quad a \quad c \\ \diagdown \quad \diagup \\ p \quad q \end{array}
\quad r \\
\hline
\begin{array}{c} q \quad r \\ \circ \quad \circ \\ c \quad p \\ a \quad q \end{array}
\end{array}
\right)
\end{array}
\tag{B23}$$

This differs from the first coefficient in Eq. (B20) by

$$-\frac{\begin{array}{c} 1 \quad a \quad b \\ \circ \quad \circ \quad \circ \\ a \quad b \\ \hline \begin{array}{c} 1 \quad 1 \\ \circ \quad \circ \\ p \quad q \end{array} \end{array}}{\begin{array}{c} 1 \quad a \quad b \\ \circ \quad \circ \quad \circ \\ a \quad b \\ \hline \begin{array}{c} 1 \quad 1 \\ \circ \quad \circ \\ p \quad q \end{array} \end{array}} = 2 \left(\frac{-p}{p+1} \right)^{\frac{1-\epsilon'}{2}} \left(\frac{-q}{q+1} \right)^{\frac{1-\epsilon''}{2}}.
\tag{B24}$$

Equation (B24) seems in conflict with the self-adjointness of the Hamiltonian. This illusory tension is a by-product of the usage of Temperley-Lieb tangles rather than normalized spinnetworks. As show in Ref. [32] (cf. Sec. VIII), tangles have to be normalized by the square root of the product of loops of the form (B3), one for each edge of the tangle, divided by the product of theta symbols of the form (B4), one for each vertex of the tangle (the indices of the symbols are the colors of the corresponding edges and vertices), i.e.

$$|\text{spinnetwork } \{j_i\}\rangle = \sqrt{\prod_v \prod_e \frac{\Delta_e}{\theta_v}} |\text{tangle } \{2j_i\}\rangle,
\tag{B25}$$

where Δ_e is given by Eq. (B3) with the same color as edge e , θ_v by Eq.(B4) for the vertex v (the arguments being the three colors of the edges connected to that vertex) and products run over edges e and vertices v . Note that the orthonormalized spinnetwork state in Eq. (B25) has a set $\{j_i\}$ of spins attached to its vertices, while the tangle has a corresponding set of colors $\{2j_i\}$. Hence, if the subgraph on the left-hand side of Eq. (B21) is associated with the spinnetwork $|A\rangle$ and the subgraph on the left-hand side of Eq. (B20) (before the application of the Hamiltonian) is associated with $|B\rangle$ (the rest of the two graphs being identical), the ratio $\langle A|A\rangle/\langle B|B\rangle$ is exactly given by Eq. (B24) (up to a minus sign). Therefore $\langle A|\hat{C}_s|B\rangle/\langle B|\hat{C}_s|A\rangle = -1$ and the scalar Hamiltonian constraint is self-adjoint.

Notwithstanding the apparently cumbersome form of Eq. (B20), a few properties can be extracted from its co-

efficients. The tetrahedral net symbol, for example, can be recast using Eq. (B9) as a spin-normalized 6j symbol, with well known properties. It is therefore clear that, if $p = q$ and $a = b$, the pairs of tetrahedral net symbols (related by $p \leftrightarrow q$, $a \leftrightarrow b$ up to symmetry) will cancel each other in the first coefficient of the right-hand side of Eq. (B20). Similarly, its second coefficient vanishes when $r = p$ and $c = a$ (owing to the swap $p \leftrightarrow r$, $a \leftrightarrow c$ between pairs of symbols), while the third coefficient vanishes for $r = q$ and $c = b$ (owing to the argument swap $q \leftrightarrow r$, $b \leftrightarrow c$).

Triangularity in Eq. (B9) requires that $(a, 1, c)$, (c, r, q) , (q, p, a) , $(r, 1, p)$, (a, c, r) , $(r, 1, b)$, (b, q, a) and $(1, c, q)$ all fulfill the triangular condition in order for the first pair of tetrahedral net symbols on the right-hand side of Eq. (B21) to be nonzero [55]. If $p = q = r = 1$, for example, the aforementioned term will give zero whenever $a = b = 0$, $c = a = 0$, $c = b = 0$, $a \neq b$, $c \neq a$ or $c \neq b$ (because, in this case, a , b and c can only assume the values 0 or 2). Additionally, if $a = b = 2$, the two pairs of tetrahedral net symbols subtracted from each other will be equal and therefore cancel out (since they differ by a $a \leftrightarrow b$ argument swap). As a result, a vertex with all edges of color 1 is annihilated by the action of the Hamiltonian [in other words, it is a zero-eigenvalue eigenstate of Eq. (1)].

Similarly, if $p = q = 1$ and $r \geq 3$, the triples $(r, 1, p)$ and $(r, 1, q)$ are not triangular. Permutation of these labels reveals that no combination of the labels 1, 1 and n (with $n \geq 3$) can simultaneously fulfill all the triangularity conditions. It is worth noting that these vertices violate the gauge constraint, therefore they are not contained in the physical Hilbert subspace. Nonetheless, 3-valent vertices with edges of colors 1, $1 + n$ and $1 + n$ with $n \in \mathbb{N}^*$ fulfill the gauge constraint, but when acted upon by the Hamiltonian constraint cannot satisfy the triangularity conditions of the 6j symbols in Eq. (B20) (giving a zero outcome), and are therefore zero-eigenvalue eigenstates of the Hamiltonian constraint when the Temperley-Lieb algebra is adopted.

[1] G. Amelino-Camelia, C. Lämmerzahl, A. Macias, and H. Müller, The search for quantum gravity signals, *AIP Conf. Proc.* **758**, 30 (2005).

[2] R. Howl, L. Hackermüller, D. E. Bruschi, and I. Fuentes,

Gravity in the quantum lab, *Adv. Phys.: X* **3**, 1383184 (2018).

[3] A. Barrau, Testing different approaches to quantum gravity with cosmology: An overview, *C. R. Phys.* **18**, 189

- (2017).
- [4] M. Bronstein, Republication of: Quantum theory of weak gravitational fields, *Gen. Relativ. Gravit.* **44**, 267 (2012).
 - [5] P. A. M. Dirac, The theory of gravitation in Hamiltonian form, *Proc. R. Soc. A* **246**, 333 (1958).
 - [6] P. A. M. Dirac, *Lectures on quantum mechanics*, Vol. 2 (Yeshiva University, New York, 2001).
 - [7] S. W. Hawking, Breakdown of predictability in gravitational collapse, *Phys. Rev. D* **14**, 2460 (1976).
 - [8] J. A. Wheeler, Superspace and the nature of quantum geometrodynamics, in *quantum cosmology*, Adv. Ser. Astrophys. Cosmol. **3**, 27 (1987).
 - [9] B. S. DeWitt, Quantum theory of gravity. i. the canonical theory, *Phys. Rev.* **160**, 1113 (1967).
 - [10] A. Ashtekar, New variables for classical and quantum gravity, *Phys. Rev. Lett.* **57**, 2244 (1986).
 - [11] J. F. Barbero G., Real ashtekar variables for Lorentzian signature space-times, *Phys. Rev. D* **51**, 5507 (1995).
 - [12] C. Rovelli and L. Smolin, Knot theory and quantum gravity, *Phys. Rev. Lett.* **61**, 1155 (1988).
 - [13] T. Thiemann, Anomaly-free formulation of non-perturbative, four-dimensional Lorentzian quantum gravity, *Phys. Lett. B* **380**, 257 (1996).
 - [14] A. Ashtekar and J. Lewandowski, Background independent quantum gravity: A status report, *Class. Quantum Grav.* **21**, R53 (2004).
 - [15] R. Koenig, G. Kuperberg, and B. W. Reichardt, Quantum computation with Turaev–Viro codes, *Ann. Phys. (Amsterdam)* **325**, 2707 (2010).
 - [16] Y.-J. Liu, K. Shtengel, A. Smith, and F. Pollmann, Methods for simulating string-net states and anyons on a digital quantum computer, *Phys. Rev. X Quant.* **3**, 040315 (2022).
 - [17] S. Trebst, M. Troyer, Z. Wang, and A. W. Ludwig, A short introduction to Fibonacci anyon models, *Prog. Theor. Phys. Suppl.* **176**, 384 (2008).
 - [18] I. Mäkinen, Introduction to SU(2) recoupling theory and graphical methods for loop quantum gravity, *arXiv preprint arXiv:1910.06821* (2019).
 - [19] L. H. Kauffman and S. Lins, *Temperley-Lieb Recoupling Theory and Invariants of 3-Manifolds* (Princeton University Press, Princeton, 1994).
 - [20] D. Brink and G. Satchler, *Angular Momentum, 2nd edition* (Clarendon Press, Oxford, 1968).
 - [21] A. Messiah, *Quantum mechanics Vol. II* (North Holland Publishing Company, Amsterdam, 1962).
 - [22] T. L. M. Guedes, G. A. Mena Marugán, F. Vidotto, and M. Müller, Computing the graph-changing dynamics of loop quantum gravity, Companion letter, *arXiv:2412.XXXXX* (2024).
 - [23] J. Yang and Y. Ma, Graphical calculus of volume, inverse volume and Hamiltonian operators in loop quantum gravity, *Eur. Phys. J. C* **77**, 1 (2017).
 - [24] R. Borissov, R. De Pietri, and C. Rovelli, Matrix elements of Thiemann’s Hamiltonian constraint in loop quantum gravity, *Class. Quantum Grav.* **14**, 2793 (1997).
 - [25] M. Gaul and C. Rovelli, A generalized Hamiltonian constraint operator in loop quantum gravity and its simplest Euclidean matrix elements, *Class. Quantum Grav.* **18**, 1593 (2001).
 - [26] E. Alesci, T. Thiemann, and A. Zipfel, Linking covariant and canonical loop quantum gravity: New solutions to the Euclidean scalar constraint, *Phys. Rev. D* **86**, 024017 (2012).
 - [27] H. Sahlmann and W. Sherif, Towards quantum gravity with neural networks: Solving the quantum Hamilton constraint of U(1) BF theory, *arXiv preprint arXiv:2402.10622* (2024).
 - [28] C. Rovelli, *Quantum Gravity* (Cambridge University Press, Cambridge, 2004).
 - [29] A. Ashtekar and P. Singh, Loop quantum cosmology: A status report, *Class. Quantum Grav.* **28**, 213001 (2011).
 - [30] G. A. Mena Marugán, A brief introduction to loop quantum cosmology, *AIP Conf. Proc.* **1130**, 89 (2009).
 - [31] T. Thiemann, *Modern Canonical Quantum General Relativity* (Cambridge University Press, Cambridge, 2007).
 - [32] R. De Pietri and C. Rovelli, Geometry eigenvalues and the scalar product from recoupling theory in loop quantum gravity, *Phys. Rev. D* **54**, 2664 (1996).
 - [33] C. Rovelli and L. Smolin, Spin networks and quantum gravity, *Phys. Rev. D* **52**, 5743 (1995).
 - [34] C. Rovelli and L. Smolin, Loop space representation of quantum general relativity, *Nucl. Phys. B* **331**, 80 (1990).
 - [35] D. Horsman, A. G. Fowler, S. Devitt, and R. Van Meter, Surface code quantum computing by lattice surgery, *New J. Phys.* **14**, 123011 (2012).
 - [36] M. Gutiérrez, M. Müller, and A. Bermúdez, Transversality and lattice surgery: Exploring realistic routes toward coupled logical qubits with trapped-ion quantum processors, *Phys. Rev. A* **99**, 022330 (2019).
 - [37] A. Ashtekar and J. Lewandowski, Quantum theory of geometry II: Volume operators, *Adv. Theor. Math. Phys.* **1**, 388 (1998).
 - [38] This choice is based on the criterion of parallelism or anti-parallelism between the Hodge dual of the wedge product of the 3 arguments of κ and the 4th unit vector perpendicular to them (in 4D Euclidean space).
 - [39] Note that the way the grasp is attached to the link along the direction p_4 is different when the temporary spin-1/2 link is present. Nonetheless, after applying Eq. (11) when we take the spin $1/2 \rightarrow 0$, the difference boils down to a braid operation and an arrow flip, giving an overall phase of $(-1)^{1+j_4+j_4}(-1)^{2j_4} = -1$, which cancels out the minus in the prefactors in Eq. (81). This shows graphically how the volume for 4-valent intertwiners can be obtained from Eq. (81).
 - [40] J. Brunnemann and D. Rideout, Properties of the volume operator in loop quantum gravity: I. results, *Class. Quantum Grav.* **25**, 065001 (2008).
 - [41] Mathematica notebook available in https://github.com/ThiagoLMGuedes/Canonical_LQG.
 - [42] M. Domagała, K. Giesel, W. Kamiński, and J. Lewandowski, Gravity quantized: Loop quantum gravity with a scalar field, *Phys. Rev. D* **82**, 104038 (2010).
 - [43] R. Gambini, J. Griego, and J. Pullin, Chern-Simons states in spin-network quantum gravity, *Phys. Lett. B* **413**, 260 (1997).
 - [44] T. Thiemann and M. Varadarajan, On propagation in loop quantum gravity, *Universe* **8**, 615 (2022).
 - [45] C. Rovelli and F. Vidotto, Stepping out of homogeneity in loop quantum cosmology, *Class. Quantum Grav.* **25**, 225024 (2008).
 - [46] M. P. Reisenberger and C. Rovelli, “Sum over surfaces” form of loop quantum gravity, *Phys. Rev. D* **56**, 3490 (1997).
 - [47] Calculations for such values of the lapse, already close to the unit, might be questionable in a perturbative study.

- Nonetheless, our results about the relative values of the 2nd-order and 4th-order contributions provide support to their validity, or at least are not in conflict with it.
- [48] M. Christodoulou and F. d’Ambrosio, Characteristic time scales for the geometry transition of a black hole to a white hole from spinfoams, [arXiv preprint arXiv:1801.03027](#) (2018).
- [49] C. Rovelli and F. Vidotto, White-hole dark matter and the origin of past low-entropy, [arXiv preprint](#) (2018), [arXiv: 1804.04147](#).
- [50] H. Huang, J. Kunz, J. Yang, and C. Zhang, Light ring behind wormhole throat: Geodesics, images, and shadows, *Phys. Rev. D* **107**, 104060 (2023).
- [51] It is worth noting that the expression given in Ref. [19] fails to retrieve the correct answer, which is zero, in certain specific cases with violation of triangularity, such as, for example, when the central color [j in Eq. (B2)] alone violates it.
- [52] Note that the original expression of the formula in Sec. 8.5 of Ref. [19], also reproduced in Refs. [24, 25, 28], has a typo (a minus sign turned into a plus) relative to the correct derivation presented in Sec. 9.11 of Ref. [19], also reproduced in Refs. [24, 25, 28]. Furthermore, the derivation only holds when the triangularity condition is fulfilled, therefore numerical evaluations using this formula require the additional inclusion of triangularity-based selection rules.
- [53] By convention, the attachment of a holonomy is always performed from the right side of an edge. This ordering will be important later, when Eq. (B8) comes into play. If one consistently attaches holonomies from the same side, however, it does not matter which side is chosen as convention.
- [54] Note that $\lambda_c^{a,b} = \lambda_b^{a,c} = \lambda_a^{b,c}$, because $(-1)^{-1} = -1$.
- [55] V. G. Turaev and O. Y. Viro, State sum invariants of 3-manifolds and quantum 6j-symbols, *Topology* **31**, 865 (1992).